NUCLEAR SHELL STRUCTURE OF ODD-A MAGNESIUM ISOTOPES WITHIN USDA HAMILTONIAN

ANWER AHMED MOHAMMED AL-SAMMARRAIE

THESIS SUBMITTED IN FULFILMENT OF THE REQUIREMENTS FOR THE DEGREE OF DOCTOR OF PHILOSOPHY

DEPARTMENT OF PHYSICS
FACULTY OF SCIENCE
UNIVERSITY OF MALAYA
KUALA LUMPUR

2015

UNIVERSITI MALAYA

ORIGINAL LITERARY WORK DECLARATION

Name of Candidate: **ANWER AHMED MOHAMMED AL-SAMMARRAIE**

Regisration/Matric No.: **SHC100052**

Name of Degree: **DOCTOR OF PHILOSOPHY**

Title of Project Paper/Research Report/Dissertation/Thesis ("this Work"): **"NUCLEAR SHELL STRUCTURE OF ODD-A MGNESIUM ISOTOPES WITHIN USDA HAMILTONIAN"**

Field of Study: **Theoretical Nuclear Physics**

I do solemnly and sincerely declare that:

(1) I am the sole author/writer of this Work,
(2) This Work is original,
(3) Any use of any work in which copyright exists was done by way of fair dealing and for permitted purposes and any excerpt or extract from, or reference to or reproduction of any copyright work has been disclosed expressly and sufficiently and the title of the Work and its authorship have been acknowledged in this Work,
(4) I do not have any actual knowledge nor do I ought reasonably to know that the making of this work constitutes an infringement of any copyright work,
(5) I hereby assign all and every rights in the copyright to this Work to the University of Malaya ("UM"), who henceforth shall be owner of the copyright in this Work and that any reproduction or use in any form or by any means whatsoever is prohibited without the written consent of UM having been first had and obtained,
(6) I am fully aware that if in the course of making this Work I have infringed any copyright whether intentionally or otherwise, I may be subject to legal action or any other action as may be determined by UM.

(Candidate Signature) Date:

Subscribed and solemnly declared before,

Witness's Signature Date:

Name **PROF. DR. HASAN ABU KASSIM**

Designation

ABSTRACT

The USDA is the latest universal shell model interaction in the SD (0s1d) shell. It is derived by fitting more than 600 energy levels from experimental data. We assess the accuracy of the USDA Hamiltonian in the nuclear structure calculations for odd-A magnesium isotopes with neutron numbers between 9 and 17 on the basis of the recently reported experimental data. This study provides an example of the applicability and the accuracy of the shell model calculations limited to the *sd* shell. The assessments rely on the evaluation of the Hamiltonian's eigenvalues with the corresponding positive parity energy states up to 10 MeV for most isotopes and the Hamiltonian's eigenvectors with the transition strength probability and inelastic electron-nucleus scattering. We show the regions in which the Hamiltonian is effective and demonstrated the possibility of confirming the known experimental data and suggesting some new nuclear energy levels.

The calculations of the energy states are performed by using the OXBASH code and the results show a good agreement with the experimental states for the $^{21-27}$Mg isotopes while a clear difference is found with the ^{29}Mg data. Many energy states are proposed and we have confirmed the existence of some states that were experimentally uncertain . The reduced electric quadrupole transition probabilities, reduced magnetic dipole transition probabilities, and multipole mixing ratio results show the same precision for related energy states. The longitudinal inelastic electron scattering form factors have been calculated for the states 0.974(J=$3/2_1^+$), 1.611(J=$7/2_1^+$), 1.964(J=$5/2_2^+$), 2.563(J=$1/2_2^+$), 2.801(J=$3/2_2^+$), 3.405(J=$9/2_1^+$), 4.059(J=$9/2_2^+$) and 5.252(J=$11/2_1^+$) MeV in the ^{25}Mg spectrum. The wave functions of the radial single-particle matrix elements have been calculated with the

Woods-Saxon and Skyrme interaction potentials with the one-body transition densities (OBTDs) obtained from the USDA calculations. The result of the longitudinal form factors C2 and C4 show good agreement with the available experimental data for all states in the first sequence whereas, in the second sequence the accuracy of the results vary according to the energy of the states. Two shell-model codes, CPM3Y and OXBASH, have been used to calculate the transverse form factors for the 1.611 and 3.405 MeV states in the ^{25}Mg spectrum with the OBTDs obtained from USDA Hamiltonian. The results of the two codes show good agreement with the available experimental data for the $J=7/2^+$ state at energy 1.611 MeV. For the second state $J=9/2^+$ at energy 3.405 MeV, the CPM3Y and OXBASH results are higher and lower than the experimental data, respectively. The effective g factors values are used as adjustable parameters to get an agreement with the experimental data for OXBASH calculations due to the core-polarization effects.

ABSTRAK

USDA adalah interaksi model petala umum terkini di dalam petala SD (0s1d). Ia telah diterbitkan oleh padanan kepada lebih daripada 600 aras tenaga daripada data eksperimen. Kami menaksirkan kejituan Hamiltonian USDA dalam pengiraan struktur nuklear bagi isotop magnesium A-ganil dengan nombor neutron antara 9 tan 17 pada asas data eksperimen yang terkini dilaporkan. Kajian ini memberikan satu contoh keterterapan dan kejituan pengiraan model petala yang dihadkan kepada petala *sd*. Penilaian ini bergantung kepada penaksiran nilai eigen Hamiltonian yang sepadan dengan keadaan tenaga pariti positif sehingga 10 MeV bagi kebanyakan isotop serta vektor eigen Hamiltonian dengan kebarangkalian kekuatan peralihan dan serakan electron-nukleus tak kenyal. Kami menujukkan kawasan di mana Hamiltonian adalah efektif dan kebarangkalian untuk mengesahkan data eksperimen yang diketahui serta mencadangkan sebahagian keputusan baru struktur nuklear. Pengiraan keadaan tenaga dilakukan dengan menggunakan kod OXBASH dan keputusannya menunjukkan persetujuan dengan keadaan eksperimen bagi isotope $^{21-27}$Mg manakala satu perbezaan nyata dijumpai pada data ^{29}Mg. Banyak keadaan tenaga yang telah dicadangkan dan kami telah mengesahkan kewujudan sebahagian keadaan yang tidak dapat dipastikan daripada eksperimen. Keputusan kebarangkalian peralihan catur kutub-elektrik terkurang, kebarangkalian peralihan dwikutub magnet terkurang dan nisbah campuran multikutub menunjukkan kepersisan yang sama bagi keadaan tenaga yang berkaitan. Faktor bentuk serakan membujur elektron tak kenyal telah dikira untuk keadaan 0.974(J=$3/2_1^+$), 1.611(J=$7/2_1^+$), 1.964(J=$5/2_2^+$), 2.563(J=$1/2_2^+$), 2.801(J=$3/2_2^+$), 3.405(J=$9/2_1^+$), 4.059(J=$9/2_2^+$) dan 5.252(J=$11/2_1^+$) MeV di dalam

spektrum ^{25}Mg. Fungsi gelombang elemen matrik jejari satu zarah telah dikira dengan menggunakan keupayaan interaksi Woods-Saxon dan Skyrme dengan ketumpatan peralihan satu jasad (OBTDs) diperolehi daripada pengiraan USDA. Keputusan faktor bentuk membujur C2 dan C4 menunjukkan persetujuan dengan data eksperimen yang sedia ada bagi semua keadaan dalam urutan pertama. manakala dalam urutan kedua kejituan keputusannya berubah bergantung kepada tenaga bagi keadaan tersebut . Dua kod model petala CPM3Y dan OXBASH telah digunakan untuk mengira faktor bentuk melintang bagi keadaan 1.611 dan 3.405 MeV dalam spektrum ^{25}Mg dengan OBTDs diperolehi daripada Hamiltonian USDA. Keputusan bagi dua kod tersebut menunjukkan persetujuan dengan data eksperimen sedia ada bagi keadaan $J=7/2^{+}$ pada tenaga 1.611 MeV. Bagi keadaan kedua $J=9/2^{+}$ pada tenaga 3.405 MeV, keputusan CPM3Y dan OXBASH masing- masing menunjukkan lebih tinggi dan rendah daripada data eksperimen. Nilai efektif faktor g digunakan sebagai parameter bolehlaras untuk mendapatkan persetujuan dengan data eksperimen bagi pengiraan OXBASH disebabkan oleh kesan pengutuban teras.

ACKNOWLEDGMENTS

First of all, I would like to thank my supervisor, Assoc. Prof. Dr. Hasan Abu Kassim, for his support and guidance throughout my research project. I would also like to express a special acknowledgment to Dr. Fadhil I. Sharrad ; University of Kerbala, who spent a year in the University of Malaya as a visting research fellow at the Department of Physics. His knowledge and experience in shell model have guided and enabled me to complete this thesis.

There are a number of people whom I would like to thank who have contributed to this work both professionally and personally. My fellow Ph.D and MSc. students and colleagues at the Theoretical Physics Lab have helped make my Ph.D an excellent experience with lots of fun along the way, for which I am grateful. I would like to thank Miss Nor Sofiah, Mrs Azni, Dr. Norhasliza, Dr. Ghassan, Dr. Maher , Dr. Saad and Dr. Abdurahim who have helped me so much. I would like to express my gratitude to the Department of Physics and the University of Malaya for the opportunity that they have given to me to pursue my study in nuclear physics and support for this work through the University of Malaya Postgraduate Research Grant No. PV089/2011A. I am also grateful to my sponsor the Islamic Development Bank for their financial support through the fellowship under Grant No. 600014283, who made these endeavors financially possible.

I could have had none better than my parents, my wife and my children who were in infinitely patient, encouraging and generousity. They have my unending thanks.

CONTENTS

LIST OF FIGURES

LIST OF TABLES

CHAPTER 1

INTRODUCTION

Understanding the composition of matter has been one of the important issues throughout human history. Breaking matter into smaller building blocks helped to provide information about the molecules which consists of atoms and each atom consists of electrons and a nucleus. The nucleus is composed of protons and neutrons and their number determines the properties of the nucleus and thus the properties of matter. The nucleus is very small, about 10^{-12} to 10^{-13} cm in diameter, and its protons and neutrons orbit relative one to another and interact with each other via the nuclear and Coulomb forces. It is common using the letter Z as the atomic number which represents the number of protons (or electrons) in the nucleus (in the atom), N the number of neutrons and A the mass number which is equal to Z+N. Isotopes are nuclei with same Z but different N [1].

Nuclei have two types of properties: time-independent properties such as mass, size, charge and spin, and time-dependent properties such as radioactive decay and artificial transmutation. The excited states of nucleus are the time-independent property where each state has a definite energy and angular momentum. Time-dependent processes also involve transition between excited states [2].

There are almost 1700 species of nuclei that occur naturally on earth and a significant number of them are created artificially or in the interior of stars [3]. For each Z

element there are usually one or more stable or long-lived isotopes. At low value of Z, the stable nucleus is usually at Z=N and this property changes when N>Z for heavier nuclei where the number of protons and the Coulomb force increases.

From the Rutherford's discovery of nucleus to till date, scientists have strived to find a thorough understanding for this system and the forces which are responsible for binding the components in this extremely small size. Our understanding of nuclear structure is "barely scratched the surface". But, we have colossal number of facts about the nucleus and we have extensive knowledge about these facts [4].

The understanding on nuclear structure means the features of the nucleus and the forces that hold it together. The goal of nuclear structure study is to develop models that combine all of the nuclear phenomena in order to produce a unified nuclear picture. The development of nuclear models has connection to other fields in physics. There are many isotopes that will never be attainable in the laboratory but their existence is possible in stars or may have existed earlier in cosmological time. The development of generalized nuclear models increases the ability to predict nuclear behavior and provides information that is required for cosmological calculations.

To describe the nuclei properties, the theoretical nuclear models must treat the weak, strong, and electromagnetic interactions. The accurate mathematical form to the nucleon-nucleon interaction cannot be represented clearly because the strong force acts non-perturbatively. The solution for this problem was established by using several different approaches either theoretically or phenomenologically [5]. The phenomenological and empirical considerations represent an alternative to the direct theoretical calculation of the effective interactions. This approach can be applied to parameterize an interaction which leads to closer correspondence to experiments. Many ways can be used for making such a

parameterization, starting from those depend highly on a model for the interaction to those that are ultimately independent of any such assumptions [6].

Shell model and collective model are the basic models that from the framework of our understanding on nuclei [4]. Shell model is one of the most important models that have been used to describe the nuclear system for more than 60 years, but the main challenges for this model appeared when the nuclei are away from closed shells, far off the stability line or in the high energy levels.

The aim of this work is to study the nuclear structure of the odd-magnesium isotopes $^{21\text{-}29}$Mg by employing the new SD-shell Hamiltonian (USDA) [7] with the proton-neutron formalism version (USDAPN) in the shell model. USDA represents the closest match between realistic and empirical Hamiltonians.

The first objective of this work is to determine the precision of the USDA calculations. The precision of the USDA is derived from the eigenvalues and eigenvectors of this Hamiltonian. The eigenvalues are investigated through the comparison with the available experimental excited-state for odd-magnesium isotopes. The Hamiltonian eigenvectors are used in the transitions calculations and the investigation of the eigenvectors is achieved through the comparison with the available experimental transition strengths and form factors. The second objective is to present new theoretical nuclear structure data specific in the regions where the USDA shows some reasonable precision. The third objective aims to study the recent modifications in some nuclear factors in compatibility with USDA calculations in order to increase the accuracy and the resulting inferences.

In order to clarify the USDA and OXBASH program characteristics, we need to illustrate the nuclear structure according to the perspective of the shell model with emphasis on the odd-magnesium isotopes properties and their importance through some previous studies. All of the above will be discussed in Chapter Two.

In Chapter Three we will present the details of the mathematical equations which are used in our calculations. The results of the state energies and reduced electric quadrupole transition probabilities, reduced magnetic dipole transition probabilities, and multipole mixing ratio are illustrated in Chapter Four. Chapter Five contains the results of the inelastic electron scattering longitudinal and transverse form factors for ^{25}Mg nucleus. Finally, the conclusions and future work are presented in Chapter Six.

CHAPTER 2

SHELL MODEL

2.1 Nuclear Structure Within Shell Model

The liquid drop model is effective in characterizing the nucleus in macroscopic terms i. e. volume, surface area, Coulomb repulsion, pairing and symmetry (neutron to proton ratio). Other nuclear microscopic properties, such as the increase in binding energy for nuclei at closed nuclear shell boundaries, cannot be described using this semi-empirical approach. There are experimental data that prove the existence of a shell-like structure that is analogous to the observed atomic shell structure [8]. It has been found in nuclei with certain values of proton number (Z) and/or neutron number (N) equal to 2, 8, 20, 28, 50, 82 and 126 that show obvious contrast from the liquid drop model behavior by being unusually stable. These values of Z and/or N are called magic numbers because the lack of interpretation to these numbers for quite a long time. This unusual behavior of magic nuclei has been explained on the basis of the analogy between nuclear and atomic magic numbers. The shell model shares remarkable similarities in the complicated details of the atomic structure and the same theory has been used to solve problems in nuclear structure. In spite of its successes, the model encounter several difficulties when applied in the nuclear field. The most important issue is from the potential, where in the atomic shell the potential supplied by the Coulomb field of the nucleus-electrons and this external agent establishes

the subshells in the atoms. In the nucleus the nucleons move in a potential that is created by the nucleons themselves without any external agent [9].

The shell model describes the filling of orbits or shells with nucleons of certain angular momentum and spins with increasing energy within the nuclear potential. Shells are filled in a manner consistent with the Pauli Exclusion Principle; it means that each nucleon has an individual set of quantum numbers and wave function. Every nucleon is considered as an individual particle orbiting in a central potential in spite of the existence of strong interactions between nucleons [1]. The central potential governs the motion of each nucleon which is designed to approximate most of the nucleons individual interactions. The only requirement for this potential *V(r)* is attractive and $V(r) \rightarrow 0$ as $r \rightarrow 0$. The Schrodinger equation for such potential is [4]:

$$H\psi = \left(\frac{P^2}{2M} + V(r)\right)\psi_{n\ell m}(r) = E_{n\ell m}\psi_{n\ell m}(r) \tag{2.1}$$

where ψ is the wavefunction, P momentum, M is the average nucleon mass and E is the eigenvalue for the Hamiltonian H . This equation is separable into radial and angular coordinates and therefore the solutions:

$$\psi_{n\ell m}(r) = \frac{1}{r}R_{n\ell}(r)\psi_{n\ell}(\theta\phi) \tag{2.2}$$

where n is the radial quantum number $n=1, 2, \ldots$., ℓ the orbital angular momentum ℓ =0, 1, 2… or *s, p, d*… , and m the eigenvalue of its z-component, ℓ_z.

The harmonic oscillator is an ideal potential because of the ease of analytical and computational manipulations. The harmonic potential is given by [4]:

$$V(r) = \frac{1}{2}m\omega^2 r^2 \tag{2.3}$$

where ω is the oscillation frequency, and r the radial distance. For a 3-dimensional harmonic oscillator , the eigenvalues, $E_{n\,\ell}$ (or energy levels), can be written as [4]:

$$E_{nl} = \left(2n + \ell - \frac{1}{2}\right)\hbar\omega \tag{2.4}$$

This leads to exactly degenerate energies of two sub levels. In Figure 2.1, the degenerate multiples of levels with more than one value of *n* (the principle quantum number) can be seen in the simple harmonic oscillator scheme. The degeneracy of each level is *2(2ℓ+1),* which is the number of nucleons in each level. This potential with no modifications reproduces only the first three shell closures and above this point, level spacing does not represent as has been observed experimentally. This shows that the simple harmonic oscillator potential represents a good first approximation to the nuclear potential and must be modified to become useful. The first modification comes from adding an ℓ^2 term to the potential which will flatten out the bottom of the harmonic oscillator potential. The effect of the ℓ^2 term makes the particles with larger angular momentum feel a stronger attractive interaction which causes a reduction of the energy of such levels. This energy reducing changes the degeneracy of the harmonic oscillator levels which results in the emergence of new subshell as shown in Figure 2.1 (Woods-Saxon potential).

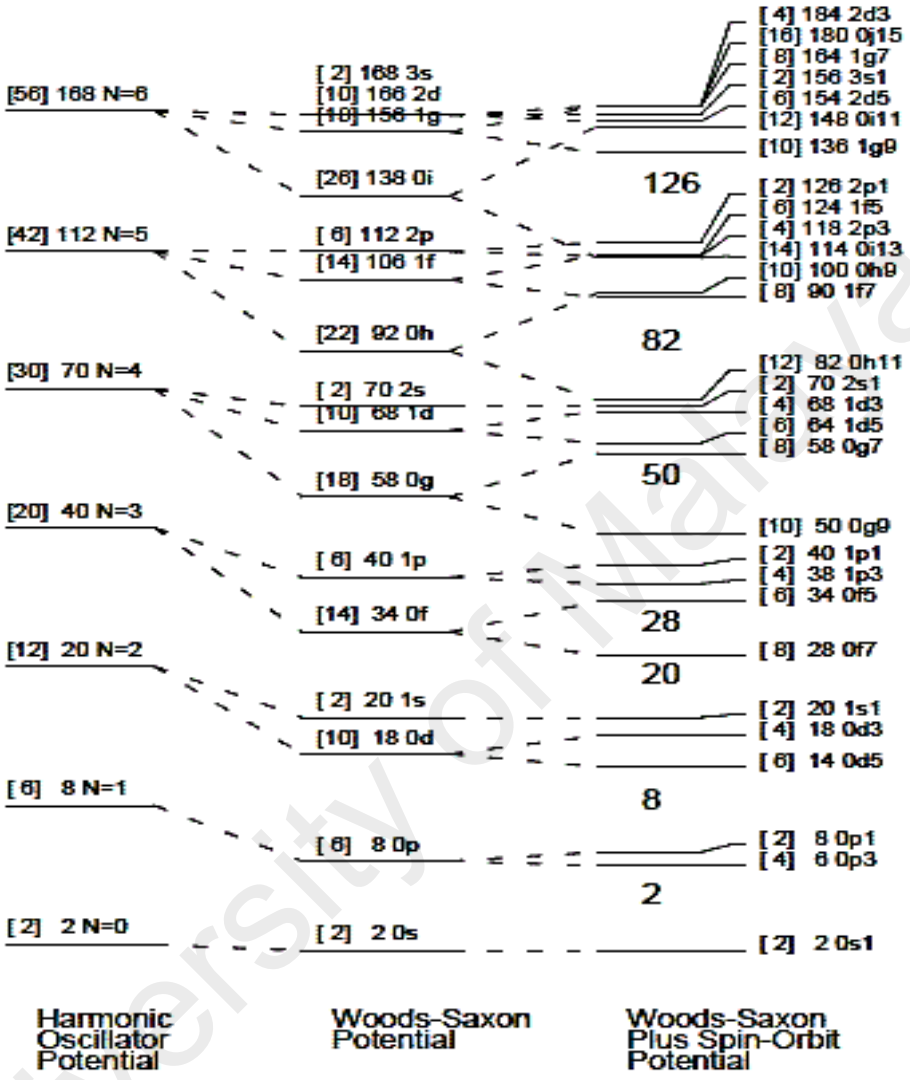

Figure 2.1: single-particle states with three potential models[10], harmonic oscillator, Woods-Saxon without spin-orbit or modified harmonic oscillator with ℓ^2term[4] (middle) and Woods-Saxon with spin orbit (right). The numbers in square brackets are the maximum number of particles in that each level can contain; the following number is a running sum of the total. In addition the harmonic oscillator is labeled by the major quantum number $N=2n+\ell$, the Woods Saxon is labeled by n, ℓ the Woods-Saxon with spin-orbit is labeled by n, ℓ, $2j$.

One of the most commonly used potentials is the Woods-Saxon potential which has the form [9]:

$$V(r) = \frac{-V_0}{1 + e^{\frac{r-R}{a}}} \tag{2.5}$$

where V_0 (well depth) ≈ 50 MeV, R (mean radius) = 1.25 $A^{1/3}$ *fm*, a (skin thickness) = 0.524 *fm* and r is the radial distance from the center of the potential. The Woods-Saxon potential represents intermediate form between the square well and harmonic oscillator potentials as we can see in Figure 2.2, and it is very similar to the harmonic oscillator potential with a modification coming from adding of an ℓ^2 term [9]. The potential model aim is to allow the construction of an appropriate Hamiltonian with the ability of reproducing the nuclear shell sequence for closed shells or magic numbers. Despite the degeneracy of the harmonic oscillator states has been broken, the reproduction of the magic numbers remains incorrect when using the harmonic oscillator potential with an ℓ^2 correction. The successful replication of the magic numbers is achieved by the inclusion of a spin-orbit coupling to the Woods-Saxon potential [1]. In addition to the net nuclear potential, each nucleon in the nucleus feels a strong inverted spin-orbit interaction proportional to the $\ell \cdot s$ value.

The spin-orbit force in generally is a surface effect, and as such can be written as :

$$V_{\ell.s} = -V_{\ell.s} \frac{\partial V(r)}{\partial r} \ell \cdot s \tag{2.6}$$

where $V(r)$ is the chosen potential, and V_{ls} is a strength constant [4]. According to the shell model perspective, nucleons have an intrinsic angular momentum, $s = \frac{1}{2}\hbar$, known as spin. The spin couples to the orbital angular momentum, ℓ, to form the total angular momentum j. There are two types of coupling: parallel or anti parallel.

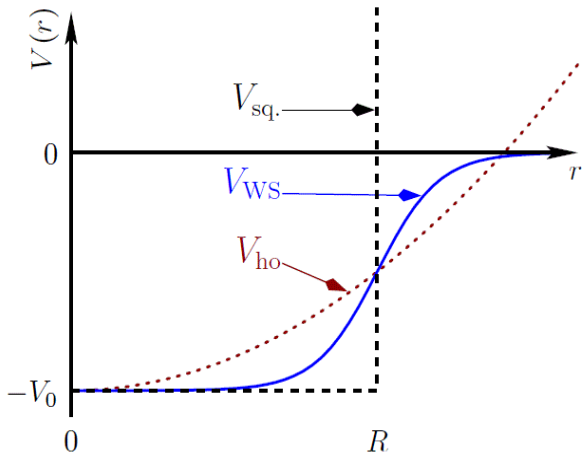

Figure 2.2: Potentials radial dependence, square well $V_{sq.}$, harmonic oscillator V_{ho}, and Woods-Saxon potential $V_{WS}(r)$ [11].

Parallel alignment favors the spin-orbit interaction that affects higher ℓ orbits more than oribits with lower ℓ , splitting $n\,\ell$ levels into components $j = \ell + \frac{1}{2}$ and $j = \ell - \frac{1}{2}$.

Due to the effects of splitting; the spin-orbit interaction reproduces the shell gaps at the correct magic numbers as shown in Figure 2.1. The energy difference between two states with the same $n\,\ell$, originating from the spin-orbit splitting can be found from [10]:

$$j^2 = \ell^2 + s^2 + 2\ell \cdot s \tag{2.7}$$

$$-\ell.s|\psi_j\rangle = -\frac{\hbar^2}{2}(j^2 - \ell^2 - s^2)|\psi_j\rangle$$

$$= -\frac{\hbar^2}{2}\big(j(j+1) - \ell(\ell+1) - s(s+1)\big)|\psi_j\rangle \tag{2.8}$$

$$\left\langle \psi_{j=\ell+\frac{1}{2}}| - \ell \cdot s \ |\psi_{j=\ell+\frac{1}{2}}\right\rangle = -\frac{\ell}{2}\hbar^2 \tag{2.9}$$

$$\left\langle \psi_{j=\ell-\frac{1}{2}}| - \ell \cdot s \ |\psi_{j=\ell-\frac{1}{2}}\right\rangle = +\frac{\ell+1}{2}\hbar^2 \tag{2.10}$$

From Equations (2.9) and (2.10), the energy splitting increases linearly with the orbital angular momentum ℓ as:

$$\Delta E_{ls} = \frac{2\ell + 1}{2}\hbar^2 V_{\ell s} \quad . \tag{2.11}$$

Every nucleon fills the nuclear shells indicated by *t n ℓ j*, where *t* represents the type of nucleon (proton and neutron). The single-particle states are associated in groups according to the principal quantum number *n*. The nuclear total angular momentum *J* caused by the coupling of all the nucleon single-particle states. Nuclei with an even number of neutrons and protons always have a ground state spin of 0^+ because the strong pairing in nuclei whereas in odd-A nuclei, the unpaired nucleon dominate the nuclear spin. The parity is the other important feature of the nucleus, which characterizes the properties of the wave function under spatial inversion. The individual nucleons are fermions with a definite parity $\pi = (-1)^{\ell}$ and the parity of the of the nucleus is found from product of all the individual nucleon parities.

2.2 The Model Space

The term "model space" refers to the orbits and the truncation in the set of the orbits that is supposed to be used in the calculation [12]. Solving Schrödinger equation in full Hilbert space becomes impossible due to the huge number of configurations. In this case, the truncation of the Hilbert space is the best technique to solve the Schrödinger equation, and there are three parts to this method :

1- The inert core; all orbits are forced to be always full.

2- The valence space; a truncated part, model space, consists of the orbits available to the valence particles. If the nuclear system consists of *N* neutron number and

Z proton number and the core consists of N_c neutrons and Z_c protons then the valence protons are $Z_v=Z-Z_c$ and the valence neutrons are $N_v=N-N_c$.

3- External space; the remaining orbits that are always empty.

In this work, the truncated model space is defined by the single-particle quantum states *0d5/2*, *1s1/2*, and *0d3/2* as shown in Figure 2.1. This states configuration is called the SD-model space which is commonly used in nuclei with mass number $16 < A < 40$ with the condition Z and $N > 8$ which represents the inert core or the so-called ^{16}O. The choice of these states is based on the shell gaps between the 0p and 0d ,1s orbits at A=16 and the 0d, 1s and 0f, 1p orbits at A=40. The gaps are sufficiently large compared with gaps between *0d5/2*, *1s1/2*, and *0d3/2* states. The essential degrees of freedom which are necessary to model the typical low-lying positive parity are incorporated in the SD-model space [13].

Generally, a large model space gives the best and most accurate result while the computation time increases exponentially with the model space size. On the other hand, the empirical Hamiltonians are more accurate when used in a small model space. Thus the choice of model space is a compromise between what we want to describe and the cost of the calculations. It has been found that the truncation of the shell-model spaces in the *sd*-shell nuclei has a strong effect in the binding energies but the effect on the excitation energies is an order of magnitude smaller [14].

2.3 Effective Interaction

Many methods have been used to calculate the nuclear states energies within higher numerical accuracy and to provide wave functions from which the calculation of other observables becomes applicable. Shell-model configuration mixing is one of the most efficient methods used for this purpose where the conventional shell-model codes provide typically 1 keV of numerical accuracy [12]. In this method the matrix is established upon all possible Slater determinants with diagonalization on a relatively small subset of valence orbits [12]. The standard shell model Hamiltonian can be written as [15]:

$$H = \sum_a \varepsilon_a n_a + \sum_{a\leq b, c\leq d} \sum_{JT} V_{JT}(ab;cd) \sum_{MT_z} A^{\dagger}_{JMTT_z}(ab) A_{JMTT_z}(cd) \qquad (2.12)$$

where ε_a is the single-particle energies, n_a denotes the number operators of an orbit *a* with quantum numbers (n_a, ℓ_a, j_a) or sometimes called the one-body transition density, OBTD [16], $V_{JT}(ab;cd)$ the two-body matrix elements. $A^{\dagger}_{JMTT_z}(ab)$ stands for the creation operator of nucleon-pair in orbits *a* and *b* with spin quantum number *JM* and isospin quantum number TT_z . Occasionally $\sum_{MT_z} A^{\dagger}_{JMTT_z}(ab) A_{JMTT_z}(cd)$ is called the scalar two-body density operator [7].

Shell-model configuration mixing results from diagonalizing a Hamiltonian which is a set of single-particle energies (SPEs) [6] or the single-particle matrix elements and two-body interaction matrix elements (TBME) for a number of particles in a given model space

[12] . This Hamiltonian represents the basic requirements for the shell model calculation and these sets have recently been referred to as the effective interaction or model space Hamiltonian [7]. The same set of SPEs and TBME are conventionally used in the entire mass region in the shell-model configuration mixing calculations. This entire mass region is covered by the model space.

There are two general methods to determine the Hamiltonians. The first method is the "realistic" method which is constructed for a given shell – model space from known data on the free nucleon-nucleon force. The second is an "empirical" method which is based on the parameters whose values are determined by agreement between shell-model eigenvalues and measured level energies [13].

One of the most important examples of a realistic Hamiltonian is the renormalized G-matrix. It is the starting point for shell-model Hamiltonians according to the nucleon-nucleon interactions [17]. The set of TBME for the model space is found by using the Brueckner G-matrix theory for an assumed closed core. The interaction behavior of the short-range repulsive core has been taken into account via the ladder diagrams and the G-matrix renormalized to contain the mixing configurations effects outside the model space plus the core-polarization correction [10]. The TBME resulting from this method incorporating the experimental SPE has shown a remarkable achievement for nuclei with a few valence particles or holes around the closed shell. When the number of the valence particles increases, the comparison with experiment shows clear differences [17]. There are several reasons for the inaccuracy of the TBME resulting from the renormalized G-matrix, the most important are:

1- The non-convergence in the perturbation expansion [18].

2- The approximation used in the oscillator basis which is employed for the matrix elements and energy denominators [7].

3- The requirement of real three-body forces as observed in light nuclei [19].

The empirical Hamiltonians have shown to be successful over a wide mass number region. In this approach the G-matrix is empirically renormalized to reduce the divergence encountered with the G-matrix. This renormalization is used to calculate the wave function and energies for all energy levels under consideration. An expansion of the theoretical energy was provided from these wave functions in terms of a linear combination of SPE and TBME which can be fitted with experiment to make a least-square matrix. The general steps for the fitting method are [16]:

1- Starting with a reasonable Hamiltonian, calculate the matrix elements and the eigenfunctions.

2- Calculate the n_a one-body transition density and scalar two-body density operator in Equation (2.12).

3- By making linear least-squares fitting to the experimental binding energy, we can find new values of SPE and TBME.

4- From the new SPE and TBME values, recalculate the new matrix elements and the eigenfunctions.

The details of the fitting method are presented in Appendix A.

Many Hamiltonians have been created during previous decades as a result of the evolution of computers and the abundance of experimental data. These Hamiltonians were classified according to the model space and the modification used in their calculations. For *p*-shell model space, the TBME was obtained empirically such as P(10-16)T interaction

which is the result of the 15 TBME + 2 SPE fit to the *A*=10-16 *p*-shell data [20]. In the *psd*-shell model space several Hamiltonians have been introduced in the shell model calculations, such as SFO [21],WPB [20] and recently obtained monopole-based universal interaction V_{MU} [22]. For the *sd*- shell model space (*0d5/2, 0d3/2, 1s1/2*), USD Hamiltonian [6, 23] is used to provide the wave functions which are used in the calculations of the structure models, nuclear astrophysics, and nuclear spectroscopy for over two decades. It also represents a main part of the Hamiltonian used for the *psd* model space [20] and *sd-pf* model spaces [24-26]. The USD Hamiltonian is defined by 63 *sd*-shell (TBME) and three single-particle energies (SPE). The direct predecessors to USD were the Chung-Wildenthal particle (CWP) and hole (CWH) Hamiltonians [27], which were obtained from fits to data in the lower and upper parts of the *sd*-shell, respectively. The Wildenthal interaction or USD ("universal" *sd* Hamiltonian) is set-up by fitting 380 energies data with experimental error of 0.2 MeV or less from 66 nuclei. The data was fitted using the lower and upper parts of the *sd*-shell by supposing that the simple mass dependence for the matrix elements within [28]:

$$TBME\ (A) = TBME\ (A = 18)\ \cdot \left(\frac{18}{A}\right)^{0.3} \tag{2.13}$$

where *A* is the mass number. The new USD interaction call USDA and USDB which represent refined derivation of the USD Hamiltonian by updating and using a complete set of energy data [7] and details on these Hamiltonians will be discussed later. The large scale *sdpf* model space has great significance in the shell model calculation according to the wide range of nuclei in this region. There are many Hamiltonians used in this region such as *sd-pf* residual interaction, known as (SDPF-U) [29] and *sd-pf* cross-shell Hamiltonian, SDPF-

MU [30]. In the *fp*- model space we have GXPF1J [31, 32] and KB3G [33] effective interactions which are currently used in the *fp*-shell calculations [34].

2.4 USDA Hamiltonian

Brown and Richter updated the USD Hamiltonian when new experimental data became available. Two modified Hamiltonians were introduced , called USDA and USDB [7]. These Hamiltonians are derived with the fitting procedure described in Appendix A by considering 608 states in 77 nuclei. The starting Hamiltonian is taken from the renormalized *G* matrix in the Bonn-A *NN* interaction with TBME presented in Table 20 of reference [17]. The OXBASH program [35] employed to calculate the wave functions, energies, occupation numbers, and scalar two-body transition densities are then used in the fitting process.

The USDA resulted through the iteration of the USD Hamiltonian with 30 well determined linear combinations and the remaining 36 poorly determined linear combinations are set to the renormalized G matrix values. The iterative process continued until the linear combinations values and the energies converged to the level of about 10 keV. In the same approach USDB was calculated with significant difference in the number of well determined linear combinations where 56 linear combinations of parameters used in three iterations were required for convergence. The two Hamiltonians possess the following attributes: the conservative USDA Hamiltonian where its features are closed to the renormalized G matrix values and gives a good but not the best fit to the data and the USDB that differs more from the renormalized G matrix values but gives a best fit to the

data [7]. The single particle energies for the *sd* model space identified from the USDA Hamiltonian are -3.9436,-3.0612 and 1.9798 MeV for shells *d5/2, s1/2* and *d3/2* respectively and the TBME values are shown in Table 2.1.

2.5 OXBASH Program

In this work the calculations are performed using the code OXBASH for Windows [35]. The OXBASH is a set of codes for carrying out shell-model calculations by using an *M*-scheme Slater determinant basis with dimensions up to about 2,000,000, wave functions with good angular momentum *J*, isospin *T* in dimensions up to about 50,000 in the *J-T* scheme, and a projection technique. This code can be used in any Windows PC without the need to use any other software with acceptable speed and accurate results. OXBASH is the only version that uses the projection technique which is make it convenient for a variety of truncations [12]. More details of these methods can found in Chapter Three.

OXBASH comes with a library of model spaces and interactions. The starting point in the use of OXBASH is the selection of an appropriate model space and interaction for that model space. For *sd*-shell there are two model space types; the first is SD which depends on the number of valence particles outside the core O^{16} and the range of *J* and *T* values. The second model space is SDPN which means that the calculation is done in the proton-neutron formalism. This means the need for determining the number of protons and neutrons out of the core O^{16} and the range of *J* values.

Table 2.1: The two body matrix elements values V ($j_1, j_2, j_3, j_4; JT$) of USDA Hamiltonian for T (isospin) = 0 and 1. The orbital labeled by *5 = d5/2, 3 = d3/2, 1 = s1/2* [7] .

T=0						*T=1*					
j_1	j_2	j_3	j_4	*J*	*USDA*	j_1	j_2	j_3	j_4	*J*	*USDA*
5	5	5	5	1	-1.4277	5	5	5	5	0	-2.4796
5	5	5	1	1	3.052	5	5	3	3	0	-3.5693
5	5	1	1	1	1.9658	5	5	1	1	0	-1.1572
5	5	1	1	1	0.3967	3	3	3	3	0	-1.505
5	5	1	1	1	-0.89	3	3	1	1	0	-0.9834
5	1	5	1	1	-6.5106	1	1	1	1	0	-1.8461
5	1	1	1	1	0.0136	5	3	5	3	1	0.251
5	1	1	1	1	1.5511	5	3	3	1	1	0.0736
5	1	1	1	1	1.9021	3	1	3	1	1	0.3105
1	1	1	1	1	-1.4927	5	5	5	5	2	-0.9899
1	1	1	1	1	-1.0014	5	5	5	3	2	-0.3092
1	1	1	1	1	0.0949	5	5	5	1	2	-0.7746
1	1	1	1	1	-3.8051	5	5	3	3	2	-1.1335
1	1	1	1	1	-0.6655	5	5	3	1	2	0.8901
1	1	1	1	1	-3.8693	5	3	5	3	2	0.2248
5	1	5	1	2	-4.5452	5	3	5	1	2	0.1022
5	1	5	1	2	-1.0254	5	3	3	3	2	-0.5208
5	1	1	1	2	-1.2803	5	3	3	1	2	0.2811
5	1	5	1	2	-0.4874	5	1	5	1	2	-0.9039
5	1	1	1	2	-2.5947	5	1	3	3	2	-0.5542
1	1	1	1	2	-1.753	5	1	3	1	2	1.7072
5	5	5	5	3	-1.4018	3	3	3	3	2	-0.157
5	5	5	1	3	2.2427	3	3	3	1	2	0.1368
5	5	5	1	3	-1.7954	3	1	3	1	2	-0.2533
5	5	1	1	3	0.9812	5	3	5	3	3	0.4777
5	1	5	1	3	-1.2963	5	3	5	1	3	-0.4507
5	1	5	1	3	0.8962	5	1	5	1	3	0.647
5	1	1	1	3	1.8985	5	5	5	5	4	-0.2136
5	1	5	1	3	-3.9337	5	5	5	3	4	-1.3155
5	1	1	1	3	0.4599	5	3	5	3	4	-1.2509
1	1	1	1	3	-2.98						
5	1	5	1	4	-4.4652						
5	5	5	5	5	-4.3811						

2.6 Magnesium Isotopes

There are 22 known isotopes of magnesium. The atomic number for these isotopes is 12 and the neutron number ranges from 7 to 28. There are three stable isotopes ^{24}Mg, ^{25}Mg, ^{26}Mg and 19 other radioisotopes have been discovered. ^{28}Mg is the longest-lived radioisotope with a half-life of 20.915 hours. The shortest-lived is the rare radioisotope ^{40}Mg with a half-life > 170 ns [6]. The lighter isotopes mostly decay to isotopes of sodium while the heavier isotopes decay to isotopes of aluminum. Magnesium isotopic chain is of particular interest because the special nuclear structure of these isotopes. This interest comes from the importance of nuclei that lie far away from β-stability where they had been proved to be well adapted for the description of nuclear systems near the valley of stability. This feature has made them good test candidates for the nuclear shell model [36]. In this work, the odd-magnesium isotopes, with 4 protons in the sd-shell, and neutrons gradually filling the sd-shell between N=9 and N=17 are excellent isotopes to study the effect of changes in the proton-neutron interaction due to the filling of the neutrons in sd-shell. These isotopes represent the extended chain on the two sides of the valley of stability, beyond the N =9 shell which represents the neutron deficient side until the N =17 shell at the neutron rich side which represents the boundaries of what is known as "islands of inversion" [37]. Island of inversion is a region where the usual shell model hypothesis filling of the single-particle levels changes as a result of models space overlap. The nuclear shell model accurately predicts phenomena occurring in nuclear systems near the valley of

stability. The validity of this model has been verified by the nuclei far away from β-stability [36].

Another reason for the surge in recent interest is the importance of odd-magnesium isotopes in astrophysics. It has become scientifically recognized that the odd-magnesium isotopes represent an important link in nuclear reactions in stars [38] . The identification of these isotopes structural properties is crucial for the description and to comprehend many of these reactions. Table 2.2 lists these isotopes and the reactions with recent research that deal with it. In the next sections we will mention the important research conducted to measure and calculate the magnesium isotopes excited states, transition probabilities, and electron scattering form factors.

2.7 Excited States and Transitions Probability

The ground state's angular momentum for the odd nuclei is determined from the shell of the last neutron according to the distribution in the model space. In this case the ground state's angular momentum, excited states angular momentum, and isospin are half integer. The experimental data of the excited states and transition probabilities are usually based on two certified references. The first reference is the Nuclear Data Sheets journal and the second is the National Nuclear Data Center database [6].

In addition to the experimental values in the previous references, we also adopted some new data for some isotopes as follows. The starting point will be with ^{21}Mg which has special significance due to the scarce knowledge of any $T_z = -3/2$ *sd*-shell nuclei [48].

The first determination of ^{21}Mg excited states had been done by using ^{24}Mg(^{3}He,^{6}He)^{21}Mg reaction [49]. Ground state and the first four excited states have been identified.

Table 2.2: Magnesium isotopes nuclear reactions in the astrophysics field.

Isotopes	Reactions	Utility	Reference
21	^{20}Na(p, γ)^{21}Mg	Important for hydrogen burning in explosive scenarios.	[38]
23	^{23}Mg(p, γ)^{24}Al	Important link between the Ne-Na and Mg-Al cycles in O-Ne classical novae.	[39, 40]
	^{22}Na(p, γ)^{23}Mg	^{22}Na consumes by hydrogen burning.	[41-43]
25	^{25}Mg(p, γ)^{26}Al	^{26}Al produce in stellar H-shell burning by proton capture process.	[44]
	^{22}Ne(α,n)^{25}Mg	Provide neutrons for the slow neutron-capture process (s process) in stars which responsible for the origin of about one half of the elemental abundances beyond iron that we observe today.	[45-47]

Later, more than 20 states have been identified with excitation energy less than 6.025 MeV and spin-parity determinations within the same reaction with different energy

for the projectile particles [50-52]. The ^{21}Mg level structure has been probed by using a resonant elastic scattering of a radioactive ^{20}Na beam incident on protons in a polyethylene target [48]. An additional three levels have been observed with energy 4.005, 4.22, and 4.538 MeV for J=3/2$^+$, 5/2$^+$, and 3/2$^+$, respectively. The shell model with USD Hamiltonian was used in the comparison and predicts corresponding states with a disparity of a few keV. Recently, the excited states in ^{21}Mg were probed in the one-neutron knockout reaction ^{9}Be(^{22}Mg, ^{21}Mg+γ)X at 74 MeV/nucleon projectile energy [38]. A new negative parity state has been found with J =1/2$^-$ at energy 1.084 MeV and determine the J value of the other two levels. The WBP shell model effective interaction [20] was used to compare with the experimental results. WBP predictions showed a clear difference with the experimental levels with only one agreement for the J = 1/2$^-$ state. Also, this study led to the first identification of the state J= 3/2$^+$ at energy 1.651 MeV.

The excited states of ^{23}Mg isotope had a great interest in previous decades. More than nine types of reactions have been used to identify these states with energy ≤ 14.56 MeV for 1/2 ≤ J ≤ 21/2 and 1/2 ≤ J ≤ 5/2 in positive and negative parities respectively [53]. As well there are two types of lower transitions probability that have been specified for many states which are the electric quadrupole transition and magnetic dipole transitions. The ^{22}Na(p,γ)^{23}Mg reaction has been used to study the ^{23}Mg excited states [42, 43]. The β-delayed proton spectrum of ^{23}Al with statistical analysis of the observed β strength has shown new energy levels in the ^{23}Mg spectrum without specifying the J values for these levels. Three levels at energy 8.579, 8.84, and 9.604 MeV have been found and revised some others [54]. Another revision was made by A. Saastamoinen *et al.* [55] with determined a new energy level at 7.917 MeV. The first five excited states were discussed in detail in A. Gade *et al*. [56] by using ^{12}C(^{22}Mg, ^{23}Mg + γ)X reaction and USDB

Hamiltonian . Research has shown that the energy level 2.714 MeV is assumed to be a $9/2^+$ state where the previous literature showed it as a cluster of two states [53]. The experimental results have been used in a theoretical calculation to substantiate that the uncertain state at 2.908 MeV is actually corresponds to $J = 3/2^+$. Recently, excited states in ^{23}Mg were populated using the ^{12}C(^{12}C,n) reaction at beam energy of 22 MeV [57]. The highly excited structures have been found and intensive investigation made up to an excitation energy of 8 MeV and spin-parity of $13/2^+$. The shell model Hamiltonian USDB used to describe positive-parity states while the PSDPF interaction [58] was used to describe negative-parity states.

In 1962, a magnetic spectrograph was used in the ^{27}Al (d, α)^{25}Mg reaction to determine 66 levels in ^{25}Mg below 8.7 MeV excitation energy [59]. Since that time to 2009, many researches had been conducted to study the structure of this nucleus. At least 75 positive parity states , and 23 negative parity states with $J \leq 15/2$ have been identified.A further 15 states with unknown parity and 28 levels with unknown J have been found below 13.33 MeV excitation energy [60]. The reduced electric quadrupole transition probability and reduced magnetic dipole transition probability have been measured for several states. Important assignments have been made using a model conducted by Longland *et al.* [47] in the J values for many energy levels in ^{25,26}Mg. The energy involved in this study was $10.693 \leq E \leq 12.343$ MeV for ^{26}Mg and $11.318 \leq E \leq 12.551$ MeV for ^{25}Mg.

The last Nuclear Data Sheets for $A = 27$ identified 54 excited states in the ^{27}Mg nucleus [61]. These states are in the energy range ≤ 7.976 MeV and $J \leq 9/2$. The positive parities are 26 and the negative parities are 9 while there are 3 states with unknown parity and 28 states with unknown J. There is one value for the reduced electric quadrupole and

dipole transition probabilities and three values for the reduced magnetic dipole transitions probability. In addition to the above values, there are other levels published previously such as 6.51 MeV at $J^{\pi}=1^{-}, 3^{-}$ with 6.876 ,7.227 and 7.309 MeV unknown J levels [62] and the state 6.443 MeV at $J^{\pi}=1^{+}$ [63].

The ^{29}Mg isotope which is considered as neutron-rich Mg isotope lies at the border of the island of inversion region. This led to the significant interest in the island of inversion recently. More information about this region will be presented in Chapter Four. As a result of the short half-life for ^{29}Mg nucleus (1.3 seconds), a few energy levels have been identified. The latest results have found five positive and four negative parity states with four unknown parity states and five unknown J within the energy range $\leq$ 4.28 MeV and $J \leq 7/2$ [64]. The J value for energy level 0.054 MeV was not identified in reference [64]. But Kowalska *et al*. [65] showed that this level should be assigned as $J^{\pi}=1/2^{+}$ inaccordance with the results of reference [66]. Kowalska *et al*. [65] measured the ground-state spins and magnetic moments of neutron-rich ^{27}Mg, ^{29}Mg, and ^{31}Mg with laser and β-NMR spectroscopy. The results for ^{29}Mg compared with the USD and USDB shell model interactions which are tailored to the *sd*-shell nuclei and restrict the valence neutrons and protons to this major shell show good agreement for the first two positive states using USDB while the USD indecated a clear difference in the ground state and the first excited state.

2.8 Inelastic Electron Scattering Form Factors

Electron high energy scattering from nuclei represents a powerful tool for studying nuclear structure using the information provided by the spectroscopy of the target nucleus. It is possible to identify the spins and parities of excited states and measures the reduced

matrix elements for nuclear transitions [67]. There are many reasons for considering electron scattering as a powerful tool for studying nuclear structure. First, the basic interaction between the electron and the target nucleus is known in which the electron interacts with the electromagnetic charge and current density of the nucleus. Since the interaction is relatively weak, one can make measurements on the target nucleus without greatly disturbing its structure [68]. The second advantage is that for a fixed energy loss to the target, one can vary the three-momentum transfer q and map out the Fourier transforms of the static and transition densities [69]. With electron scattering, one can immediately relate the cross section to the transition matrix elements of the local charge and current density operators and thus directly to the structure of the target nucleus itself [70].

Electron scattering is of two kinds: the first one is elastic scattering of electrons which can be used to study the ground-state properties such as the static distributions of charge and magnetization. The second kind is inelastic electron scattering, which determines transition densities corresponding to the initial and final nuclear states in question, for the three quantities in the nucleus that interact with the passing electron, namely, the distribution of charge, current and magnetization [68].

The scattering cross-section for relativistic electrons from spinless nuclei of charge Ze was first derived by Mott in 1929 [71]. The nuclear size can be taken into account by multiplying the Mott's cross-section by a factor which depends on the charge, current and magnetization distributions in the target nucleus. This factor is called the nuclear form factor.

The Born approximation was used to describe the electrons interaction with a nucleus as an exchange of a virtual photon carrying a momentum. In the Born approximation, the form factor depends only on energy and scattering angle (θ) through the

momentum transfer q, where the incident and scattered particles are considered as free, i.e., represented by plane waves [72, 73]. The electron scattering form factor is divided into two types;

1- Longitudinal form factor, in which the virtual photon carries angular momentum 0 along $\vec{q}$.

2- Transverse form factor, in which the virtual photon carries angular momentum ±1 along $\vec{q}$. Transverse form factor is divided into two parts, electric (E) and magnetic (M) form factor [74].

Many attempts have been made to explain the electron scattering and to understand the nature of nuclear forces and the structure of the nuclei. The ^{25}Mg isotope is of special interest in these experiments and theoretical studies because it is a stable isotope. This is the only odd-mass magnesium isotope where there is experimental data and, therefore in this study we will deal with it in the form factor calculation. Some of the previous work which deal with the ^{25}Mg isotopes could be listed as follows:

For the elastic electron scattering in ^{25}Mg , there are many experimental [75-77] and theoretical [73, 78, 79] works that have been done. The inelastic scattering was used to study the excited states in ^{25}Mg by Fagg *et al*. [80]. Longitudinal form factors (C2 and C4) were measured by Okazaki *et al*. [81] for ^{25}Mg states $J^{\pi}=1/2^{+}$, $3/2^{+}$, $5/2^{+}$, $9/2^{+}$, and $11/2^{+}$ at energies 2.56, 2.801, 3.909, 4.059 and 5.251 MeV respectively. The experimental data were compared with the values calculated in the strong-coupling model [82]. Less *et al.* [83] made many longitudinal form factor measurements in the ^{25}Mg nucleus. The longitudinal form factors for the states $J^{\pi}=7/2^{+}$ and $9/2^{+}$ at energies 1.611 and 3.405 MeV respectively [83] and $J^{\pi}=3/2^{+}$, $5/2^{+}$, $1/2^{+}$, $3/2^{+}$, $9/2^{+}$ and $11/2^{+}$ at energy 0.974,1.964, 2.563, 2.801, 4.059

and 5.251 MeV respectively [84]. Marinelli and Moreira [85] used inelastic electron scattering to measure the transverse form factor for the transitions $5/2^+ \rightarrow 7/2^+$ (1.611 MeV) , $5/2^+ \rightarrow 3/2^-$ (3.413 MeV) and $5/2^+ \rightarrow 9/2^+$ (3.405 MeV) using electron beam with energy 120 to 260 MeV. Projection and cranking models were used for the theoretical calculations to compare with the experimental data.

CHAPTER 3

METHODS OF CALCULATIONS

3.1 Introduction

In order to calculate the properties of nuclear ground state and excited states one must have obtained the wave functions of these states. The wave functions can be obtained by solving the many-body Schrödinger equation for a nucleus of A nucleons represented by space vectors *r(1),r(2)….,r(A)* [86]:

$$H\Psi\big(r(1), r(2), \dots\dots, r(A)\big) = E\Psi\big(r(1), r(2), \dots\dots, r(A)\big) \qquad (3.1)$$

Because of the complexity of the nuclear many-body problem, the time-independent Schrödinger equation cannot be solved exactly for more than a few particles. Various methods have been developed to approximate this equation and to provide theoretical estimation of nuclear properties. Configuration Interaction (CI) method and Energy Density Functional (EDF) methods are two commonly used sets of nuclear structure techniques that expand the range of theoretical calculations beyond the lightest-mass region of the nuclear chart.

The most part of the study on nuclear structure problems may be classified as a study on bound states depending on the perspective of quantum mechanics. The energy level values and wave functions can be obtained from solving the eigenvalue problem for

the proposed interaction. We can use the eigenfunctions to calculate the matrix elements of the operators corresponding to the observables. The strong force between nucleons is regarded as the primary interaction while the effects of the Coulomb force often, can be treated as perturbation to the dominant nuclear interaction [3]. In this chapter we will present the mathematical formulas and concepts that are used in our calculations.

3.2 Nuclear Excited States

The nuclear excited states are unstable. Like atomic excited states, they usually decay rapidly by emission of electromagnetic radiation to the ground state. According to the excitation mechanism, the excited states can give valuable information about the orbits of the individual nucleons [9]. On the other hand, these states represent an ideal laboratory for studying the quantum many-body effects. They also provide important information on the essential nature of the weak and strong interactions, provided that the many body aspects are sufficiently well understood. The nuclear shell model is the one of the principal approaches for such understanding [6].

The original nuclear shell model [1] assumed a single configuration for each nuclear level which means corresponding to a single nucleon in one single-particle orbit. A significant improvement in the modern nuclear shell model calculation has been found when the assumption of configuration interaction (CI) method was used [87, 88]. Configuration interaction means a large number of configurations mixed by the residual interaction. In this configuration the valence protons and neutrons of the nucleus simultaneously occupy several different, partially filled, single –particle quantum states in the intended model space. Adoption of the configuration mixing method resulted in the increase of the accuracy of calculations and comprehensiveness of the theoretical understanding of nuclear states [6].

3.3 M-scheme Approach And Projection Technique

As mentioned in section 2.5, the OXBASH code uses the *M*- scheme with projection technique in shell model calculation. Therefore, we will present the M- scheme and projection technique in this section. The first task in understanding the method of calculating excited states is to know which values of the total angular momenta *J* that are permissible for *n* particles configuration under the restrictions imposed by the Pauli principle. There are several ways of approaching this issue [4]. In our calculation we used the M-scheme computational approach. In this approach, we can construct the many-body wave functions with the maximum angular momentum and isospin projection (M_J, T_z) [89]. The M-scheme set of states is convenient since M_J is an additive quantum number and one need only to consider the subset of basis states Φ with a single value of M in the construction of the many-particle wave functions Ψ. In order to provide for good total angular momentum (J), one has to include all states of fixed M_J within a given configuration. To illustrate this approach we will give an example of two-nucleon configuration in the first shell of the sd-space, $(5/2)^2$ in identical configuration (p-p or n-n coupling) and unidentical configuration (p-n or n-p coupling) in Table 3.1. In this simple example, the two-particle wave function consists of the subset of basis states with a single value of m, t_z for the two particles under the restrictions of the Pauli principle which is intended to not allowing for any two nucleons to have same wave function in the M_J, T_z scheme. The basis state for every nucleon has $(2j+1)$ m-states and the value of $m = j, j-1, \ldots, -j$. In Table 3.1(a) we have two identical particles (T = 1). Therefore, Φ_1 and Φ_2 have the

same t_z and the difference will be in the m-values. In Table 3.1(b), Φ_1 and Φ_2 have different t_z values therefore we can take all possible m-values.

Table 3.1: J and T values for two-particle wave function for $(5/2)^2$ configuration. Only the positive m_1- values are listed; the table is symmetric for $m_1<0$ and will shows the negative projections for M.

(a) For identical coupling

$\Phi_1(m_1, t_{z1})$	$\Phi_2(m_2, t_{z2})$	M	Ψ (J,T=1)
$\frac{5}{2},\frac{1}{2}$	$\frac{5}{2},\frac{1}{2}$	Not Allowed	
$\frac{5}{2},\frac{1}{2}$	$\frac{3}{2},\frac{1}{2}$	4	J=4
$\frac{5}{2},\frac{1}{2}$	$\frac{1}{2},\frac{1}{2}$	3	
$\frac{5}{2},\frac{1}{2}$	$\frac{-1}{2},\frac{1}{2}$	2	
$\frac{5}{2},\frac{1}{2}$	$\frac{-3}{2},\frac{1}{2}$	1	
$\frac{5}{2},\frac{1}{2}$	$\frac{-5}{2},\frac{1}{2}$	0	
$\frac{3}{2},\frac{1}{2}$	$\frac{3}{2},\frac{1}{2}$	Not Allowed	
$\frac{3}{2},\frac{1}{2}$	$\frac{1}{2},\frac{1}{2}$	2	J=2
$\frac{3}{2},\frac{1}{2}$	$\frac{-1}{2},\frac{1}{2}$	1	
$\frac{3}{2},\frac{1}{2}$	$\frac{-3}{2},\frac{1}{2}$	0	
$\frac{1}{2},\frac{1}{2}$	$\frac{1}{2},\frac{1}{2}$	Not Allowed	
$\frac{1}{2},\frac{1}{2}$	$\frac{-1}{2},\frac{1}{2}$	0	J=0

(b) For unidentical coupling

$\Phi_1(m_1, t_{z1})$	$\Phi_2(m_2, t_{z2})$	M	Ψ (J,T=0)
$\frac{5}{2},\frac{1}{2}$	$\frac{5}{2},\frac{-1}{2}$	5	J=5
$\frac{5}{2},\frac{1}{2}$	$\frac{3}{2},\frac{-1}{2}$	4	
$\frac{5}{2},\frac{1}{2}$	$\frac{1}{2},\frac{-1}{2}$	3	
$\frac{5}{2},\frac{1}{2}$	$\frac{-1}{2},\frac{-1}{2}$	2	
$\frac{5}{2},\frac{1}{2}$	$\frac{-3}{2},\frac{-1}{2}$	1	
$\frac{5}{2},\frac{1}{2}$	$\frac{-5}{2},\frac{-1}{2}$	0	
$\frac{3}{2},\frac{1}{2}$	$\frac{3}{2},\frac{-1}{2}$	3	J=3
$\frac{3}{2},\frac{1}{2}$	$\frac{1}{2},\frac{-1}{2}$	2	
$\frac{3}{2},\frac{1}{2}$	$\frac{-1}{2},\frac{-1}{2}$	1	
$\frac{3}{2},\frac{1}{2}$	$\frac{-3}{2},\frac{-1}{2}$	0	
$\frac{1}{2},\frac{1}{2}$	$\frac{1}{2},\frac{-1}{2}$	1	J=1
$\frac{1}{2},\frac{1}{2}$	$\frac{-1}{2},\frac{1}{2}$	0	

In order to adopt J value, we should have the M-scheme extension for all *J* values (i.e. for *J = 4* we must have *M=4,3,2,1,0,-1,-2,-3,-4*). The resulting J and T values for the two cases achieve antisymmetric condition which requires in this case *J+T=odd* [86]. We can find the J-dimension *D(J)*, which is the total number of states for a given *J*, from the M-scheme dimensions *d(M)* as follows [10]:

$$D(J) = d(M = J) - d(M = J + 1) \tag{3.2}$$

In Table 3.1(a), we have two configurations with M = 2, Φ_1 (5/2, 1/2) with Φ_2 (-1/2, 1/2) and Φ_1 (3/2, 1/2) with Φ_2 (1/2, 1/2). The first configuration is associated with the J-states that has *J*=4 and the second with *J*=2. The linear combination for any desired *J*- value can be obtained by applying the angular-momentum projection operator [90] which constructs explicit linear combinations of the M-scheme Slater determinants have good total angular momentum. This operator given by [10]:

$$\bar{P}_{J_i,J_0} \equiv \frac{\hat{J}^2 - J_0(J_0+1)}{J_i(J_i+1) - J_0(J_0+1)} \tag{3.3}$$

where J_0 is the unwanted components and J_i is the unchanged components. So we can use the J_0 to projects out many unwanted components with $J=J_0$ and leaving only one component with $J=J_i$. Then we can use:

$$\hat{P}_{J_i} \equiv \prod_{J_0=M, J_0 \neq J_i}^{J_{max}} \bar{P}_{J_i,J_0} \quad . \tag{3.4}$$

The unwanted components from the isospin can also be projected out by changing the operator formula as follows [89]:

$$\bar{P}_{T_i,T_0} \equiv \frac{\hat{T}^2 - T_0(T_0+1)}{T_i(T_i+1) - T_0(T_0+1)} \quad . \tag{3.5}$$

Hence, if we have the linear combination of M-states wave function $|\Phi_a(M)>$, we can choose the component of J (or J and T) by operating with $\hat{P}_{J_i}$(or $\hat{P}_{J_i}\hat{T}_{T_i}$) on this wave function [10]:

$$\hat{P}_{J_i}|\Phi_a(M)>=\sum_{w=1}^{D(J)} d_{wj_i}\,|\Psi(\mathrm{w}J_iM)> \tag{3.6}$$

where $\Psi(\mathrm{w}J_iM)$ is the wave function in the J-scheme, D*(J)* is J-dimension found from Equation (3.2). Here, w is an additional quantum number which must be introduced when there is more than one state for a given value of *J* and d_{wj_i} is the probability of finding the component *J* in the partition w. Partition is defined as a specific distribution of the particles into the allowed (active) set of *k* states. The summation in the above equation is also being a linear combination of M-states:

$$\sum_{w=1}^{D(J)} d_{wj_i}\,|\Psi(\mathrm{w}J_iM)>=\sum_{b=1}^{d(M)} a_b|\Phi_b(M)> \tag{3.7}$$

The square of a_b represents the probability of finding the component J_i in the state $|\Phi_b(M)>$ [10].

3.4 Hamiltonians Eigenvalues And Eigenvectors

We can rewrite the Hamiltonian Equation (2.12) as follows:

$$H = H^0 + H^1 \tag{3.8}$$

where H^0 represents the unperturbed part and H^1 is the perturbed component or the residual interaction. If we have linear combinations for r states as [86]:

$$\Psi_p = \sum_{k=1}^{r} a_{kp}\Phi_k^0 \quad (p = 1, \ldots . r) \tag{3.9}$$

and when applying the Hamiltonian operator on this function and multiply the left-hand side with $\langle \Phi_l^0 |$ we get:

$$\sum_{k,l=1}^{r} \langle \Phi_l^0 \big| H^0 + H^1 \big| \Phi_k^0 \rangle \, a_{kp} = E_p a_{lp} \tag{3.10}$$

or

$$\sum_{k,l=1}^{r} H_{lk} a_{kp} = E_p a_{lp} \tag{3.11}$$

The last equation possesses the solution under the condition of vanishing determinant:

$$\begin{vmatrix} H_{11} - E_p & H_{12} & \ldots\ldots & H_{1r} \\ H_{21} & H_{22} - E_p & \ldots\ldots & H_{2r} \\ \vdots & \ldots\ldots\ldots & & \vdots \\ H_{r1} & \ldots\ldots\ldots & & H_{rr} - E_p \end{vmatrix} = 0 \tag{3.12}$$

If we multiply Equation (3.11) with $a_{lp'}$, we will obtain:

$$\sum_{k,l=1}^{r} a_{lp'} H_{lk} a_{kp} = E_p \delta_{pp'} \tag{3.13}$$

$$\sum_{k=1}^{r} a_{kp} a_{kp'} = \delta_{pp'} \text{ for } E_p \neq E_{p'} \tag{3.14}$$

Equation (3.12) gives the eigenvalue E_p (state energy) with r roots (p=1,…,r) and containing two parts, first is the diagonal part when ($l = k$) which can be expressed as follows:

$$H_{kk} = e_k^0 + H_{kk}^1 \tag{3.15}$$

where e_k^0 is the single-particle energy and H_{kk}^1 is the residual interaction. The second is the off- diagonal part when ($l \neq k$) which contain only the residual interaction with symmetric property:

$$H_{kl}^1 = H_{lk}^1 \, . \tag{3.16}$$

In Equation (3.13), a_{kp} matrices diagonalize the matrix H_{lk} according to the normalized and orthogonal relation (3.14). After we identify the eigenvalue E_p one can find the eigenvector (mixed-configuration wave functions) from equation (3.13).

A convenient way to express the many-body wave functions by using the second-quantized form in terms of creation and destruction operators. In addition to taking into account the wave functions antisymmetry we can represent the basis states Φ by binary bit patterns with (1) denoting an occupied state and (0) an unoccupied state. In this method the computations are based on some finite set of single-particle quantum numbers ($\alpha_1, \ldots, \alpha_n$), where $\alpha=(n, \ell, j, m)$ [10]. By using creation and destruction operators we can rewrite the Hamiltonian in Equation (3.8) as follows [35]:

$$H = \sum_k e_k a_k^+ a_k + \sum_{k>k'=1, l>l'=1} V_{k\,k'll'}\, a_k^+ a_{k'}^+ a_{l'} a_l \tag{3.17}$$

where a_k^+ creates one-particle in the *k* (*k* =(*n*, ℓ, *j*,)) state and a_l eliminates the one-particle from the *l* state. In the shell model the perturbed Hamiltonian part can be written as a sum of two-particle interactions:

$$H^1 = \sum_{k>k'=1, l>l'=1} V_{kk'll'}\, a_k^+ a_{k'}^+ a_{l'} a_l \tag{3.18}$$

where $V_{kk'll'}$ is the two-body matrix elements with state *k* for the first particle and k' for the second particle. Equation (3.17) shows the importance of the residual interaction in obtaining the eigenvalue E_p (state energy) and the eigenvector (state wave functions) by providing the two-body matrix elements and the single-particle energy in the model space. It becomes clear that in the sd-shell model space there are 63 independent *(J, T)* formed for two particles through d5/2, s1/2 and d3/2 shells.

For *n* particles distributed over three *k*-states in the sd- model space, there are *w* partitions that give states with J value. The diagonal Hamiltonian matrix elements have the form [10]:

$$\langle nwJ|H|nwJ\rangle = n_1 e_{k_1} + n_2 e_{k_2} + n_3 e_{k_3} + \sum_i D_i(w, w, J)\langle V\rangle_i \tag{3.19}$$

and the off-diagonal matrix elements have the form:

$$\langle nwJ|H|nw'J\rangle = \sum_i D_i(w, w', J)\langle V\rangle_i \tag{3.20}$$

where e_{k_j} is the energy of a single-particle in state k_j and n_j is the number of particles in the state k_j, $n = n_1 + n_2 + n_3$, w is the same as in Equation (3.6), $\langle V\rangle_i$ represents the list of possible two-body matrix elements in the model space and D_i are numerical coefficients

which are called double fractional parentage coefficients. This coefficient is used when the many-body wave function is converted into the two-body wave function.

Nuclear binding energy is defined as the energy required in breaking up a given nucleus into its constituent parts of N neutrons and Z protons [10]. After determining the eigenvalues, the binding energy for the *n* particles in the k_j shell is given by [86]:

$$E_{JT}^{b}\left(core + k_j\right) = E_C + E^b(core) + \sum_{j=1}^{3} n_j e_{k_j} \delta_{ww'} + \sum_i D_i(w, w', J)\langle V\rangle_i \qquad (3.21)$$

where E_C is the Coulomb energy, $E^b(core)$ is the binding energy of the core which is equal to 127.62 MeV [86], and other symbols as in Equations (3.19) and (3.20). For the calculation of the Coulomb energy, E_C, various approximate expressions exist. One of the most important approximations for sd-shell is the approach [86]:

$$E_C(Z') = cZ' + \frac{1}{2}Z'(Z'-1)a + [\frac{1}{2}Z']b \qquad (3.22)$$

where Z' is the number of protons outside the core, the parameters a, b and c depend on the orbital and $[\frac{1}{2}Z']$ stands for the largest integer not exceeding $\frac{1}{2}Z'$. The highest binding energy is identified as the ground state binding energy ($E_B(gr)$) and the excitation energy for state *n* ($E_x(n)$) is the difference between the binding energy in state n, ($E_B(n)$), and the ground state binding energy ($E_B(gr)$) [86]:

$$E_x(n) = E_B(n) - E_B(gr) \qquad (3.23)$$

It is clear from the equation (3.23) that E_C and $E^b(core)$ did not have any effect in the calculations of the excitation energies while they have effect in the calculations of binding energies.

3.5 Reduced Transition Probability

A wide range of knowledge on nuclei is found from the study of electromagnetic transitions. For example, it is the main source of information about the spin assignments of nuclear states. Theoretically, we can calculate the transition rates for the multipole radiations if the nuclear wave functions are known [86]. The interaction of the electromagnetic field with the nucleons can be expressed in terms of a sum of tensor operators of rank λ called electric $O(E\lambda)$ and magnetic $O(M\lambda)$ operators. The decay rate between an initial state $|J_i, M_i\rangle$ and final state $|J_f, M_f\rangle$ is given by [10]:

$$W = \sum_{\mathcal{E},\lambda} \left(\frac{8\pi(\lambda+1)}{\lambda[2\lambda+1)!!]^2}\right)\left(\frac{\kappa^{2\lambda+1}}{\hbar}\right)\frac{\left|\langle J_f||O(\mathcal{E}\lambda)||J_i\rangle\right|^2}{(2J_i+1)} \tag{3.24}$$

where $\mathcal{E} = E$ for electric or $\mathcal{E} = M$ for magnetic and κ is the wave-number for the electromagnetic transition. The last factor in Equation (3.24) is the reduced transition probability, which is defined by the reduced matrix elements of one-body operator as given in the following equation:

$$B(i \to f) = \frac{\left|\langle J_f||O(\mathcal{E}\lambda)||J_i\rangle\right|^2}{(2J_i+1)} \tag{3.25}$$

where $\langle J_f||O(\mathcal{E}\lambda)||J_i\rangle$ is the reduced matrix operator and it has the property $\left|\langle J_f||O(\mathcal{E}\lambda)||J_i\rangle\right|^2 = \left|\langle J_i||O(\mathcal{E}\lambda)||J_f\rangle\right|^2$, λ is the transition multipolarity and $O(\mathcal{E}\lambda)$ is the one body operator. The factor $(2J_i+1)$ determines the direction of the transition. The notation $B(\downarrow)$ symbolizes the electromagnetic transitions in which J_i is the initial state has the higher energy. $B(\uparrow)$ is the Coulomb excitation which is usually the J_i is the ground state.

The electric transitions operator, $O(E\lambda)$, is given by:

$$O(E\lambda) = r^{\lambda} Y_{\mu}^{\lambda}(\hat{r}) e_t e \tag{3.26}$$

where Y_{μ}^{λ} is the spherical harmonic wave function, λ is the rank of the tensor operators $O(E\lambda)$, $\mu = -\lambda, -\lambda+1, .., \lambda$, r is the orbital radius for the nucleon and $e_{\acute{q}}$ is the effective charge with $\acute{q}$ stand for proton ($t = p$) and neutron ($t = n$), for free nucleon $e_p = 1$ and $e_n = 0$.

The magnetic transitions operator, , is given by:

$$O(M\lambda) = \sqrt{\lambda(2\lambda+1)} \left[\left[Y^{\lambda-1}(\hat{r}) \otimes \vec{\ell} \right]_{\mu}^{\lambda} \frac{2g_t^{\ell}}{(\lambda+1)} + \left[Y^{\lambda-1}(\hat{r}) \otimes \vec{s} \right]_{\mu}^{\lambda} g_t^{s} \right] r^{\lambda-1} \mu_N \tag{3.27}$$

where g_t^{ℓ} (g_t^{s}) is the orbital (spin) g-factors for proton and neutron (according to t) respectively which are $g_p^{\ell} = 1$, $g_n^{\ell} = 0$, $g_p^{s} = 5.586$ and $g_n^{s} = -3.826$. Here μ_N is the nuclear magneton and its value is 0.105 *e fm* and the cross symbol $\otimes$ denotes the Clebsch-Gordan product.

The electromagnetic transition between two states should be subject to the selection rules as a result of the conservation laws. These rules express certain symmetry conditions that hold for the system under consideration. Thus, the electromagnetic transitions take place only if the emitted gamma ray carries away an amount of angular momentum λ in order to achieve the formula $J_i = J_f + \lambda$. This means that λ in the electromagnetic transitions has the values [86] :

$$|J_i - J_f| \leq \lambda \leq J_i + J_f \tag{3.28}$$

This selection rule is known as the triangle condition. Another important selection rule results from the conservation of parity. The parity change classifies the elements of the operators $E\lambda$ and $M\lambda$ according to their transformation. The parity selection rule for electromagnetic mulipole transition is given by [10, 86]:

$$\pi_i \pi_f \pi_o = +1 \tag{3.29}$$

where π_i and π_f is the parity for initial and final states, respectively, and π_o is the parity of the operator. For Y^λ operator $\pi_o = (-1)^\lambda$ and $\pi_o = -1$ for $\vec{r}$. Equation (3.29) divides the transitions into classes, ones with unchanged parity $\pi_i \pi_f = +1$, which is done by the operators with $\pi_o = +1$. These operators are for example :

$$\pi_i \pi_f = +1 \text{ for } M1, E2, M3, E4, \ldots \tag{3.30}$$

and others change the parity $\pi_i \pi_f = -1$, which is done by the operators with $\pi_o = -1$. These operators are for example:

$$\pi_i \pi_f = -1 \text{ for } E1, M2, E3, M4, \ldots \tag{3.31}$$

In this work we are dealing with positive parity states, therefore, the operators in Equation (3.30) is the type that will be used in our calculations. The most measurable transitions are the minimum λ values, which are *M1* and *E2* from Equation (3.30). The formula of these operators can be found from Equations (3.26) and (3.27) and given as follows [10]:

$$O(E2) = r^2 Y_\mu^{(2)}(\hat{r}) e_t e \tag{3.32}$$

$$O(M1) = \sqrt{\frac{3}{4\pi}} \left[\vec{\ell} g_t^\ell + \vec{s} g_t^s \right] \mu_N \ . \tag{3.33}$$

The reduced matrix operator in Equation (3.25) can be expressed as a sum over one-body transition densities times the single-particle matrix elements [10]:

$$\langle J_f||O(\lambda)||J_i\rangle = \sum_{k_\alpha k_\beta} OBTD(J_f J_i\, k_\alpha k_\beta \lambda)\langle k_\alpha||O(\lambda)||k_\beta\rangle \tag{3.34}$$

where $\langle k_\alpha||O(\lambda)||k_\beta\rangle$ is the redued single-particle matrix elements and $OBTD(fik_\alpha k_\beta\lambda)$ is the one-body transition densities which are calculated from [10]:

$$OBTD(fik_\alpha k_\beta\lambda) = \frac{\langle nwJ||[a^+_{k_\alpha}\otimes a_{k_\beta}]^\lambda||nw'J'\rangle}{\sqrt{(2\lambda+1)}} \tag{3.35}$$

where n is the number of nucleons, $w'J'$ and wJ are the initial and final state quantum numbers, respectively. Here $a^+_{k_\alpha}, a_{k_\beta}$ are the creation and destruction operators, respectively in which k_α k_β are the quantum numbers $(n_\alpha \ell_\alpha j_\alpha)$ and $(n_\beta \ell_\beta j_\beta)$, respectively.

3.6 Electron Scattering Form Factors

The differential cross section for an electron has initial energy E_i and final energy E_f scattering from nucleus of mass M and charge Z through an angle θ in the one-photon exchange can be given by the following Equation [10]:

$$\frac{d\sigma(\theta,q,f,i)}{d\Omega} = \sigma_{Mott}\eta[\epsilon^2 F_c^2(q,f,i) + f(\theta)F_T^2(q,f,i)] \tag{3.36}$$

where

$$\sigma_{Mott} = \left[\frac{Z\alpha_0\cos(\frac{\theta}{2})}{2E_i sin^2(\frac{\theta}{2})}\right]^2, f(\theta) = \left[\frac{\epsilon}{2} + tan^2(\frac{\theta}{2})\right],\ \eta = \frac{1}{\left[1+\frac{2E_i}{M}sin^2(\frac{\theta}{2})\right]} \text{ and } \epsilon = 1 - \left[\frac{\omega}{(q\hbar c)}\right]^2.$$

F_c and F_T are the Coulomb and transverse form factors, respectively, q three-momentum transfer, $\alpha_0 = \frac{e^2}{\hbar c}$ is the fine structure constant, $\omega = E_i - E_f$ is the energy loss, the indices i and f stand for all quantum numbers that are needed to specify uniquely the initial and final nuclear states, and $(\hbar cq)^2 = 4E_iE_f sin^2\left(\frac{\theta}{2}\right) + \omega^2$.

In Section 2.8, we mentioned the two types of the form factors, the Coulomb or longitudinal electric $F(C\lambda, q, f, i)$, and the transverse with both types magnetic $F(M\lambda, q, f, i)$ and electric $F(E\lambda, q, f, i)$ where λ is the multipolarity. The total form factors are given by [10]:

$$F_c^2(q, f, i) = \sum_{\lambda} F^2(C\lambda, q, f, i) \tag{3.37}$$

$$F_T^2(q, f, i) = \sum_{\lambda} [F^2(M\lambda, q, f, i) + F^2(E\lambda, q, f, i)] \tag{3.38}$$

Every transverse form factors types have two components, λ_c and λ_m , arising from the convection currents (due to the orbital motion of the nucleons) and the magnetization currents (due to the intrinsic magnetic moments of the nucleons), respectively [91]. Therefore, we have:

$$F(E\lambda, q, f, i) = F(E\lambda_c, q, f, i) + F(E\lambda_m, q, f, i), \tag{3.39}$$

$$F(M\lambda, q, f, i) = F(M\lambda_c, q, f, i) + F(M\lambda_m, q, f, i). \tag{3.40}$$

The final form factor expression is given by [10]:

$$F^2(X\lambda, q, f, i) = N_p G_{cm}^2(q)\left[\sum_{t_z,x} W_{fs}(X\lambda x, q, f, i, t_z)\right]^2 \tag{3.41}$$

where:

$$N_p = \left[\frac{4\pi}{Z^2(2J_i+1)}\right] . \quad (3.42)$$

G_{cm} is the center-of-mass correction which is given:

$$G_{cm}(q) = e^{(\frac{b^2q^2}{4A})} \quad (3.43)$$

where *b* is the oscillator length parameter chosen to reproduce the root mean square radius (rms) of the nucleus and *A* is the mass number , its value determined from [10]:

$$b = \sqrt{\frac{41.4\ MeV\ fm^2}{\hbar\omega}} \quad (3.44)$$

and $\hbar\omega$ found from [92]:

$$\hbar\omega = 45A^{-\frac{1}{3}} - 25A^{-\frac{2}{3}} \ . \quad (3.45)$$

The character *x* specifies the convection (c) and magnetic current (m) contributions for the electric (*X* = *E*) and magnetic (*X* = *M*) form factors, and *x* stands for the single term of Equation (3.40), in the case of the Coulomb (*X* = *C*) form factor. $W_{fs}(X\lambda x, q, f, i, t_z)$ are the reduced matrix elements calculated by taking into account the finite-size of the nucleons. Here t_z is the proton ($t_z = \frac{1}{2}$) or neutron ($t_z = -\frac{1}{2}$) isospin. These matrix elements can be found from:

$$W_{fs}(X\lambda x, q, f, i, t_z) = W(X\lambda x, q, f, i, t_z)\frac{g_{fs}(Xx, q, t_z)}{g(Xx, t_z)} \quad (3.46)$$

where $W(X\lambda x, q, f, i, t_z)$ is the point-nucleon reduced matrix elements [10] or multiparticle form factors [91], $g(Xx, t_z)$ is the free-nucleon g factors, where for *Xx*=*Mc*, *Ec*, or *C* $g(Xx, t_z) = g_l(t_z)$ and for *Xx*=*Mm* or *Em*, $g(Xx, t_z) = g_s(t_z)$. $g_{fs}(Xx, q, t_z)$ are the

equivalent q-dependent form factors for free nucleons which are found experimentally in reference [93]. The multiparticle form factors $W(X\lambda x, q, f, i, t_z)$ are given by [10]:

$$W(X\lambda, q, f, i, t_z) = \sum_{k,\acute{k}} OBTD\big(\lambda, k, \acute{k}, f, i, t_z\big) w\big(X\lambda, q, k, \acute{k}, t_z\big) \tag{3.47}$$

where X stands for C, *Mc*, *Mm*, *Ec or Em*. The sum $(k, \acute{k})$ runs over all pairs of single-particle states in the model space. $OBTD\big(\lambda, k, \acute{k}, f, i, t_z\big)$ are the same as in Equation (3.35) but in the isospin formalism which is given by [70] :

$$OBTD(\lambda, k, k', f, i, t_z) = \frac{1}{2}(-1)^{T_f - T_Z}[\sqrt{2}\begin{pmatrix} T_f & 0 & T_i \\ -T_z & 0 & T_z \end{pmatrix} OBTD^{\Delta T=0}(\lambda, k, k', f, i)$$

$$\pm\sqrt{6}\begin{pmatrix} T_f & 1 & T_i \\ -T_z & 0 & T_z \end{pmatrix} OBTD^{\Delta T=1}\big(\lambda, k, \acute{k}, f, i\big)] \tag{3.48}$$

$$OBTD^{\Delta T}(\lambda, k, k', f, i) = \frac{\langle f \| [a_k^+ \otimes a_{k'}]^{(\lambda, \Delta T)} \| i \rangle}{\sqrt{(2\lambda + 1)(2\Delta T + 1)}} \tag{3.49}$$

where T_z is the projection of the total isospin., T_i and T_f are the total nucleus initial and final state isospins, respectively. Here k and $\acute{k}$ are the initial and final state quantum numbers and $w(X\lambda, q, k, k', t_z)$ is the reduced single-particle form factors which are given by the integrals of the appropriate multipole operators over the nucleon coordinates $\vec{r}$:

$$w(C\lambda, q, k, k', t_z) = \int \langle k, t_z \| Y^{(\lambda)}(\hat{r}) j_\lambda(qr) \rho_{t_z}(\vec{r}) \| k', t_z \rangle d^3r \tag{3.50}$$

$$w(M\lambda c, q, k, k', t_z) = \int \langle k, t_z \| \vec{M}(\lambda, \lambda, q, \vec{r}).\vec{J}_{t_z}(c, \vec{r}) \| k', t_z \rangle d^3r \tag{3.51}$$

$$w(M\lambda m, q, k, k', t_z) = \int \langle k, t_z \| \vec{M}(\lambda, \lambda, q, \vec{r}).\vec{J}_{t_z}(m, \vec{r}) \| k', t_z \rangle d^3r \tag{3.52}$$

$$w(E\lambda c, q, k, k', t_z) = \frac{1}{q}\int \langle k, t_z \| \left[\vec{\nabla}\otimes\vec{M}(\lambda, \lambda, q, \vec{r}).\vec{J}_{t_z}(c, \vec{r})\right] \| k', t_z\rangle d^3r \quad (3.53)$$

$$w(E\lambda m, q, k, k', t_z) = \frac{1}{q}\int \langle k, t_z \| \left[\vec{\nabla}\otimes\vec{M}(\lambda, \lambda, q, \vec{r}).\vec{J}_{t_z}(m, \vec{r})\right] \| k', t_z\rangle d^3r \quad (3.54)$$

where $\langle k, t_z|$ is the single-particle wave function in the proton-neutron (p/n) formalism, $j_\lambda(qr)$ is the spherical Bessel functions and $\rho_{t_z}(\vec{r})$ is the charge density operator,

$$\rho_{t_z}(\vec{r}) = g_l(t_z)e\sum_k \delta\left(\vec{r} - \vec{r}_{k,t_z}\right) \ . \quad (3.55)$$

In OXBASH code, the charge density operator was adopted from reference [93] to include the Darwin-Foldy and spin-orbit corrections by using a Gaussian formula and fitting to experimental data, as

$$\rho(\vec{r}) = \frac{1}{(4\pi r_0^2 q)} e^{-\frac{r^2}{a^2}} B(k, k', r_0, b) \quad (3.56)$$

where r_0 and a are parameters with values given in reference [93] and B is a function of the initial-final state quantum numbers (k and k') and b is the harmonic oscillator length parameter, see Equation (3.44).

We define $\vec{J}_{t_z}(c, \vec{r})$ as the convection current operator,

$$\vec{J}_{t_z}(c, \vec{r}) = -ig_l(t_z)\mu_N\sum_k \left[\vec{\nabla}_k\delta\left(\vec{r} - \vec{r}_{k,t_z}\right) + \delta\left(\vec{r} - \vec{r}_{k,t_z}\right)\vec{\nabla}_k\right], \quad (3.57)$$

$\vec{J}_{t_z}(m, \vec{r})$ is the magnetic current operator,

$$\vec{J}_{t_z}(m, \vec{r}) = g_s(t_z)\mu_N\sum_k \left[\vec{\nabla}\otimes\left(\frac{\vec{\sigma}_k}{2}\right)\right]\delta\left(\vec{r} - \vec{r}_{k,t_z}\right) \quad (3.58)$$

$$\vec{M}(\lambda,\lambda,q,\vec{r}) = j_\lambda(qr)\vec{Y}^{(\lambda,\lambda)}(\hat{r}) \ , \tag{3.59}$$

and

$$\vec{Y}^{(\lambda,\lambda)}(\hat{r}) = \frac{\vec{\lambda}Y^{(\lambda)}(\hat{r})}{\sqrt{\lambda(\lambda+1)}} \quad . \tag{3.60}$$

The quantities g_l and g_s are the free-nucleon g factors, μ_N is the nuclear magniton and $\vec{\sigma}_k$ is the Pauli spin vector [5].

The longitudinal form factor can be approximated in terms of the point proton form factor as follows [10]:

$$F^2(C\lambda,q,i,f) = N_p G_{cm}^2(q)\left[g_{fs}(c,q,p) + \frac{N}{Z}g_{fs}(c,q,n)\right]^2 W^2(C\lambda,q,f,i,t_z)^2 \ . \tag{3.61}$$

In the calculation of the shell model, it has been assumed that the nuclei consist of a core and valence nucleons. The core is inert and only the motion of the valence nucleons in the sd shell model space needs to be considered. However, it can be shown theoretically that the effects of the virtual excitations of nucleons from the core shells into higher orbits are important. One can use the effective charges and g factors values to take into account the model-space truncation effects [10]. The effective charges and g factors are often used as an approximation in the renormalization of the single-particle matrix elements in shell model calculations. The g factors are fairly well described with the experimental magnetic moments in the sd-shell model predictions. The values were determined by using the least-squares fits to the experimental measurements. The effective charges are determined empirically in the sd-shell by using the electrical transition (E2 and E4) matrix elements which are found from the observables *B(E2)* and *B(E4)* values [94]. The latest g factors and effective charges for the sd-shell model space are calculated from Richter *et al*, [95] using the USDA and USDB Hamiltonians. New g factors values are determined by fitting the

calculated magnetic dipole moments (*M1*) matrix elements with those from experiments. The least-square fit to the *E2* data gave essentially the same effective charges values, e_p = 1.36(5) and e_n = 0.45(5), for all Hamiltonians. The OXBASH default values are e_p = 1.35 and e_n = 0.35 for effective charges, and free nucleon g factors and the recent values [95] of the effective charges and the g factors are investigated in the present work through the calibration of the USDA calculations with experimental data. This investigation aims to determine the most appropriate values from the previous studies and adjust them for some cases as described in the following.

CHAPTER 4

ENERGY STATES AND TRANSITION STRENGTH

4.1 Introduction

The first stage in assessing almost any theoretical study of nuclear structure consists of comparing the eigenvalues obtained from the diagonalizations of the model space Hamiltonian with the energies measured for the excited states with the matching quantum numbers in the corresponding actual nucleus. The precision of the Hamiltonians are illustrated in both the energy levels (the Hamiltonian eigenvalues) and the transition probabilities which mainly depend on the state wave functions (eigenvectors). The comparison of the theoretical and experimental states can be form by the emphasis on the spin sequences and energy gaps and state-to-state correspondences became paramount [13]. In this chapter, we explore the assessments of the observables in the odd-A isotopes. The assessments rely on the calculations of the energy levels, reduced electric quadrupole transition probabilities, reduced magnetic dipole transition probabilities, and multipole mixing ratio. The nuclei with odd number of nucleons (A = odd) are known to have half-integer spins, total angular momentum and intrinsic spin of all the nucleons.

The comparison between the theoretical and the experimental energies is based on different methods. Two of these methods are the spin sequences and energy gaps and state-

to-state correspondences [13]. The calculated energy levels obtained with USDA effective interactions for odd-A Mg isotopes are shown in Figures 4.1 to 4.9. A comparison has been made for the first three sequences between the energy obtained from the effective interaction calculations and the states obtained from experimental data with non-negative parity J values. In the case of non-availability of experimental data, the calculations were carried out for the states with $J \leq 13/2^{+}$. The illustration of the first three sequences clarifies the corresponding theoretical and experimental energy states due to the energy gaps between the first three sequences states with the same J values. Furthermore, it assists in identifying the change in the accuracy of the Hamiltonian for each sequence. Levels with "( )" correspond to cases in which the spin and/or parity of the corresponding states are not experimentally well established.

Transition probability is considered as one of the most sensitive parameters in determining the effective interactions. In order to elucidate this sensitivity, the reduced electric quadrupole transition probability, B(E2), and the reduced magnetic dipole transition probability, B(M1), are calculated. These calculations are performed with the available experimental data; two sets of effective charges and g factors are used. For the first set, we use the default values in the OXBASH program [91] ; the values of the effective charges are e_p=1.35e and e_n=0.35, and the free nucleon g factors are $g_s(p)$ = 5.586, $g_s(n)$ = -3.826, g_l (p) = 1, and g_l (n) = 0. In the second set, we use new effective charges e_p = 1.36e and e_n = 0.45, and the effective g factors values g_s (p) = 5.0, g_s (n) = -3.5, g_l (p) = 1.175, and g_l (n) = -0.106[95]. The purpose of this calculation is to identify an optimal set in the USDA calculations for the above transitions. The experimental data that were adopted in this work is the latest results for the corresponding nucleus and sometimes we use the mirror nucleus data in our discussion of the results.

4.2 ^{21}Mg Nucleus

Figure 4.1 illustrates the ^{21}Mg energy levels with the experimental values for the first three sequences. The predictions of USDA for the first sequence show good agreement for the states J=1/2$^+$, 3/2$^+$ and 7/2$^+$ with the experimental data. But the state J = 9/2$^+$ is found experimentally to have energy higher than the theoretical prediction for the two Hamiltonians. This can be explained as a result of the possible existence of state with J = 9/2$^+$ equivalent to the first theoretical state which is not found experimentally. Our interpretation is based on the compatibility of USDA predictions to the other J-states in the first sequence and the prediction of USDA for second J_2 = 9/2$^+$ (3.439 MeV) which is close to the experimental first J = 9/2$^+$ (at 3.643 MeV [52]). Other evidence enhances that our interpretation comes from the existence of the first J_1 = 9/2$^+$ state in the ^{21}Mg mirror nucleus, ^{21}F, at energy 1.754 MeV [52] which approaches the USDA prediction value at 1.730 MeV. The USDA calculation and the new experimental energy for the J = 3/2$^+$ states exhibit an interesting convergence pattern. Previous studies [27, 48, 52] have shown the energy of this state to be 3.08 MeV, whereas recent measurements [38] place the value at 1.651 MeV, comparable with the USDA calculation value of 1.849 MeV which places it at the first sequence. No experimental data have been published for J = 11/2 and 13/2 in the ^{21}Mg spectrum. However, these states have been found for J = 11/2 in ^{21}Na and ^{21}Ne with $E_{ex.}$ (experimental energy) = 4.419 and 4.431 MeV, respectively [52]. The USDA prediction for this state is 4.604 MeV. In addition, J = 13/2 was found in the ^{21}Ne spectrum with E_{ex} = 6.448 MeV [52]; and the calculation value for this state is 4.620 MeV.

A clear difference is found in the second and third sequences. The doublet consisting of two states with J=3/2$^+$and 5/2$^+$ have been found experimentally in the second and third

sequences but only the second sequence is found theoretically with clear contrast energy. There are three states found in [48] (not shown in Figure 4.1), which have $J=3/2^+$, $5/2^+$ and $3/2^+$ with energies 4.005, 4.228 and 4.538 MeV respectively. The first state with $J=3/2^+$ agrees with the third sequence of $J=3/2^+$ of the USDA calculations ($J_3=3/2^+$, 4.122 MeV) and the theoretical value closest to $J=5/2^+$ is $J_3=5/2^+$ with energy 4.578 MeV, while USDA did not predict any energy state equivalent to the second $J=3/2^+$ at energy 4.538 MeV.

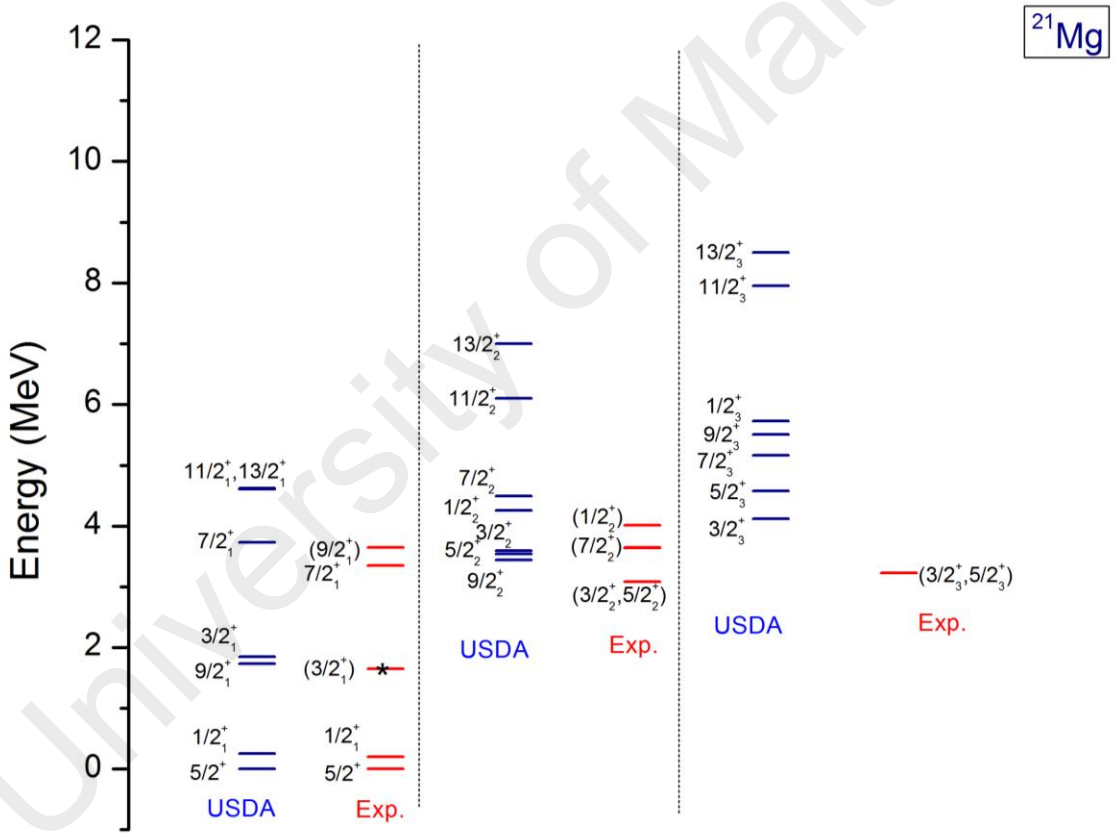

Figure 4.1: Comparison of the experimental energy levels with the energy levels calculated in the present theoretical work for the ^{21}Mg nucleus. The experimental data (—) are taken from[27, 52] while (*) are taken from[38].

4.3 ^{23}Mg Nucleus

The experimental [27, 53, 57] and theoretical energy spectra for ^{23}Mg are shown in Figure 4.2. Many states have been observed recently [57] and are marked with (*), and the other states are adopted from references [27, 53]. The comparison between theoretical and experimental values show an agreement with USDA for states with J ≤ 15/2$^+$ for the yrast states, while J=17/2$^+$ is found theoretically higher than the experimental value.

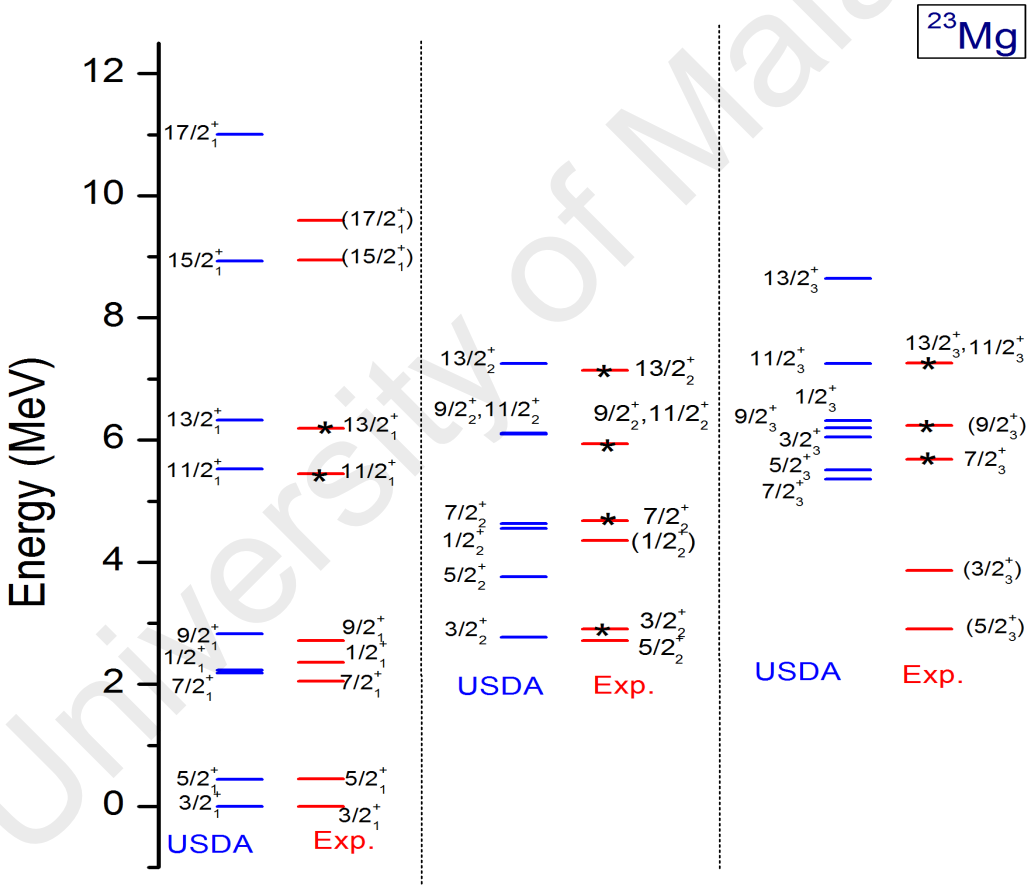

Figure 4.2: Comparison of the experimental energy levels with the energy levels calculated in the present theoretical work for the ^{23}Mg nucleus. The experimental data (—) are taken from[27, 52] while (*) are taken from[57].

In the second sequence, the USDA calculation shows a remarkable agreement with the experimental states especially with recent measurements for the J = $7/2^+$ and $13/2^+$ states. The grouping of the two states J=$9/2^+$ and $11/2^+$ demonstrates the accuracy of the USDA. It is worth to mention about the position of the state J=$5/2^+$ in the second sequence. References [27, 53] reported that 2.714 MeV energy level is identified to the two J values, J_1= $9/2^+$ and J_2= $5/2^+$. Recent experimental work [57] showed that the energy level 2.714 MeV is identified as the J_1= $9/2^+$ only and the J_2= $5/2^+$ state is found at energy 3.859 MeV , while in references [27, 53], the energy value 3.859 MeV is identified as the uncertain state J_3= $5/2^+$, which corresponds to the energy spectrum of the ^{23}Mg mirror nucleus, ^{23}Na [27, 53]. Another indication appears from the calculation of the B(M1), which shows that the energy level at 2.714 MeV is more likely to be J_1= $9/2^+$ than J_2= $5/2^+$ as shown in Table 4.2. The previous discussion is compatible with the USDA calculation for states with J= $5/2^+$ in the second and third sequences where the energy value for the J_3= $5/2^+$ will be 5.286 MeV [57]. The energy state at 2.908 MeV has been identified as the J_2=$3/2^+$ in reference [57], which agrees with the theoretical prediction, but unfortunately, reference [57] just provide few states with J=$3/2^+$. In references [27, 53], the uncertain J values energy states at 3.864 and 5.287 MeV are presented with two J values, $5/2^+$ and $3/2^+$. As stated above, these states are set to the J=$5/2^+$ based on reference [57].

The next state with J=$3/2^+$ in the energy spectrum from [27, 53] is found at 7.648 MeV, and it is unlikely to be the value of J_3= $3/2^+$ if it is compared to the energies of the other states in the third sequence. Therefore, the experimental state of J_3= $3/2^+$ is not present in Figure 4.2. The third state with J=$3/2^+$ in the ^{23}Na spectrum has been determined at energy 5.766 MeV and the closest energy state observed in the ^{23}Mg spectrum is found at 5.711 MeV and identified to be J= $1/2^+$ to $9/2^+$ [27, 53]. Comparing with the theoretical

calculation, this state could be the $J_3 = 3/2^+$ if we take into account that this state is not identified within the other states with $J = 1/2^+$ to $9/2^+$ as shown in Table 4.1. In the third sequence, the states $7/2^+$, $9/2^+$, and $11/2^+$ have only been detected recently, while the $J=5/2^+$ state is found in all the aforementioned references and an acceptable agreement is found in the USDA calculations. The third $J=13/2^+$ state has been experimentally confirmed [57] with an energy of 7.26 MeV, which is similar to that of the $J=11/2^+$ state. However, because USDA predicts an energy of 8.644 MeV for the third $J=13/2^+$ state, some reservations are raised about this state when the theoretical energy is taken into consideration, Moreover, there is a lack of discussion on this state in reference [57]. The agreement of the USDA results with the experimental data leads us to make a comparison with the higher sequence states for $J = 3/2^+$ to $9/2^+$, as shown in Figure 4.3. Theoretical calculations have been performed according to the extent of available experimental energies and each J value is compared separately.

From Figure 4.3-a, we can see the lack in the experimental data with $J=3/2^+$ from the difference in the number of the theoretical states compared with the experiment, and this starts from the third sequence in Figure 4.2. The need for more experimental data also includes the transition probability, which represents an important characteristic for comparison in order to determine the states. This problem has led to the unresolved comparison of the determination of equivalent states between experimental and theoretical results. In Figure 4.3-b, the arrangement that has been presented in the first three sequences for the states with $J=5/2^+$ leads to a remarkable consensus between the experimental and USDA states of energy up to 7.183 MeV. States with energy higher than this show a clear difference in the number of available theoretical states compared with the observed experimental data. Reference [57] has identified several new $J=7/2^+$ states.

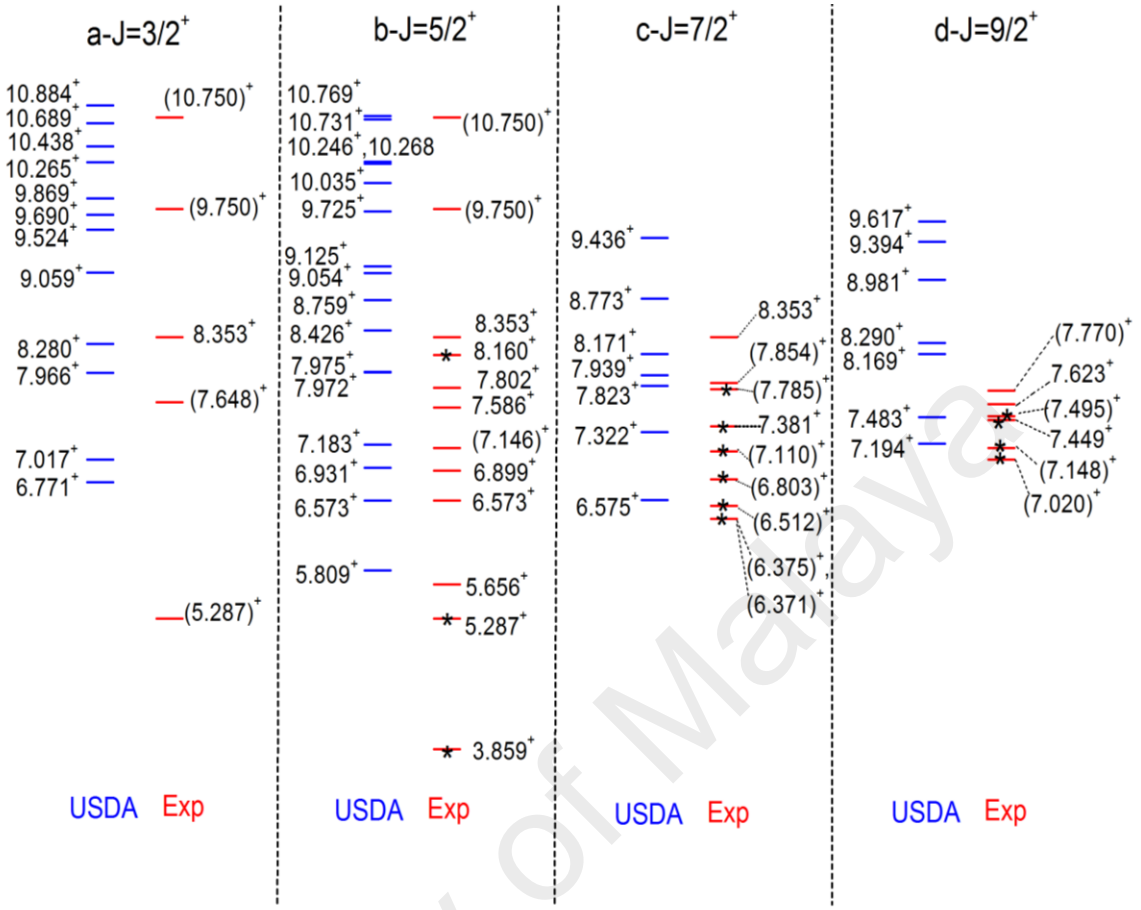

Figure 4.3: Comparison between experimental energy levels and the energy levels calculated in the present theoretical work for the ^{23}Mg nucleus for sequences higher than three. Experimental data (—) are taken from [27, 53] while (*) are taken from[57].

The new states show significant agreement with the theoretical values in Figure 4.3-c with the experimental states more than the theoretical in the energy range ≤ 8.353 MeV. The same behaviour is shown in the J=9/2$^+$ spectrum in the energy range ≤ 7.770 MeV with a remarkable agreement for many states. These variations could be resolved by expanding the model space to get more energy states within the intended range. Many states appear in the references [27, 53] with J= (1/2 to 9/2)$^+$. The USDA prediction for these states is compatible with the new experimental observations [57]. Table 4.1 shows these states with the new experimental values and the theoretical prediction. The states with J= (19/2)$^+$ at energy 14.560 MeV and (21/2)$^+$ at energy 14.130MeV found in references [27, 53] do not

appear in Figure 4.2. The USDA predictions for these states are 14.623 and 16.844 MeV respectively, which confirms the advantage of USDA for the high J- values states as the case of $J = 19/2^+$.

Table 4.1: Theoretical and new experimental energy for states with J= $(1/2 \text{ to } 9/2)^+$ in ^{23}Mg spectrum.

References[27, 53]		***Reference[57]***		***USDA***	
J	**E (MeV)**	**J**	**E(MeV)**	**J**	**E(MeV)**
$(1/2 \text{ to } 9/2)^+$	4.685	$7/2^+$	4.680	7/2	4.634
	5.691	$(7/2)^+$	5.689	7/2	5.363
	6.236	$(9/2)^+$	6.238	9/2	6.198
	6.507	$(7/2)^+$	6.512	7/2	6.575
	6.538	$5/2^+$	6.573	5/2	6.573
	7.493	$9/2^+$	7.495	9/2	7.483

The theoretical and experimental B(E2) (in units of e^2fm^4) and B(M1) (in units of μ^2, μ Bohr magneto) values for ^{23}Mg isotope are presented in Table 4.2. The symbols n_i and n_f in Table 4.2 represent the sequences of the closest theoretical J states to the experimental data, *Set1* represents the results obtained by using the default effective charge and free nucleon *g* factor, while *Set2* is obtained by using the new effective charge and nucleon *g* factor values. In general, acceptable agreement is found for the Hamiltonians in ^{23}Mg for B(E2) and B(M1) results at low energy states and diverge at high energy states. *Set1* B(E2) results are more consistent with experimental than those of Set2 while no clear disagreement is found in the B(M1) results when *Set1* and *Set2* are used. The fourth state with $J=11/2^+$ in ^{23}Mg spectrum had recently been observed at energy 7.780 MeV and it has one B(E2) transition to $J_1=7/2^+$ as shown in Table 4.2. Predictions of USDA for this state is 7.627 MeV.

Table 4.2 Theoretical and experimental B(E2) and B(M1) values for ^{23}Mg . Experimental data are taken from [53].

Experimental					*USDA*			
							B(E2) e^2fm^4	
E_i MeV	*$2J_i$*	*E_f MeV*	*$2J_f$*	*B(E2) e^2fm^4*	*n_i*	*n_f*	*Set1*	*Set2*
0.450	5	0.0	3	85.48(15)	1	1	104.2	117.4
2.052	7	0.450	5	31.08(4)	1	1	56.69	63.79
		0.0	3	50.51(4)	1	1	41.65	46.60
2.359	1	0.450	5	26.80(15)	1	1	25.52	27.52
7.624	9	0.450	5	7.38(10)	5	1	0.05	0.04
7.780	11	2.052	7	30.30(8)	4	1	2.45	2.65
Experimental					*USDA*			
							B(M1) μ^2	
E_i MeV	*$2J_i$*	*E_f MeV*	*$2J_f$*	*B(M1)μ^2*	*n_i*	*n_f*	*Set1*	*Set2*
0.450	5	0.0	3	0.343(13)	1	1	0.288	0.295
2.052	7	0.450	5	0.139(20)	1	1	0.214	0.201
2.714	5	2.052	7	0.429(5)	2	1	0.008	0.029
	9	2.052	7	0.429(5)	1	1	0.519	0.538

4.4 ^{25}Mg Nucleus

The broad experimental spectrum [27, 60] and the nuclear structure of ^{25}Mg give special significance for this nucleus in the shell model calculations. As shown in Figure 4.4, a good agreement is found for the USDA calculations for the ^{25}Mg spectrum in the three sequences of $J \leq 13/2^+$ with energies up to 8 MeV. However, the states with $J=15/2^+$ show a clear contrast in the first and second sequences. The correspondence of these data indicate

the existence of J = $13/2^+$ in the second and third sequences as well as the J = $11/2^+$ and J = $7/2^+$ states in the third sequence, the existence of which was uncertain in the experiments.

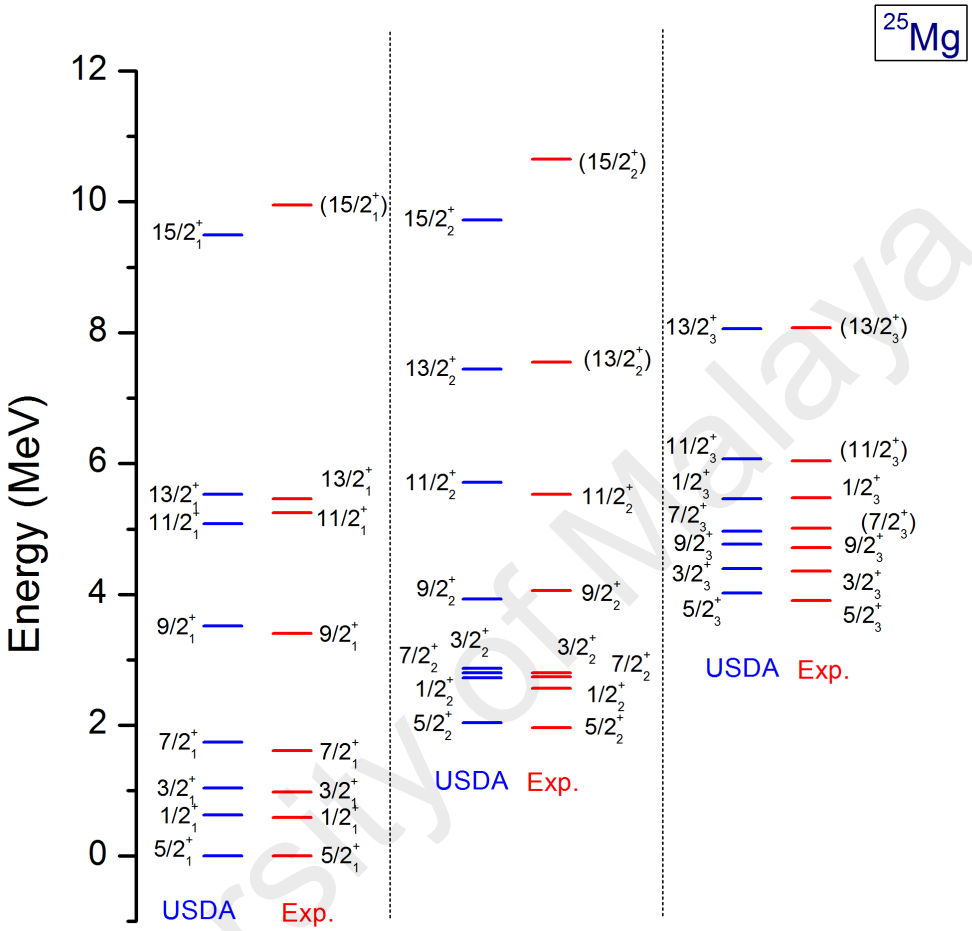

Figure 4.4 Comparison of the experimental energy levels with the energy levels calculated in the present theoretical work for the ^{25}Mg nucleus. The experimental data are taken from [27, 60].

Higher energies for the J ≤ 11/2 spectrum are compared with USDA calculations, as shown in Figures 4.5 and 4.6 with the same approach used in Figure 4.3. The calculation of higher sequences aided the comprehensive evaluation of USDA results for A = 25 as well as the study of some of the states in ^{25}Mg. In general, one can see that many of the experimental states have equivalent theoretical states while the other states are not specified, and vice versa.

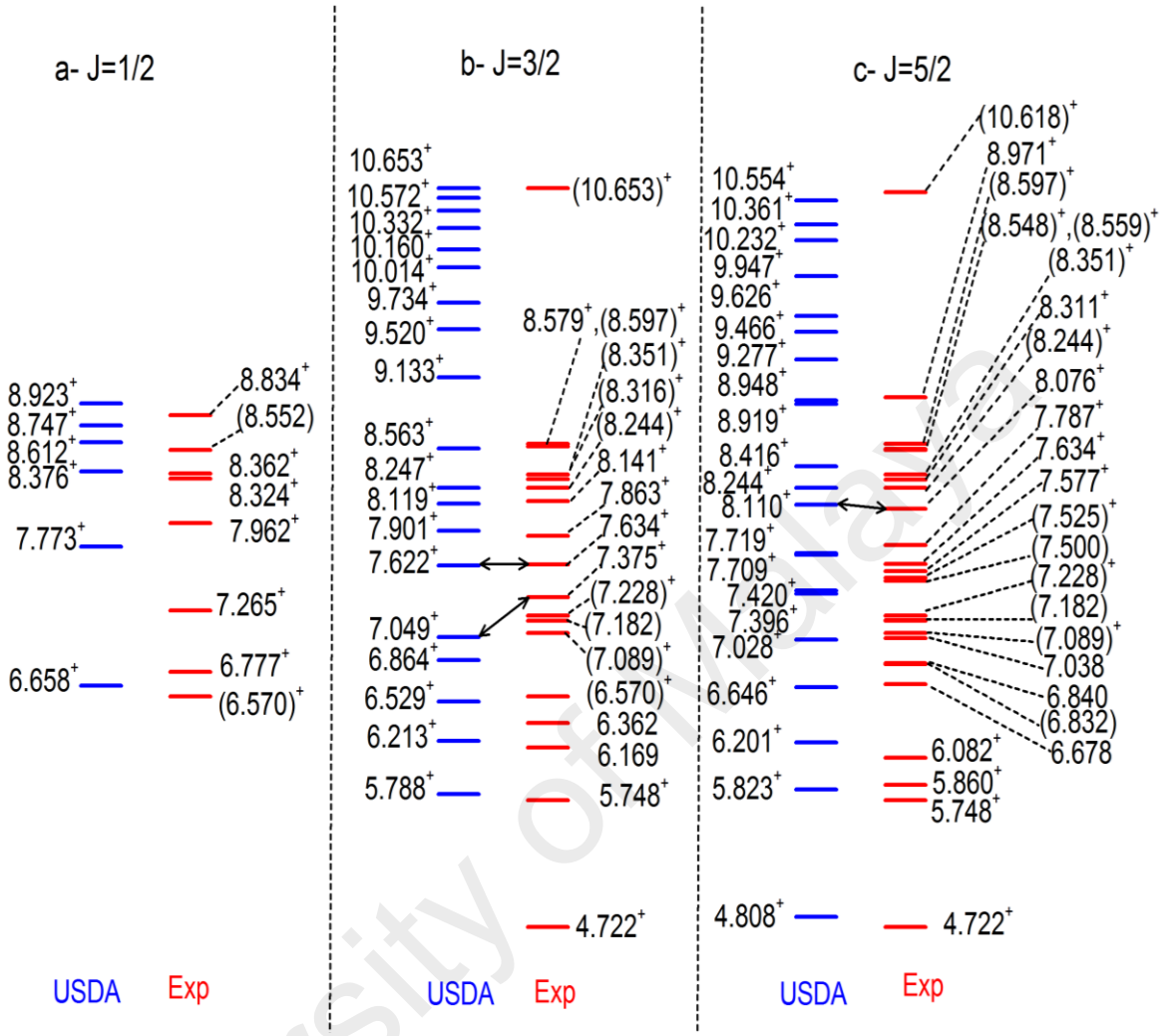

Figure 4.5: Experimental data [27, 60] and energies calculated using USDA for J = 1/2, 3/2, and 5/2 states in the ^{25}Mg nucleus. The equivalent theoretical and experimental states are connected by arrows based on matching transition probabilities, see Tables 4.3 and 4.4.

The energy intervals have theoretical states higher than the experimental giving an indication of the need for more experimental works in these intervals, while in the opposite case the theoretical solution could be obtained through the expansion of the model space as mentioned for ^{23}Mg.

Transition probabilities (B(E2) and B(M1)) and the multipole mixing ratio (δ) have been used in the determination of the corresponding states in the theoretical and experimental spectra. The multipole mixing ratio is used to calculate the ratios of the reduced transition probabilities from [96]:

$$\frac{B(M1)}{B(E2)} = 0.697 \frac{E_\gamma^2}{\delta_{E2/m1}^2} \qquad (4.1)$$

where E_γ is the gamma energy in units of MeV. Reference [60] reported B(E2), B(M1) and δ values for many states in ^{25}Mg spectrum and all the B(E2) and B(M1) transitions are calculated and illustrated in Table 4.3. While for δ calculations, only the states which achieved agreement with the experimental data are illustrated in Table 4.4. These results are used in conjunction with the discussion on the higher energy states in ^{25}Mg.

The states with J = 1/2 are shown in Figure 4.5-a. The experimental energy range of these states is found laying between the interval 6.570 and 8.834 MeV. The USDA calculations are considered satisfactory for this energy interval by the closeness of the results for several states. The state with energy 8.552 MeV, unknown parity, is located near the theoretical state at 8.612 MeV. This finding indicates the possibility of this state having a positive parity. Figure 4.5-b illustrates an experimentally observed state attributed to J = 3/2. One easily notices the state with energy 4.772 MeV without an equivalent theoretical state. This state has been found experimentally with two J values, $3/2^+$ and $5/2^+$, whereas shell model predicts a state with J=$5/2^+$ has energy near to this value as indicated in Figure 4.5-c.

Figure 4.6: Experimental data [27, 60] and energies calculated using USDA for J = 7/2,

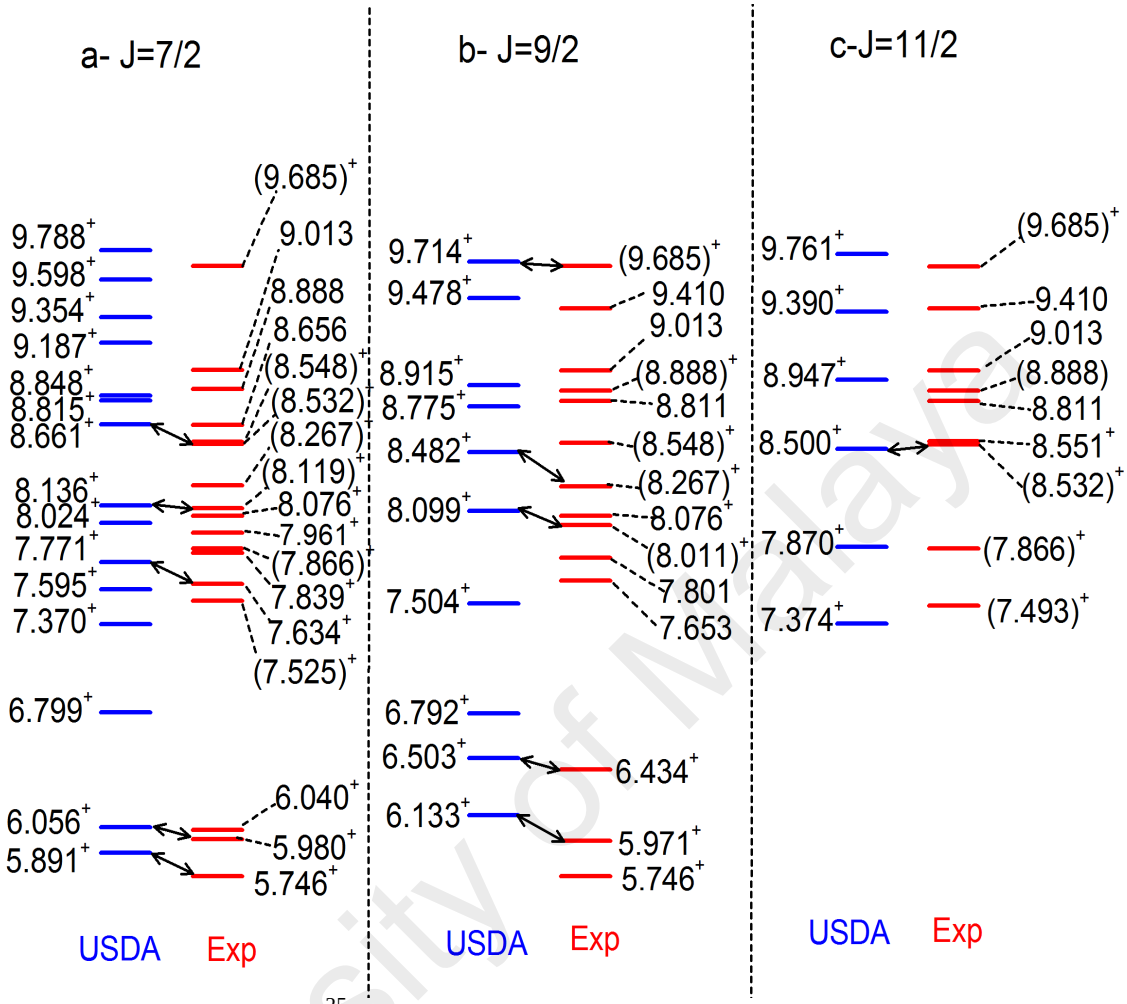

9/2, and 11/2 states in the ^{25}Mg nucleus. The equivalent theoretical and experimental states are connected by arrows based on matching transition probabilities, see Tables 4.3 and 4.4.

The two unknown parity states with energies 6.169 and 6.362 MeV have one equivalent theoretical positive parity state with energy 6.213 MeV. Identifying one of them to the theoretical state is not possible due to the lack of experimental data but one of these states undoubtedly has positive parity. Calculated values of B(M1) confirm that the theoretical state with $J_8=3/2^+$ at energy 7.049 MeV is the equivalent to the experimental state at 7.375 MeV as seen in Table 3.3. The state at energy 7.634 MeV has been found experimentally with $J=3/2^+$, $5/2^+$ and $7/2^+$ (see Figures 4.5-a,c and 4.6-a). According to $|\delta|$, Table 4.4, this state seems to be $J_9= 3/2^+$ and $J_9= 7/2^+$ rather than $J_{11}= 5/2^+$. Except for case

4.722 MeV, the J=3/2 spectrum achieves a remarkable consensus with USDA calculations. Due to the abundance of the theoretical states in the energy interval between 8.597 and 10.653 MeV, we would expect new experimental values for $J=3/2^+$.

In Figure 4.5-c and Figure 4. 4, one can see the agreement between the experimental $J=5/2^+$ states and USDA calculations to the first fifth sequences. For energy between 5.860 MeV and 8.971 MeV, experimental results show the number of states is more than the theoretical calculations with a notable agreement for several states. The state with energy of 6.646 MeV appearing in the USDA spectrum Figure 4.5-c indicates that the unknown parity state with energy of 6.678 MeV probably has positive parity. Figure 4.5-c shows the uncertain positive parity state at energy 7.089 MeV which is more likely to be the theoretical state at energy 7.028 MeV compared to the non-specific party 7.038 MeV. The comparison between experimental and theoretical $|\delta|$ values, Table 4.4, indicates that the experimental state $J=5/2^+$ at 8.076 MeV is equivalent to the theoretically state with $J_{13}=5/2^+$ at energy 8.110 MeV. The $J=5/2^+$ spectrum achieves a remarkable consensus with USDA calculations when taking the first and last state values. As a result of the theoretical calculations, it is expected that the energy interval between 8.971 and 10.618 MeV promises new experimental values for $J=5/2^+$.

The J = 7/2 spectrum is shown in Figure 4.6-a, and a greater number of experimental states compared to the number of USDA-calculated states is evident. The gap in the sequence of experimental states (6.040 MeV to 7.525 MeV) also appears in the theoretical spectrum but with a 6.79 MeV state appearing in the middle.

Table 4.3: Theoretical and experimental B(E2) and B(M1) values for ^{25}Mg . Experimental data taken from [60].

Experimental					*USDA*			
							B(E2) e^2fm^4	
E_i	$2J_i$	E_f *MeV*	$2J_f$	*B(E2)* e^2fm^4	n_i	n_f	*Set1*	*Set2*
0.585	1	0.0	5	2.44(10)	1	1	3.23	4.27
0.974	3	0.585	1	47.76(5)	1	1	55.06	63.04
		0.0	5	3.95(13)	1	1	3.93	4.75
1.611	7	0.0	5	104.21(6)	1	1	102.9	114.1
1.964	5	0.974	3	15.20(7)	2	1	19.05	21.70
		0.585	1	68.61(14)	2	1	63.03	71.40
		0.0	5	1.95(12)	2	1	2.59	3.23
2.563	1	0.0	5	17.37(3)	2	1	11.99	14.80
2.737	7	1.964	5	86.84(15)	2	2	5.13	5.19
		0.974	3	99.44(24)	2	1	72.22	82.66
		0.0	5	0.43(5)	2	1	0.69	0.82
2.801	3	1.964	5	21.71(5)	2	2	1.93	2.09
		0.585	1	6.51(13)	2	1	0.483	0.435
		0.0	5	7.38(4)	2	1	7.66	9.54
3.405	9	1.611	7	52.11(6)	1	1	59.57	66.16
		0.0	5	29.53(9)	1	1	35.10	39.05
3.907	5	0.974	3	0.13(+14-3)	3	1	0.14	0.20
		0.0	5	2.08(19)	3	1	3.90	4.59
4.059	9	1.611	7	9.11(8)	2	1	21.65	24.60
		0.0	5	6.55(17)	2	1	2.64	3.21
4.711	9	1.964	5	130.26(5)	3	2	83.91	92.94
5.251	11	4.059	9	347.37(40)	1	2	54.09	60.23
		3.405	9	14.33(12)	1	1	10.89	11.85
		2.737	7	45.59(18)	1	2	14.12	16.06
		1.611	7	22.15(12)	1	1	20.34	23.14
5.461	13	3.405	9	10.68(23)	1	1	6.28	6.99
5.533	11	3.405	9	18.67(17)	2	1	18.83	20.97
		1.611	7	39.07(4)	2	1	22.79	25.19
Experimental					*USDA*			
							B(M1) μ^2	
E_i	$2J_i$	E_f *MeV*	$2J_f$	*B(M1)* μ^2	n_i	n_f	*Set1*	*Set2*
0.974	3	0.585	1	0.029(17)	1	1	0.035	0.022
		0.0	5	0.002(12)	1	1	0.006	0.005
1.611	7	0.0	5	0.537(6)	1	1	0.524	0.593
1.964	5	0.974	3	0.016(9)	2	1	0.006	0.008
		0.0	5	0.001(11)	2	1	0.000	0.001
2.737	7	1.964	5	0.016(20)	2	2	0.022	0.010
		0.0	5	0.0001(6)	2	1	53×10^{-7}	0.00
2.801	3	1.964	5	1.091(8)	2	2	0.947	0.832
		0.585	1	0.050(4)	2	1	0.024	0.021
		0.0	5	0.009(8)	2	1	0.024	0.020
3.405	9	1.611	7	0.716(4)	1	1	0.646	0.726
3.907	5	2.737	7	0.537(11)	3	2	0.387	0.361
		0.974	3	0.179(4)	3	1	0.163	0.149
		0.0	5	0.010(4)	3	1	0.007	0.006
4.059	9	1.611	7	0.018(14)	2	1	0.088	0.107
5.251	11	4.059	9	0.340(3)	1	2	0.161	0.208
		3.405	9	0.103(9)	1	1	0.192	0.202
5.533	11	3.405	9	0.411(8)	2	1	0.410	0.451
7.375	3	0.0	5	0.408	8	1	0.538	0.493

An unknown parity state has been observed at energy 8.656 MeV. This state has an equivalent theoretical state at energy 8.661 MeV. A grouping of three J value states has been found experimentally in the energy state 8.888 MeV. The J=9/2 is found with a positive party while in J=7/2 and 11/2, the parity is not identified. For J=7/2 the USDA predicts two energy states (8.815 and 8.848 MeV) close to this experimental value. With regard to $J=9/2^+$, the closest USDA prediction (see Figure 4.6-b) is at energy 8.915 MeV while the theoretical $J=11/2^+$ shows a state (see Figure 4.6-c) with energy 8.947 MeV and it represents non-unknown case as a result of the existence of undetermined parity state for J=11/2 with energy 9.013 MeV.

The calculations of $|\delta|$ values, in Table 4.4, enable us to determine the theoretical and experimental counterpart states in Figure 4.6. For states with J=7/2, Figure 4.6-a, first case is the energy state at 5.746 MeV which was found experimentally with $J= 7/2^+$and $9/2^+$ [60]. The difference between the experimental and theoretical values of E_γ and $|\delta|$ suggest this state to be $J= 7/2^+$ rather than $9/2^+$ and the equivalent theoretical state is $J_4= 7/2^+$ at energy 5.891 MeV. States at energies 5.980 and 8.119 MeV are observed with $J= 7/2^+$ [60], the USDA equivalent predictions for these states are J_5 and $J_{11} = 7/2^+$ at energies 5.980 and 8.119 MeV, respectively. Equal theoretical values are obtained when calculating the $|\delta|$ for the state at energy 8.532 MeV which was found experimentally with $J=7/2^+$ and $11/2^+$ [60]. This result means that the theoretical $J_{12}=7/2^+$ (Figure 4.6-a) and $J_6=11/2^+$ (Figure 4.6-c) have the same possibility to be the equivalent to the experimental state. In Figure 4.6-b, the experimental J=9/2 spectrum shows an energy state 5.746 MeV without equivalent theoretical value while the same energy is found in J=7/2 spectrum (see Figure 4.6-a) and the theoretical equivalent is determined.

Table 4.4: Theoretical and experimental values of absolute multipole mixing ratio |δ| in units of $(\mu/eb)^2$ for ^{25}Mg isotopes.

Experimental [60]					*Theoretical*					
E_i *(MeV)*	$2J_i$	E_γ *(MeV)*	$2J_f$	$\|\delta\|$.	n_i	n_f	E_γ *(MeV)*	*B(M1) μ^2*	*B(E2) $\times 10^{-4}$ e^2b*	$\|\delta\|$
4.359	3	3.384	3	0.09(7)	3	1	3.36	0.381	1.1	0.05
	3	0.585	1	0.19(19)	3	1	0.626	0.354	9.86	0.17
5.746	7	1.686	9	0.18(+7-2)	4	2	1.961	0.019	0.549	0.09
	9	1.686	9	0.18(+7-2)	4	2	2.203	0.287	0.038	0.01
5.971	9	4.359	7	0.31(3)	4	1	4.394	0.036	3.351	0.35
5.980	7	4.014	5	0.14(3)	5	2	4.022	0.235	3.09	0.12
6.434	9	0.899	11	0.03(13)	5	2	0.794	0.246	1.402	0.02
	9	4.821	7	1.0(+15-6)	5	1	4.764	0.0047	2.762	0.96
7.634	3	7.634	5	0.1(+12-25)	9	1	7.622	0.373	0.652	0.08
	5	7.634	5	0.1(+12-25)	11	1	7.709	0.042	0.023	0.05
	7	7.634	5	0.1(+12-25)	9	1	7.771	0.066	0.233	0.12
8.011	9	2.761	11	0.18(1)	8	1	3.02	0.006	0.106	0.11
	13	2.761	11	0.18(1)	3	1	2.98	0.021	12.45	0.61
8.076	5	6.463	7	0.14	13	1	6.371	0.025	0.096	0.1
8.119	7	8.119	5	0.04(+5-17)	11	1	8.136	0.074	0.04	0.05
8.267	9	6.655	7	1.2(+2-3)	9	1	6.743	8.9×10^{-4}	0.235	0.91
8.532	7	5.127	9	0.1(6)	12	1	5.146	0.017	0.295	0.18
	11	5.127	9	0.1(6)	6	1	4.985	0.013	0.244	0.18
9.685	9	6.280	9	0.14(7)	13	1	6.199	0.018	0.13	0.14
	11	6.280	9	0.14(7)	9	1	6.246	0.004	0.001	0.03
9.947	15	2.399	13	0.16(4)	1	2	2.051	0.09	6.93	0.15
	15	4.487	13	0.5(5)	1	1	3.962	0.35	22.22	0.26

Theoretical states at 7.504, 8.775 and 9.478 MeV with positive parity appear near the experimental unknown parity states at 7.653, 8.811 and 9.410 MeV respectively. Four experimental energies of states with $J=9/2^+$ have been theoretically identified in the spectrum. States at energy 5.971 and 6.434 MeV have theoretical equivalents to J_4 and $J_5=9/2^+$ at energies 6.133 MeV and 6.503 MeV respectively. Calculations of $|\delta|$ values show that the equivalent theoretical state to the experiment at energy 8.011 MeV is $J_8=9/2^+$ where this state was found experimentally with $J=9/2^+$ and $13/2^+$ [60]. The last case is found experimentally with energy 9.685 MeV with $J=9/2^+$ and $11/2^+$. Calculation of $|\delta|$ values with $J_{13}=9/2^+$ and $J_9=11/2^+$ has shown that $J_{13}=9/2^+$ has the value approaching to the experimental data.

Figure 4.6-c shows a good agreement for the USDA predictions for J=11/2 states. Differences appear only in the three experimental energy states with unknown parity at 8.811, 8.888 and 9.013 MeV whilst the USDA calculations suggest a positive parity state at 8.947 MeV. These states also had appeared in the J=9/2 spectrum and the determination of the equivalent to the theoretical values is not possible; but it is worth mentioning that one of these states has $J=11/2^+$.

The results of B(E2) and B(M1) in Table 4.3, show that USDA has an acceptable accuracy in the calculation of the transition probabilities, which indicates that the wavefunction obtained from USDA is appropriate to describe the nuclear states. The results of USDA for ^{25}Mg indicate that the default values of effective charge [91], rather than the new values are valid, and the new effective g factors values [95] improve the calculated values of B(M1).

4.5 ^{27}Mg Nucleus

In Figure 4.7, the USDA effective interaction shows a clear agreement for the first and second sequences, and the doublet consisting of the state J= $1/2^+$ and $3/2^+$ in the second sequence is present amongst the theoretically predicted states. This agreement suggests a new energy value for J = $13/2^+$ in the first sequence with an energy of 7.33 MeV, which is not experimentally observed, and the possible existence of the J = $11/2^+$ and $13/2^+$ states in the second and third sequences on the basis of the theoretical values.

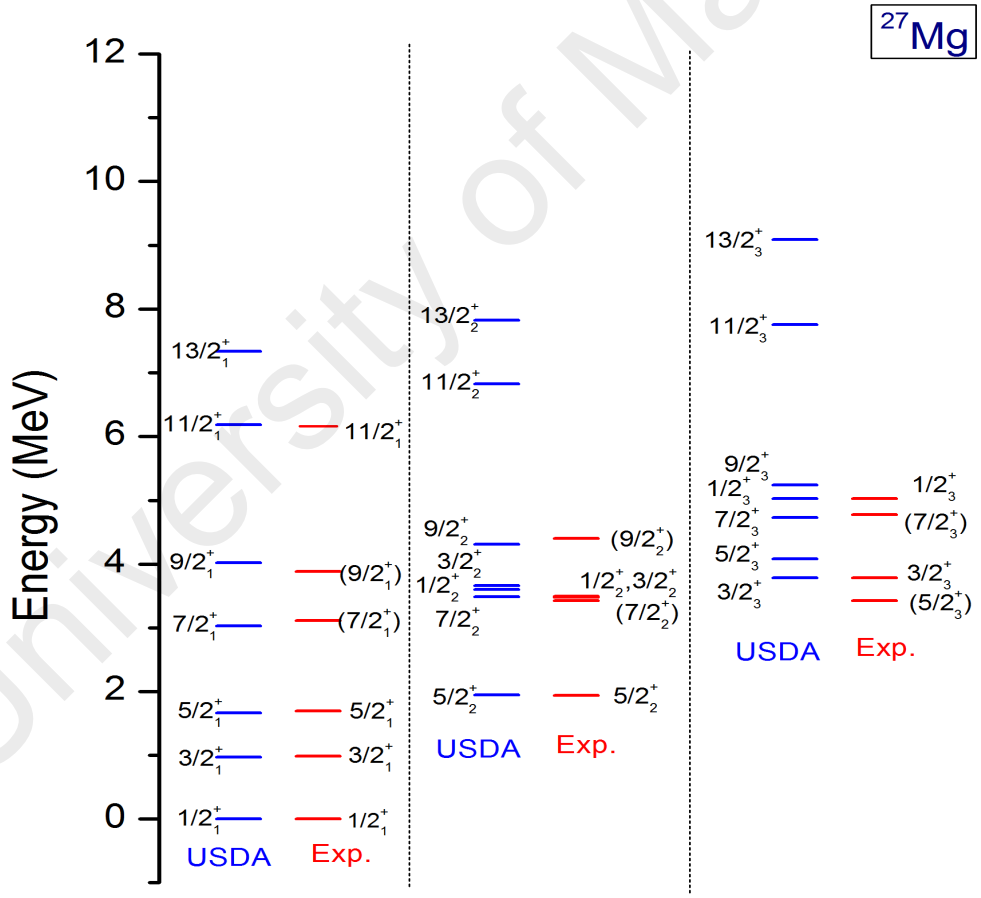

Figure 4.7: Comparison of the experimental energy levels with the energy levels calculated in the present theoretical work for the ^{27}Mg nucleus. The experimental data are taken from [27, 61].

The third sequence shows four experimental states, and we can observe an opposite trend in J = $5/2^+$ as the theory and experiment are in agreement for the first and second sequences of this state only. Figure 4.8 shows the USDA calculations and the available experimental energy states for J= $3/2^+$ and $5/2^+$ in sequences higher than the third sequence. Comparison between theoretical and experimental data for J= $3/2^+$ (Figure 4.8-a) shows states at energies 4.150 and 4.553 MeV without any corresponding theoretical values. Other experimental values for J= $3/2^+$ have corresponding theoretical states including the first three sequences.

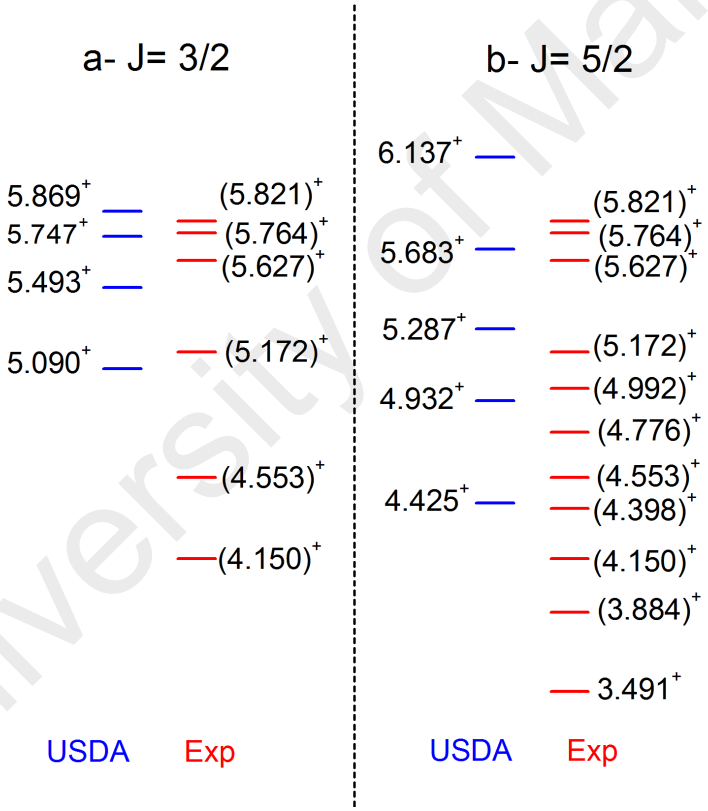

Figure 4.8: Experimental data [27, 61] and USDA calculations of energy states for J = $3/2^+$ and $5/2^+$ for the ^{27}Mg nucleus.

Inaccuracies in the predictions of USDA for $J=5/2^+$ spectrum as we can observe in Figure 4.8-b compared to the experimental data which can starts from the third sequence. The $J=5/2^+$ spectrum also shows the number of states observed experimentally is more than the theoretical prediction. This conclusion indicates that the USDA accuracy decreases as the sequence increases in the ^{27}Mg configuration.

Results of the B(E2) and B(M1) calculations are shown in Table 4.5. Clearly, the USDA shows less accuracy than with ^{25}Mg in the two transitions types. The comparison between *Set1* and *Set2* did not present any favouritism to the any one of them within the two Hamiltonians.

Table 4.5 Theoretical and experimental B(E2) and B(M1) values for ^{27}Mg . Experimental data are taken from [61].

Experimental					***USDA***			
							B(E2) e^2fm^4	
E_i MeV	***$2J_i$***	***E_f MeV***	***$2J_f$***	***B(E2) e^2fm^4***	***n_i***	***n_f***	***Set1***	***Set2***
0.984	3	0.0	1	28.87(19)	1	1	39.55	43.69
1.698	5	0.0	1	48.60(23)	1	1	23.73	26.58
1.940	5	0.984	3	3.85(+13-8)	2	1	9.87	11.24
3.109	7	1.940	5	192.45(+60-40)	1	2	37.32	43.06
Experimental					***USDA***			
							B(M1) μ^2	
E_i MeV	***$2J_i$***	***E_f MeV***	***$2J_f$***	***B(M1)μ^2***	***n_i***	***n_f***	***Set1***	***Set2***
0.984	3	0.0	1	0.041(6)	1	1	0.040	0.027
1.940	5	0.984	3	0.046(7)	2	1	0.015	0.021
3.109	7	1.940	5	0.322(5)	1	2	0.208	0.223

4.6 ^{29}Mg Nucleus

There are six states with positive and unknown parities observed in ^{29}Mg spectrum [64, 97]. These states are illustrated in Figure 4.9 with USDA calculation in one sequence. The first difference between the USDA calculation and experimental data appears in the prediction of the ground state and the first excited state. Although convergence of energy for the ground state and the first excited state, but with constrasting J values refer to an important indication about the difference between configuration mixing used in the USDA calculation and the real configuration of the nucleus.

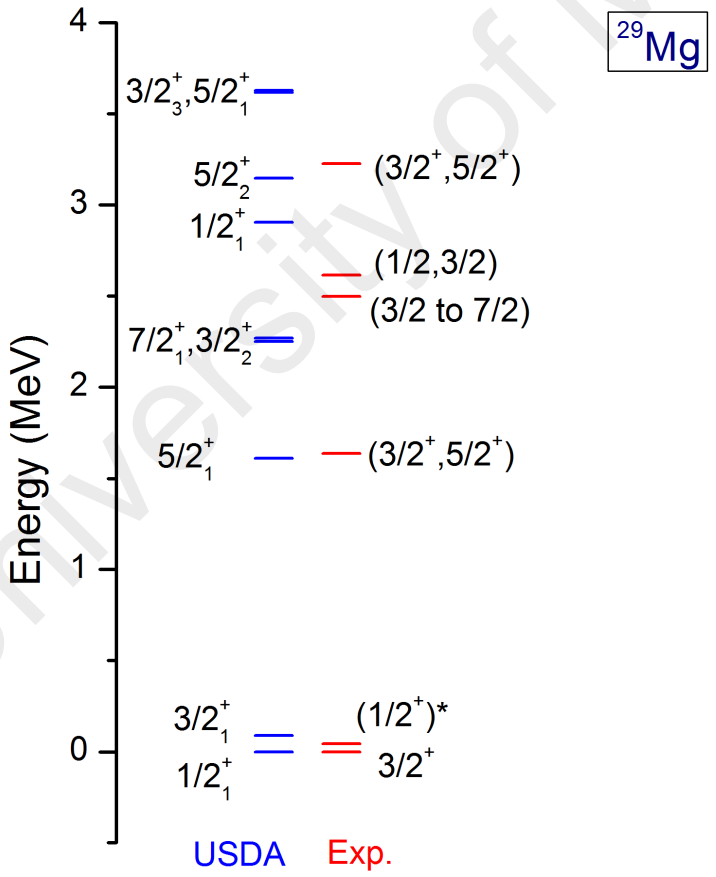

Figure 4.9: Comparison of the experimental energy levels with the energy levels calculated in the present theoretical work for the ^{29}Mg nucleus. The experimental data are taken from [64, 97], * refers to states with J value specified by [66].

This difference between the configurations led to the inaccuracy in the USDA predictions for the highest energy states as we can see in Figure 4.9. The reason of this inaccuracy is due to the nuclear structure of the ^{29}Mg nucleus. We have mentioned in the Section 2.7 that ^{29}Mg lies at the border of the "island of inversion" region. Island of inversion, located around Z = 10–12 and the magic N = 20, is an exotic part of the nuclear landscape where the nuclear ground states are much more deformed than expected for semi-magic nuclei. This behavior represents a collapse of the ordinary filling of the single-particle levels when neutrons occupying the *pf* shell before the lower *sd* shell is fully closed [65]. From the above it is clear that USDA is not the appropriate effective interaction that can be used in the calculations of the ^{29}Mg or the other higher odd-A magnesium isotopes because USDA is limited to the *sd* shell only. However, it is appropriate to use as an effective interaction that includes *pf and sd* shell model spaces for these isotopes.

CHAPTER 5

INELASTIC ELECTRON SCATTERING FORM FACTORS OF ^{25}Mg

5.1 Introduction

In Section 3.4, we have illustrated the mathematical formulae which are used to calculate the inelastic electron scattering form factors; both types of longitudinal and transverse. These formulae have shown the dependence of the form factors on the final and initial states wave functions or the Hamiltonian eigenvectors. In other words, the form factors values represent a rigorous test to evaluate USDA Hamiltonian and provide important knowledge on the nuclear structure of the target nucleus. As we mentioned in Chapter Two, the ^{25}Mg is the only odd-A magnesium isotope that has experimental data for the longitudinal and transverse electron scattering form factors. In Chapter Four, the comparison with experimental data showed a good accuracy for the eigenvalues and eigenvectors obtained from USDA calculations for ^{25}Mg isotope. Therefore, in this chapter we will employ the USDA Hamiltonian to calculate the longitudinal and transverse electron scattering form factors for this isotope.

The form factor calculations are based on the model space transition densities which combine the single-nucleon wave functions generated by the potential model [70].

Therefore, the potential is an important attribute in the form factor calculations that requires identification in this process. OXBASH program contains three types of potentials; harmonic-oscillator, Woods-Saxon and Skyrme interaction. In this work, the calculations are performed with these potentials and we only present the curves of the potential that shows a compatible results with the experimental data. For most excitations, the potential taken from Skyrme interaction showed the best results. The potentials can be analytically calculated using the Skyrme interaction in terms of the densities that resulted in rapid self-consistent calculations. The Skyrme interaction has been proven to be remarkably useful and successful for nuclear Hartree-Fock calculations. This interaction is based on a set of parameters that must be determined from the experimental data because it is a phenomenological interaction [10]. The default Skyrme interaction in OXBASH program, symbolizes by Sk20, is described in Reference [92] with details of all parameters and formulas. In the current work, we use the latest version of these parameters, symbolized by Sk42 [98].

In Section 5.2, we present the one-body transition density, OBTD. In Sections 5.3 and 5.4, the results of the theoretical longitudinal and transverse electron scattering form factors are presented and compared with the available experimental data, respectively.

5.2 One-Body Transition Density (OBTD)

The single-particle matrix elements are universal for all nuclear models since they only characterize the properties of the transition operators. The one-body transition densities (OBTDs), on the other hand, are model and case specific [99], and in the context of shell-model the expression for the OBTD given by Equation (3.49). The OBTD, represented in a compact form, which is the most general information needed to calculate the matrix elements of one-body operators between a given initial and final state [10] or in

other words, the OBTD contains all the information about transitions of given multipolarities, embedded in the model wave functions. In some references, the OBTD also known as one-body density matrix (OBDM) which is evaluated in a J-scheme basis [70] and it has the same values in the M-scheme. The calculated OBTD values which are used in this work are presented in Table 5.1. In this table, all the initial states are the ground state with $J=5/2^{+}$. The J_f and n_f are the total angular momentum and sequence number for the final state, respectively. E_{exp} is the experimental energy taken from [60, 97] and $E_{theo.}$ is the USDA prediction values. ΔJ determines the possible transition type from the multipolarity relation (3.28) , where ΔJ =1, 3 and 5 for magnetic transverse M1, M3 and M5, respectively , and ΔJ =2 for electric transverse E2 and / or longitudinal C2, and ΔJ =4 electric transverse E4 and / or longitudinal C4. $(n\ \ell\ j)_i$ and $(n\ \ell\ j)_f$ are the quantum numbers for the initial and final subshells. *OBTD* is the one-body transition density calculated using USDA Hamiltonian in proton – neutron formalism version (USDAPN).

Table 5.1: The USDA Hamiltonian one-body transition density (OBTD) matrix elements for each transition studied in this work in ^{25}Mg nucleus with $\Delta T=0$. The experimental energy is taken from [60, 97]. The definition of the terms in the table is explained in the text.

J_f	n_f	$E_{exp.}$(MeV)	$E_{theo.}$(MeV)	ΔJ	$(n\ \ell\ j)_i$	$(n\ \ell\ j)_f$	OBTD	
							Proton	Neutron
3/2	1	0.974	1.035	2	*1d5/2*	*1d5/2*	-0.05490	-0.17693
					1d5/2	*1d3/2*	-0.06300	-0.08043
					1d5/2	*2s1/2*	-0.04014	-0.00405
					1d3/2	*1d5/2*	0.07168	-0.24528
					1d3/2	*1d3/2*	-0.05922	-0.07005
					1d3/2	*2s1/2*	-0.00407	0.01129
					2s1/2	*1d5/2*	-0.04798	-0.36788
					2s1/2	*1d3/2*	0.00275	0.03094
				4	*1d5/2*	*1d5/2*	0.03222	0.07628
					1d5/2	*1d3/2*	0.02903	0.02713
					1d3/2	*1d5/2*	-0.04538	-0.21702

Table 5.1 (Continued.)

J_f	n_f	$E_{exp.}$(MeV)	$E_{theo.}$(MeV)	ΔJ	$(n\ell j)_i$	$(n\ell j)_f$	OBTD	
							Proton	Neutron
7/2	1	1.611	1.739	1	1d5/2	1d5/2	0.24688	-0.28368
					1d5/2	1d3/2	0.09438	-0.06034
					1d3/2	1d5/2	-0.06998	-0.07832
					1d3/2	1d3/2	0.03737	0.04533
					1d3/2	2s1/2	0.02945	0.02594
					2s1/2	1d3/2	-0.01353	-0.07044
					2s1/2	2s1/2	-0.00876	-0.03507
				2	1d5/2	1d5/2	0.74614	0.2362
					1d5/2	1d3/2	0.31902	0.27801
					1d5/2	2s1/2	0.34663	0.36697
					1d3/2	1d5/2	-0.30048	-0.32018
					1d3/2	1d3/2	0.08133	0.08431
					1d3/2	2s1/2	-0.16429	-0.15971
					2s1/2	1d5/2	0.55338	0.56743
					2s1/2	1d3/2	0.21122	0.16991
				3	1d5/2	1d5/2	-0.0214	-0.24781
					1d5/2	1d3/2	0.00134	-0.01237
					1d5/2	2s1/2	0.00967	0.01176
					1d3/2	1d5/2	-0.00656	-0.00583
					1d3/2	1d3/2	0.01039	0.0052
					2s1/2	1d5/2	-0.01446	-0.06678
				4	1d5/2	1d5/2	0.21688	0.02635
					1d5/2	1d3/2	-0.00253	0.02692
					1d3/2	1d5/2	0.01601	-0.05765
				5	1d5/2	1d5/2	-0.03308	0.37811
5/2	2	1.964	2.034	2	1d5/2	1d5/2	0.06439	0.07107
					1d5/2	1d3/2	0.03894	0.08143
					1d5/2	2s1/2	0.07006	0.02823
					1d3/2	1d5/2	-0.07208	0.06594
					1d3/2	1d3/2	0.02994	0.03898
					1d3/2	2s1/2	-0.02755	-0.03963
					2s1/2	1d5/2	0.00521	0.40507
					2s1/2	1d3/2	-0.01665	0.04167
				4	1d5/2	1d5/2	-0.05158	0.23973
					1d5/2	1d3/2	-0.06022	-0.04662
					1d3/2	1d5/2	0.07529	-0.01297

Table 5.1 (Continued.)

J_f	n_f	$E_{exp.}$(MeV)	$E_{theo.}$(MeV)	ΔJ	$(n\ell j)_i$	$(n\ell j)_f$	OBTD	
							Proton	Neutron
1/2	2	2.563	2.722	2	1d5/2	1d5/2	0.1358	0.14057
					1d5/2	1d3/2	0.07951	0.07879
					1d5/2	2s1/2	-0.01788	-0.00302
					1d3/2	1d5/2	-0.12181	-0.45313
					1d3/2	1d3/2	0.07572	0.10153
					1d3/2	2s1/2	0.03918	0.03857
					2s1/2	1d3/2	0.03823	0.22116
					2s1/2	1d3/2	-0.01951	-0.00515
3/2	2	2.801	2.868	2	1d5/2	1d5/2	0.12789	0.15314
					1d5/2	1d3/2	0.04458	0.00389
					1d5/2	2s1/2	0.04188	0.08456
					1d3/2	1d5/2	-0.10153	-0.41231
					1d3/2	1d3/2	0.06317	0.04007
					1d3/2	2s1/2	0.00449	0.01689
					2s1/2	1d5/2	0.04939	0.39369
					2s1/2	1d3/2	-0.03222	-0.06091
				4	1d5/2	1d5/2	0.01309	0.00108
					1d5/2	1d3/2	-0.06865	-0.0929
					1d3/2	1d5/2	0.05403	-0.20064
9/2	1	3.405	3.515	2	1d5/2	1d5/2	0.57224	0.18925
					1d5/2	1d3/2	0.25582	0.21305
					1d5/2	2s1/2	0.08321	0.24093
					1d3/2	1d5/2	-0.3053	-0.30754
					1d3/2	1d3/2	0.13028	0.12346
					1d3/2	2s1/2	-0.09927	-0.09559
					2s1/2	1d5/2	0.28222	0.29506
					2s1/2	1d3/2	0.08008	0.05081
				3	1d5/2	1d5/2	0.13551	-0.2148
					1d5/2	1d3/2	0.03425	-0.02721
					1d5/2	2s1/2	-0.04393	0.00217
					1d3/2	1d5/2	-0.07429	-0.10215
					1d3/2	1d3/2	-0.00026	-0.01522
					2s1/2	1d5/2	0.02409	0.09315
				4	1d5/2	1d5/2	0.26129	0.16461
					1d5/2	1d3/2	-0.07578	-0.09148
					1d3/2	1d5/2	0.18501	0.19611
				5	1d5/2	1d5/2	0.00417	-0.27563

Table 5.1 (Continued.)

J_f	n_f	$E_{exp.}$(MeV)	$E_{theo.}$(MeV)	ΔJ	$(n\ell j)_i$	$(n\ell j)_f$	OBTD	
							Proton	Neutron
9/	2	4.059	3.93	2	1d5/2	1d5/2	0.01042	0.22552
					1d5/2	1d3/2	0.0091	0.12201
					1d5/2	2s1/2	0.12893	0.16418
					1d3/2	1d5/2	-0.22466	-0.25496
					1d3/2	1d3/2	0.14729	0.14184
					1d3/2	2s1/2	0.00492	-0.0019
					2s1/2	1d5/2	0.05706	-0.00568
					2s1/2	1d3/2	-0.13216	-0.07951
				4	1d5/2	1d5/2	-0.19956	-0.14192
					1d5/2	1d3/2	-0.12721	-0.09662
					1d3/2	1d5/2	0.19026	0.18869
1	1	5.251	5.079	4	1d5/2	1d5/2	-0.14083	-0.02819
					1d5/2	1d3/2	-0.28082	-0.23595
					1d3/2	1d5/2	0.4703	0.53665

5.3 Longitudinal Form Factors

In this work, the longitudinal form factors are obtained by applying Equation (3.61). The effective charges for C2 transition (and E2 transverse) are taken from reference [95] with e_p = 1.36 and e_n = 0.45, while for C4 transition (and E4 transverse) are taken from reference [91] with e_p = 1.5 and e_n = 0.5.

Reference [84] showed the experimental values for the electron scattering longitudinal form factors for transition from ground state ($J^\pi = 5/2^+$) to the excited state with $J^\pi = 3/2^+$ at energy 0.974 MeV in the momentum transfer range 0.3 to 1.15 fm^{-1}. According to the multipolarity relation (3.28), there are two types of transitions C2 and C4 for this case. The theoretical and experimental results are illustrated in Figure 5.1.

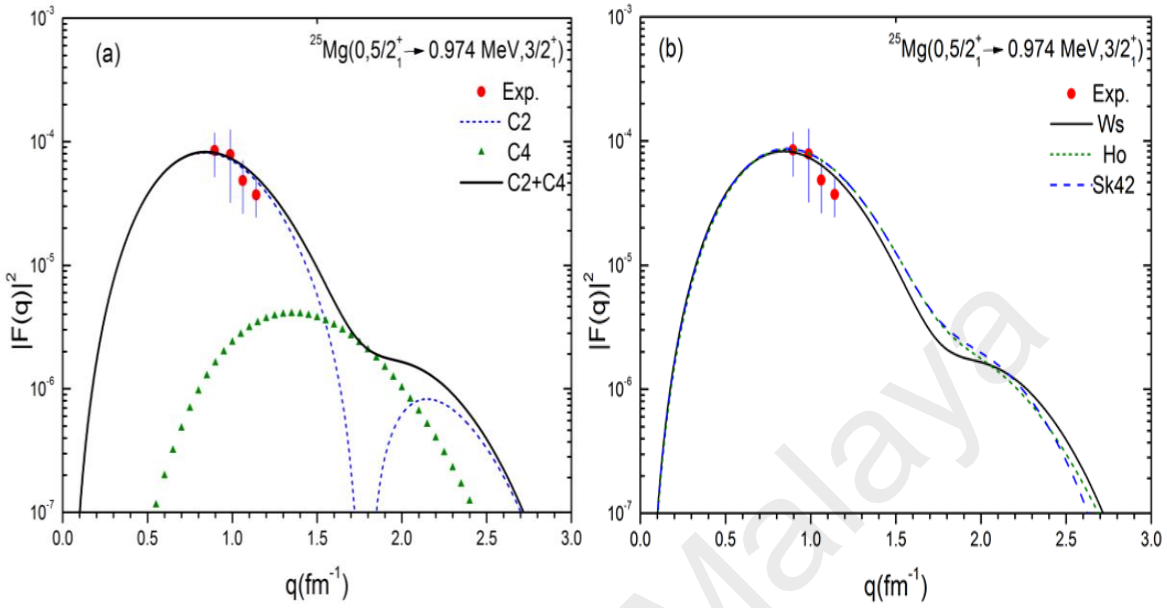

Figure 5.1: a- Longitudinal C2 and C4 electron scattering form factors for the $5/2^+_1 \rightarrow 3/2^+_1$ transition in the ^{25}Mg obtained using the Woods-Saxon potential and USDA Hamiltonian. b- The total longitudinal form factor obtained by the three potentials. The experimental data are taken from [84].

The theoretical calculation is performed for $q \leq 3\ fm^{-1}$ in order to show a wide range of theoretical values. The two types of transitions C2 and C4 are shown in Figure 5.1, (a) by using the Woods-Saxon potential [100] and (b) shows that the three potentials harmonic-oscillator, Woods-Saxon and Skyrme interactions which are used for this transition to investigate which interaction can estimate the experimental values better. The three potentials are in good agreement with the available experimental data. The C2 shows dominance in the region with $q \leq 1.5\ fm^{-1}$ while, for $q > 1.5\ fm^{-1}$ C4 becomes most dominant. The contribution for the quadrupole Coulomb transition C2 and the hexadecapole Coulomb transition C4 transition can be known from the values of the reduced transition probability of each transition. For this transition, the theoretical $B(C2,\uparrow)_{Theo.}$ is 3.16 $e^2\ fm^4$ and the experimental $B(C2,\uparrow)_{Exp.}$ is 2.3 ±0.6 $e^2\ fm^4$ [84], whereas

the theoretical B(C4,↑)$_{Theo.}$ is 314.2 $e^2\ fm^8$. The comparison between transition probabilities will be more prenounced if we convert B(C2↑) and B(C4↑) to the Weisskopf unit [$W.u.$] by using the following equations [10]:

$$B(C2\uparrow)[W.u.] = 16.820 * A^{\frac{-4}{3}} * B(C2\uparrow)e^2fm^4 \quad (5.1)$$

$$B(C4\uparrow)[W.u.] = 15.8633 * A^{\frac{-8}{3}} * B(C4\uparrow)e^2fm^8 \quad (5.2)$$

where A is the atomic mass number. Using Equations (5.1) and (5.2), we found B(C2↑)$_{Theo.}$ [$W.u.$] = 0.729 and B(C4↑)$_{Theo.}$ [$W.u.$] = 0.932 . It is clear that the probability of C4 transition is higher than the C2 which emphasizes the importance of C4 in this transition.

The longitudinal C2 and C4 form factors, obtained by using the USDA Hamiltonian and Skyrme interaction potential Sk42 [98], are in good agreement with the experimental data [83] as shown in Figure 5.2-(a), for the transition from the ground state to the first J=7/2$^+$ at energy 1.611 MeV. In this transition, C4 has a small contribution to the total form factor value whereas C2 is dominant for over all q. The comparison between the three potentials is shown in 5.2-(b).

The experimental transition strength B(C2↑)$_{Exp.}$ is equal to 158±7 $e^2\ fm^4$ [84] and the theoretical B(C2↑)$_{Theo.}$ = 152.1 $e^2\ fm^4$. The compatiblility between experimental and theoretical B(C2↑) values demonstrates the accuracy of the USDA Hamiltonian for this transition. The theoretical B(C4↑)$_{Theo.}$ = 232.9 e^2fm^8 and following the conversion to Weisskopf units we found B(C2↑)$_{Theo.}$ [$W.u.$] = 34.97 and B(C4↑)$_{Theo.}$ [$W.u.$] = 0.688. It is clear that the C2 dominates this transition.

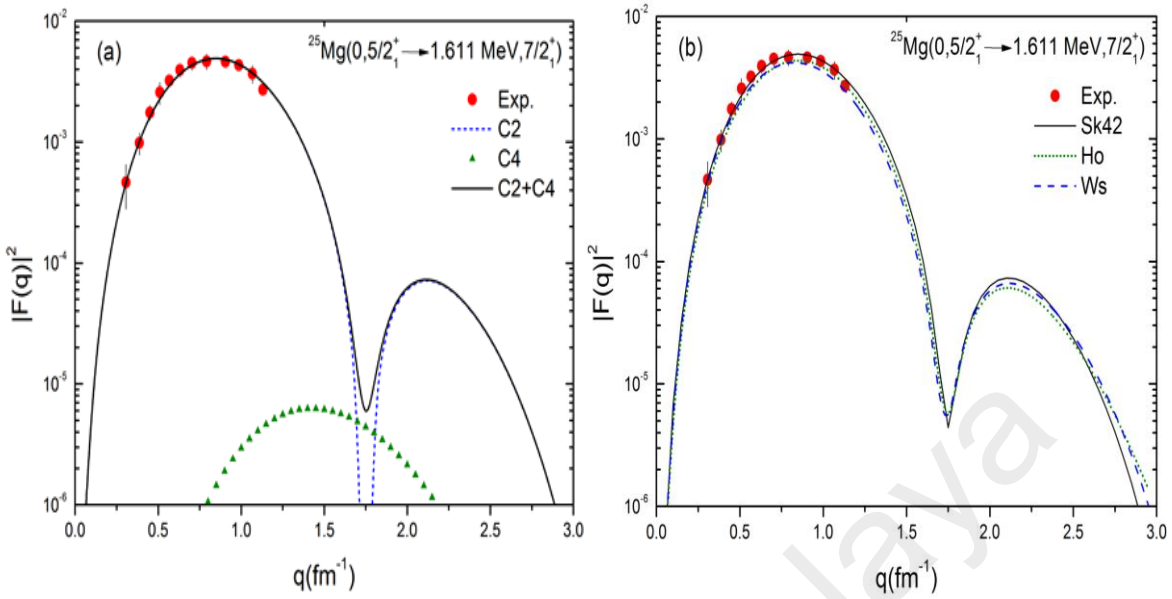

Figure 5.2: a-Longitudinal C2 and C4 electron scattering form factors for the $5/2_1^+ \rightarrow 7/2_1^+$ transition in the ^{25}Mg obtained using the Sk42 potential and USDA Hamiltonian. b-The total longitudinal form factor obtained by the three potentials. The experimental data are taken from [83].

The comparison between the theoretical and experimental data [84] C2 and C4 form factors for the transition $5/2_1^+ \rightarrow 5/2_2^+$ is shown in Figure 5.3. Obviously, the experimental measurements have been performed in the area of dominance C2. The C2 curve shows an acceptable agreement with the experimental data especially when the experimental errors are taken into account. On the other hand, the C4 is dominant within the range of q >1.5 fm^{-1} as that found in the transition $5/2_1^+ \rightarrow 3/2_1^+$ (Figure 5.1-(a)). The comparison between the three potentials is shown in Figure 5.3-(b).

Our theoretical results for this transition shows that B(C2↑) is the most probable transition than B(C4↑) in this excitation. The $B(C2\uparrow)_{Theo.}$ (3.23 $e^2\ fm^4$) is closed to the experimental $B(C2\uparrow)_{Exp.}$ value (3.0±0.5 $e^2\ fm^4$ [84]) and B(C4↑) is 130.5 $e^2\ fm^8$.

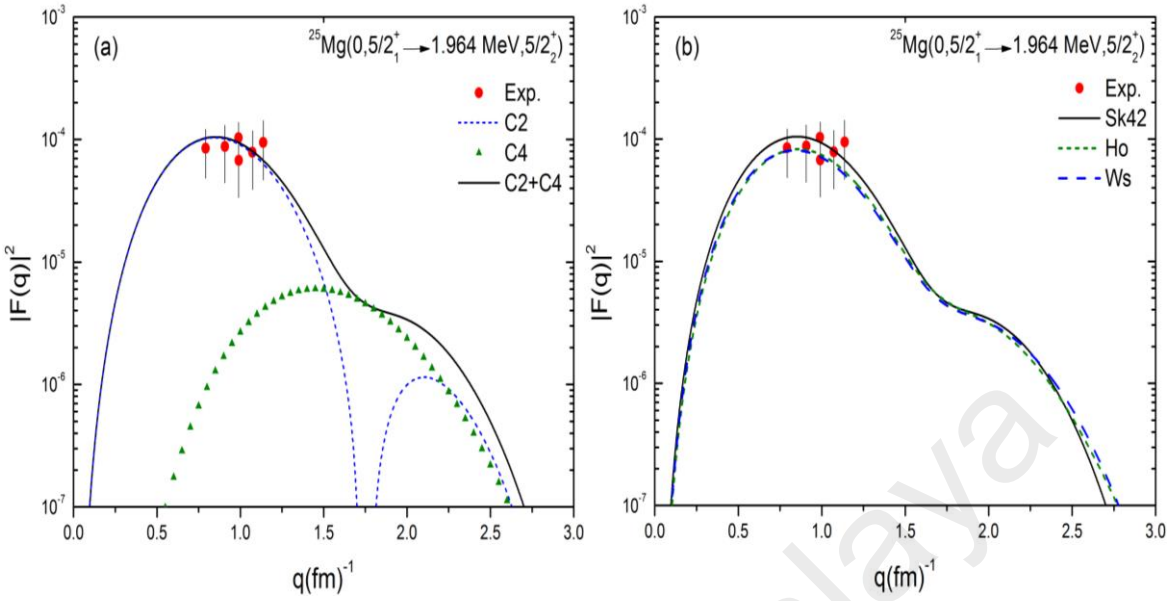

Figure 5.3: a-Longitudinal C2 and C4 electron scattering form factors for the $5/2^+_1 \rightarrow 5/2^+_2$ transition in the ^{25}Mg obtained using the Sk42 potential and USDA Hamiltonian. b-The total longitudinal form factor obtained by the three potentials. The experimental data are taken from [84].

According to the multipolarity relation (3.28), C2 is the only allowed electrical transition when ^{25}Mg is excited from the ground states to the excited state with J=$1/2^+_2$ at energy 2.563 MeV. The theoretical results when three potentials are used are shown in Figure 5.4. The best agreement between the theoretical C2 and the experimental data [84] was found when Sk42 potential is used. Reference [84] indicated that $B(C2\uparrow)_{Exp.}$ value for this transition equals to 4.3±0.8 $e^2\,fm^4$ and the theoretical calculation of $B(C2\uparrow)_{Theo.}$ is 4.95 $e^2\,fm^4$.

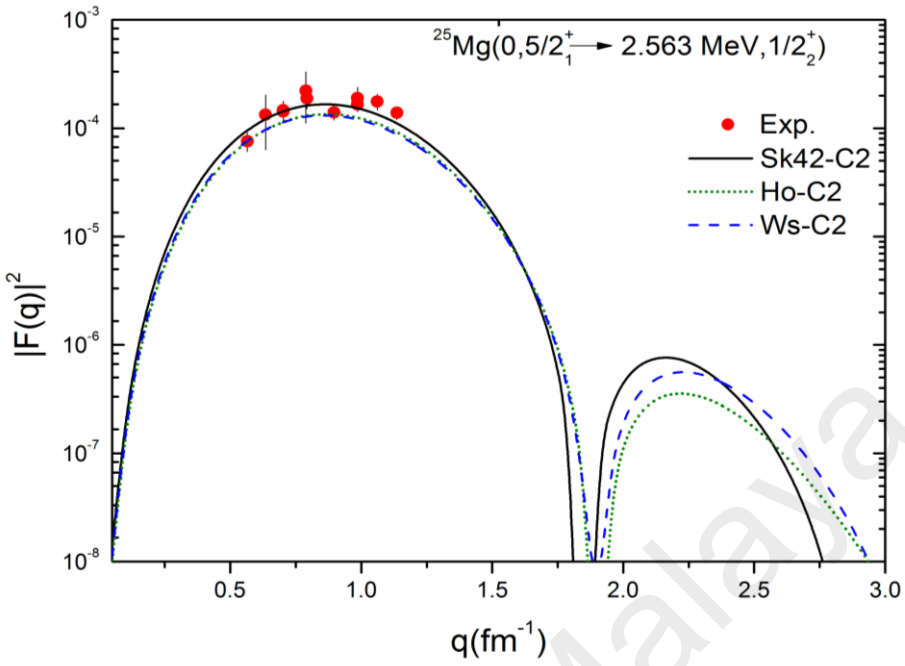

Figure 5.4: Longitudinal C2 electron scattering form factors for the $5/2^+_1 \rightarrow 1/2^+_2$ transition in the ^{25}Mg obtained using the three potentials potential and USDA Hamiltonian. The experimental data are taken from [84].

In Figure 5.5-(a), the theoretical C2 and C4 form factors are in good agreement with the experimental data for the *q* value ranging from 0.5 to 1.0 fm^{-1} when the ^{25}Mg nucleus is excited from the ground state to the excited state of J = $3/2^+_2$ at energy 2.801 MeV. We found that Sk42 potential is the best potential that agrees with the experimental data as we can see in Figure 5.5-(b). In this transition, the theoretical calculations show a predominance of C4 for the limited range of *q* that lies between 1.7 and 1.8 fm^{-1} with a clear dominance of C2 for the rest of the *q* values. The dominance of C2 also appears from the different between $B(C2\uparrow)_{Theo}[W.u.]$ = 1.46 and $B(C4\uparrow)_{Theo.}$ $[W.u.]$ = 0.144 where the probability of C2 is approximately tenfold of C4. The experimental B(C2↑) was found to be equal to 5.3±0.4 e^2fm^4 [84] while $B(C2\uparrow)_{Theo.}$ = 6.36 e^2fm^4.

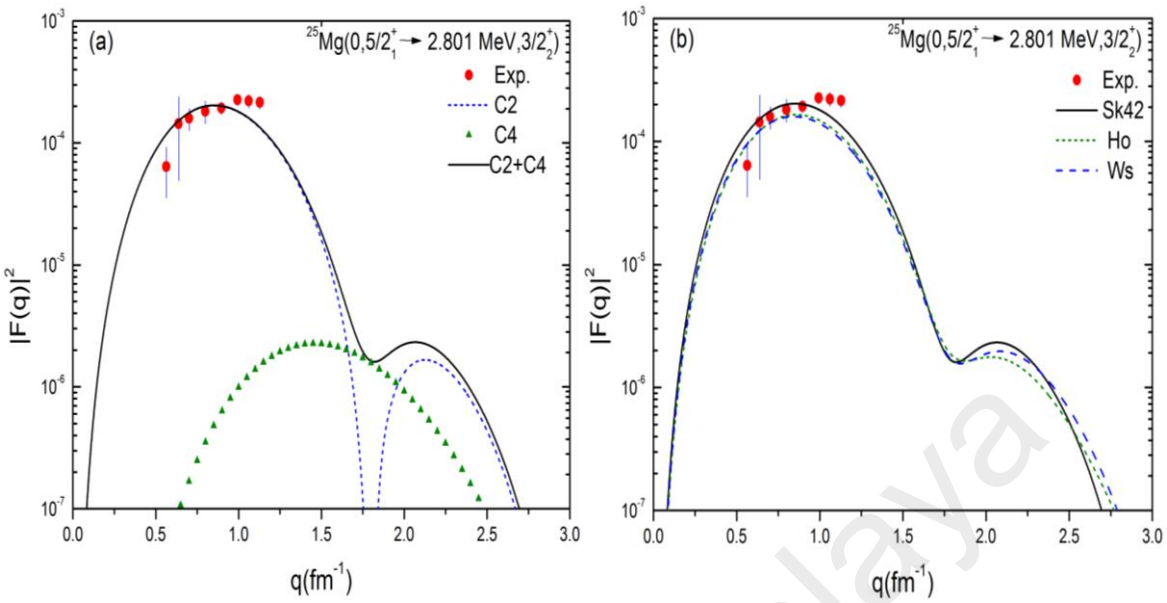

Figure 5.5: a-Longitudinal C2and C4 electron scattering form factors for the $5/2_1^+ \rightarrow 3/2_2^+$ transition in ^{25}Mg obtained using the Sk42 potential and USDA Hamiltonian. b- The total longitudinal form factor obtained by the three potentials. The experimental data are taken from [84].

Our calculation shows a good accuracy in the description of the longitudinal form factors C2 and C4 for the transition $5/2_1^+ \rightarrow 9/2_1^+$ at energy 3.405 MeV as shown in Figure 5.6. The comparison with the experimental data [83] indicates that C2 has the dominant contribution for most of the q values in this transition; in contrast C4 contribution is limited to $1.8 < q < 1.9$ fm^{-1}. The comparison between the three potentials is shown in Figure 5.6-(b). From this figure, all potentials are in good agreement with the experimental data. The quadrupole Coulomb transition probability B(C2↑) was found experimentally to be 57±4 e^2fm^4 [83] while the predicted value is $B(C2\uparrow)_{Theo.}$ = 57.29 e^2fm^4. The disparity between the probability of C2 and C4 in this excitation can be distinguished from the theoretical calculations, where we found that $B(C2\uparrow)_{Theo.}$ $[W.u.]$ = 13.18 and $B(C4\uparrow)_{Theo.}$ $[W.u.]$ = 0.427.

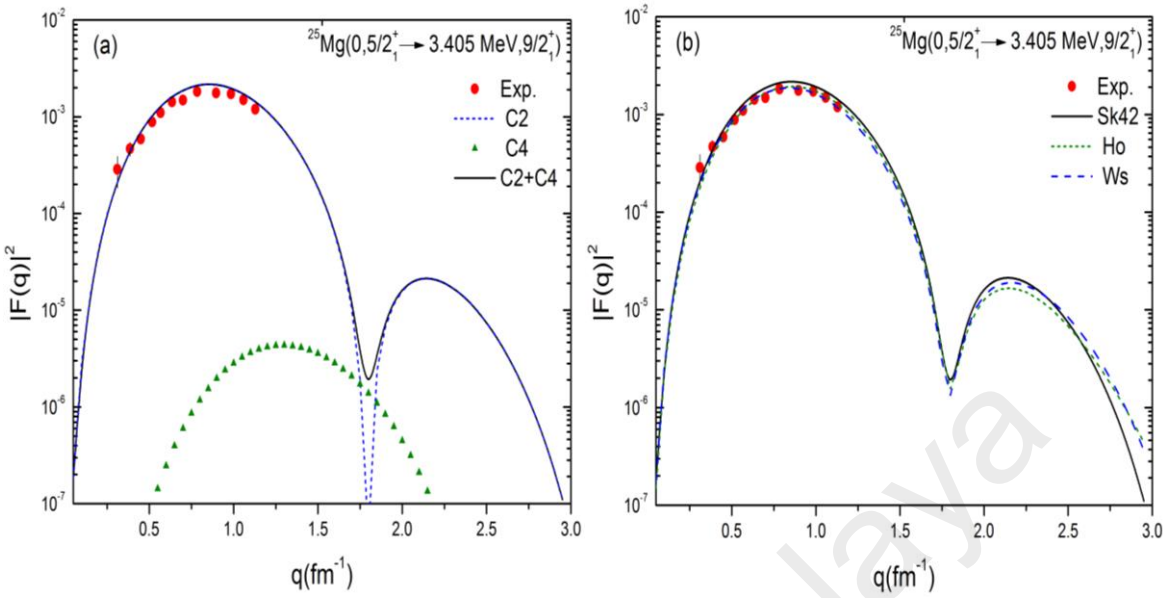

Figure 5.6: a-Longitudinal C2and C4 electron scattering form factors for the $5/2_1^+ \rightarrow 9/2_1^+$ transition in the ^{25}Mg obtained using the Sk42 potential and USDA Hamiltonian. b-The total longitudinal form factor obtained by three potentials. The experimental data are taken from [83].

The theoretical C2 and C4 values have shown results lower than the experimental data in the transition $5/2_1^+ \rightarrow 9/2_2^+$ with the excited energy 4.059 MeV as shown in Figure 5.7. None of the three potentials does a good job in describing the data for the transition. According to theoretical calculations for this excitation, C4 form factor has the largest contribution in this transition and this dominance is illustrated by $B(C2\uparrow)_{Theo.}$ $[W.u.]$ = 1.01 versus $B(C4\uparrow)_{Theo.}$ $[W.u.]$ = 14.26. Actually, we can say that the result using USDA and Sk42 potential are less accurate in this case in each of the longitudinal form factors and reduced transition C2 probability due to the difference between the $B(C2\uparrow)_{Exp.}$ = 9.6±1.0 e^2fm^4 [84] and $B(C2\uparrow)_{Theo.}$ = 4.41 e^2fm^4.

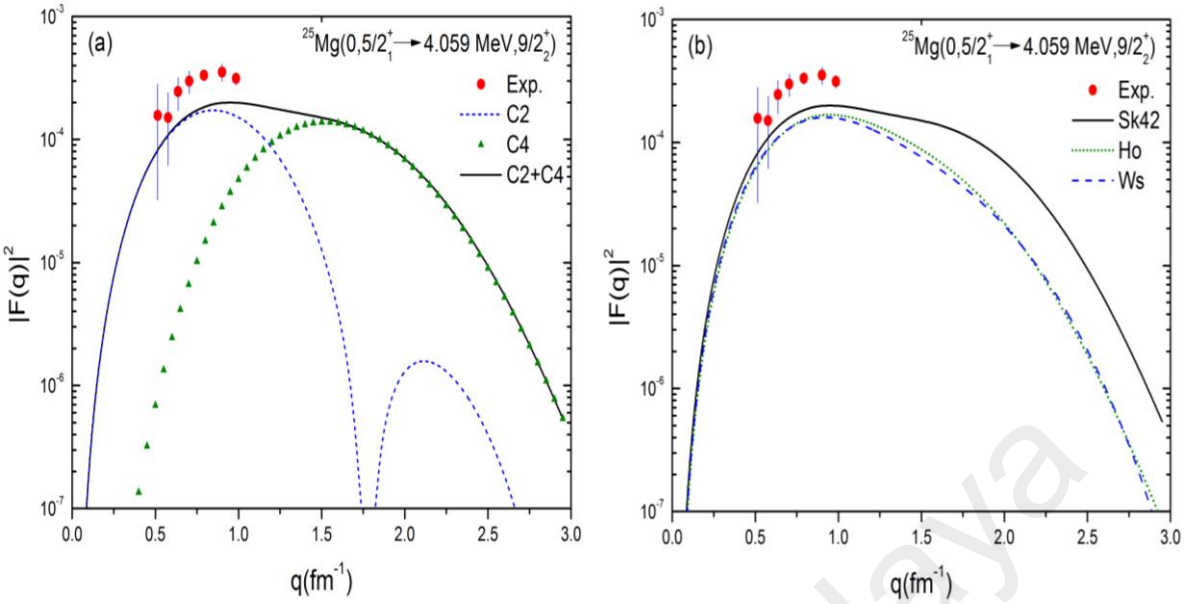

Figure 5.7: a-Longitudinal C2 and C4 electron scattering form factors for the $5/2_1^+ \rightarrow 9/2_2^+$ transition in the ^{25}Mg obtained using the Sk42 potential and USDA Hamiltonian. b-The total longitudinal form factor obtained by the three potentials. The experimental data are taken from [84].

The last available experimental longitudinal transition is $5/2_1^+ \rightarrow 11/2_1^+$ with excited energy 5.252 MeV. When applying the selection rule Equation (3.28), we find that C4 is the only allowed transition. In Figure 4.8, the calculation using USDA and three potentials produces results in good agreement with the experimental data for this excitation [84]. While $B(C4\uparrow)_{Theo.} = 10.11\times10^3\ e^2fm^8$ which is higher than the experimental value $B(C4\uparrow)_{Exp} < 6.5\times10^3$ [84]. It is worth mentioning that all the longitudinal form factors are in good agreement for all states of different *J* (3/2, 7/2, 9/2 and 11/2) and energy (0.974, 1.611, 3.405 and 5.252 MeV) in the first sequence. While the agreement of the calculated longitudinal form factors with the experimental data varies for the excitations of the states in the second sequence. From Figures 5.3, 5.4, 5.5 and 5.7, it is possible to observe that the accuracy in the calculations depends on the state energy value in inverse proportion.

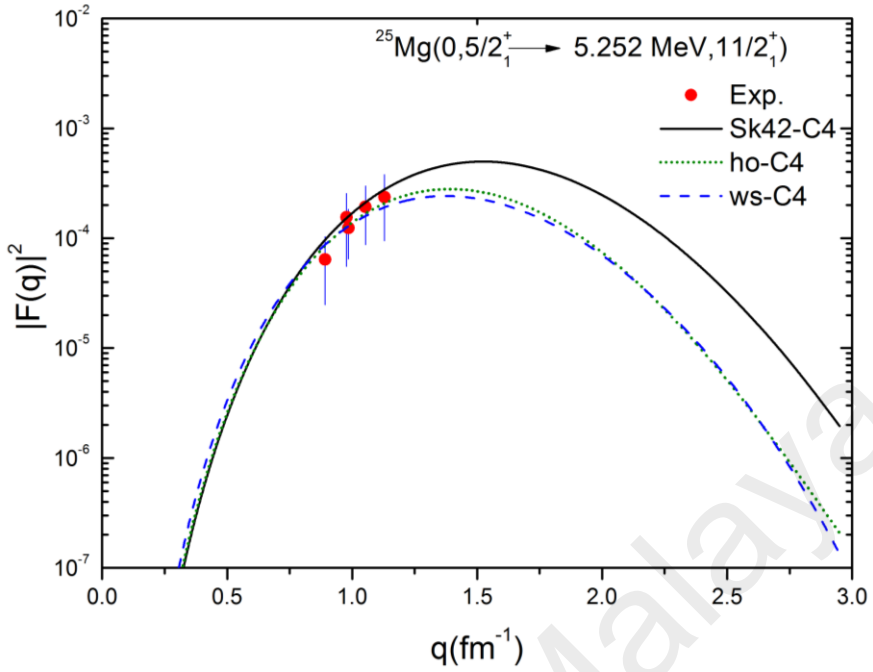

Figure 5.8: Longitudinal C2and C4 electron scattering form factors for the $5/2^+_1 \rightarrow 11/2^+_1$ transition in ^{25}Mg nucleus obtained using the three potentials and USDA Hamiltonian. Experimental data from [84].

5.4 Transverse Form Factors

The general formula used to calculate the transverse form factor has been given in Equation (3.41) which includes two parts: magnetic and electric transverse form factors. Therefore, we have mixed multipolarities for every excitation in the odd nucleus according to the selection rule, Equation (3.28).

In this work, the transverse form factors for inelastic scattering on ^{25}Mg have already been calculated using OXBASH code. Results of the OXBASH code are compared with available experimental data and the theoretical results obtained from employing the Michigan three-range Yukawa (M3Y) interaction [101] with the shell-model code CPM3Y. The details of this code are given in reference [102]. The OXBASH and CPM3Y codes use

the same OBTD values which are obtained from the USDA Hamiltonian as listed in Table 5.1. In the CPM3Y code, the reduced matrix elements consist of two parts, one is for the model-space (MS) matrix elements, and the other is for the core polarization (CP) matrix elements, whereas in the OXBASH code, the core-polarization effects are introduced through effective charges and effective g factors by considering that the core-polarization is one of the model-space truncation effects as we have clarified at the end of Chapter Three. Therefore, the comparison between the two theoretical models shows the core-polarization effects from the perspective of both models.

The electron excites the ^{25}Mg nucleus from the ground state to the $7/2_1^+$ state with the excitation energy of 1.698 MeV [85]. The total transverse form factor for this transition has mixed multipolarities as shown in Figures 5.9 and 5.10. The theoretical individual multipoles are shown in the same figures. The calculated individual multipoles values are obtained by using the USDA and Sk42 potential for OXBASH and the results are shown in Figure 5.9. The new g factors values (g_s *(p)* = 5.0, g_s *(n)* = -3.5, g_l *(p)* = 1.175, and g_l *(n)* = -0.106) [95] are used in the M1 and M3 magnetic transitions calculations, and the free-nucleon g factors are used for M5 [103]. The new effective charge (e_p = 1.36 and e_n = 0.45) are used with M1 and E2 calculations while e_p = 1.5 and e_n = 0.5 [91] are used for the M3, E4 and M5 transitions. In Figure 5.9, the curves of M1 and M3 are cut out for high q values for more obvious viewing and the values are taken into consideration in total range from $0 < q < 3$ fm^{-1}. The main contribution in most of the regions of q comes from M1 and M5. M1 has the dominant contribution in the region between 0 and 1.05fm^{-1} and M5 has the dominant contribution in the range of momentum transfer from 1.1 to 3.0 fm^{-1}. The total transverse form factor (as a solid curve) is in good agreement with the available experimental data. The results of our calculations using CPM3Y code are shown in Figure

5.10. A comparison between Figure 5.9 and Figure 5.10 shows approximately similar individual dominant contribution for every multipoles with the remarkable agreement for the OXBASH data in the region q < 1.75 fm^{-1}. The total transverse form factor from the CPM3Y code is closed to the experimental data of the sum of M1+E2+M3+M5 although the OXBASH calculations containing all the allowed multipolarities, M1+E2+M3+E4+M5 for this transition.

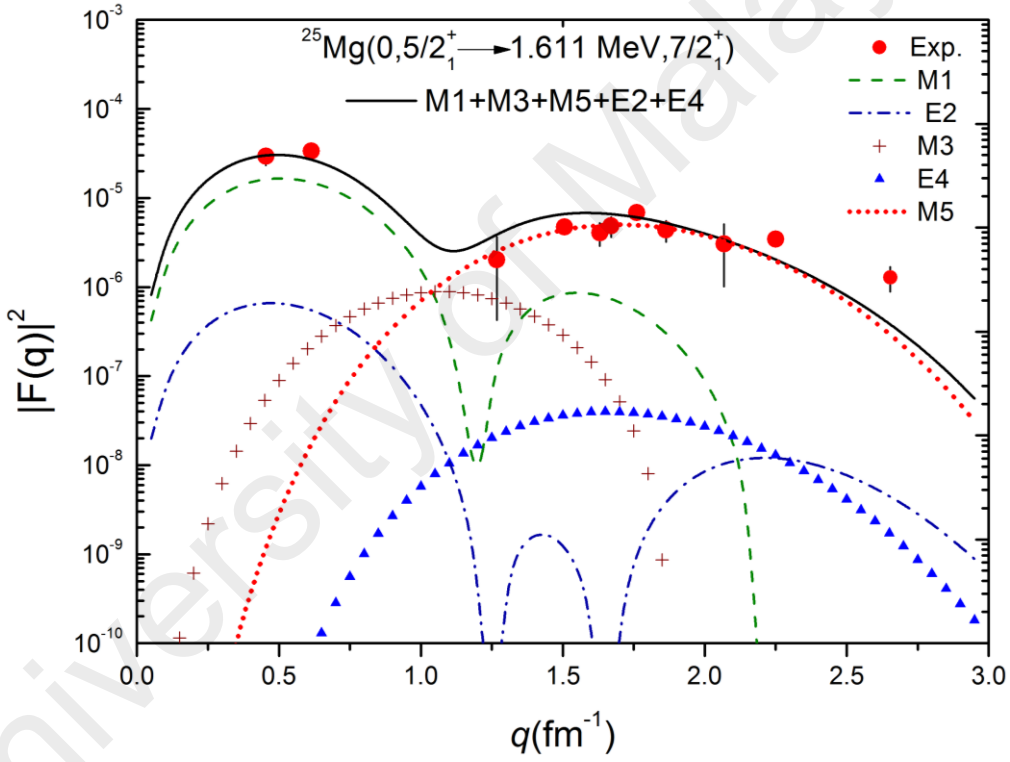

Figure 5.9: Transverse M1, E2, M3, E4, and M5 electron scattering form factors for the $5/2_1^+ \rightarrow 7/2_1^+$ transition in ^{25}Mg nucleus obtained with the Sk42 potential and USDA Hamiltonian using OXBASH code. Experimental data from [85].

Agreements in the data shown in Figure 5.9 indicate that the new values of the free-space of the one-body operator's constants (effective charges and g factors) is a good assignment to describe the core-polarization effects.

The OXBASH code is used to calculate the transverse form factor for the transition $5/2_1^+ \rightarrow 9/2_1^+$ by employing the USDA effective interaction and Sk42 potential. The individual multipoles of E2, M3, E4 and M5 are shown in Figure 5.11 with the total transverse form factor (E2+M3+E4+M5) shown as a solid curve.

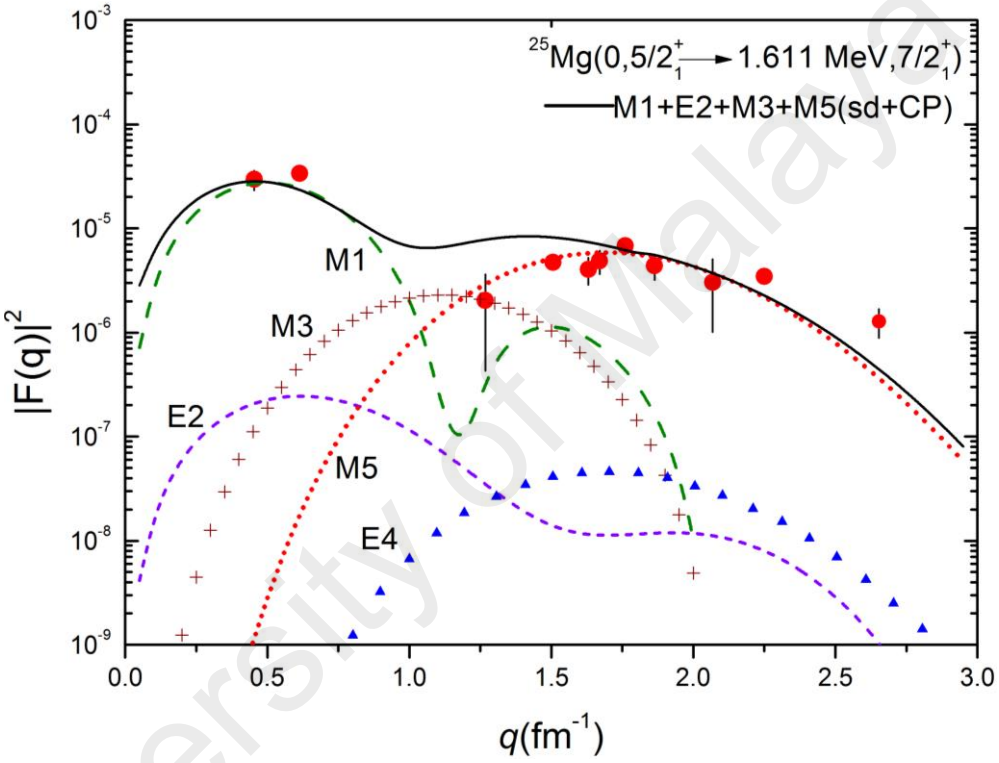

Figure 5.10: Transverse M1, E2, M3, E4, and M5 electron scattering form factors for the $5/2_1^+ \rightarrow 7/2_1^+$ transition in ^{25}Mg nucleus calculated with the core-polarization effects on the sd-shell-model wave function using the CPM3Y code. Experimental data from [85].

From the comparison with the experimental data [85] , the theoretical results (total transverse form factor) are less than the experimental data. On the other hand, we find that the results of CPM3Y code (E2+M3+M5), shown in Figure 5.12, overestimate the experimental data when the same OBTD obtained from USDA are used [102]. We can

analyze this case as follows: the difference between OXBASH and CPM3Y results indicate the presence of significant core-polarization effects in this excitation. We have mixed multipolarities of four types E2, M3, E4 and M5. The electrical multipolarities E2 and E4 show good agreement with the longitudinal transition as shown in Figure 5.6. This means that it is appropriate to use the effective charges and effective g factors to describe the core-polarization effects for this electrical multipolarities transition. The individual multipoles M3 is sensitive to the experimental data and describes it very well in the momentum-transfer range $1.25 < q < 1.6\ fm^{-1}$. The M5 is the residual multipoles which has the dominant contribution in the experimental data range. Compared with the CPM3Y results, we could attribute the differences to the significant core-polarization effects in the M5 excitation. To investigate this effect, we change the free-space values for the M5 excitation which are in this case the g factors values. In Figure 5.11, we use the following free-nucleon g factors values: $g_s(p) = 5.586$, $g_s(n) = -3.826$, $g_l(p) = 1.0$, and $g_l(n) = 0$. The calculations are individually achieved with different values for every g component, and we found that the M5 form factor has higher sensitivity to $g_s(n)$ than to the other components $g_s(p)$, $g_l(p)$, and $g_l(n)$. We have identified the value of $g_s(n) = -5.5$ and an increase of 43% in the absolute $g_s(n)$ value, as the best value used to obtain M5 and total form factor estimate the experimental data for the transition $5/2_1^+ \rightarrow 9/2_1^+$, as shown in Figure 5.13.

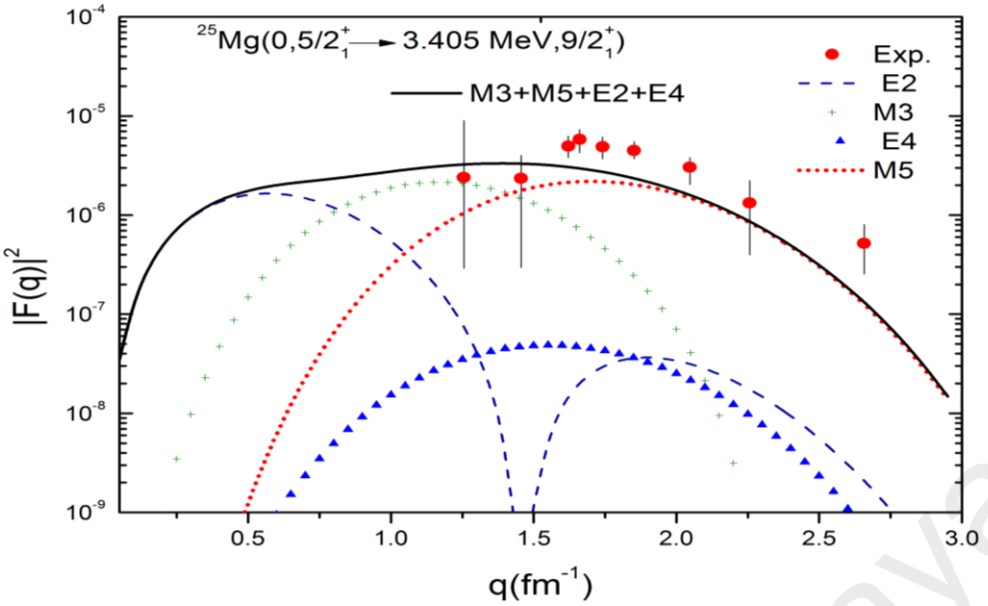

Figure 5.11: Transverse E2, M3, E4, and M5 electron scattering form factors for the $5/2_1^+ \rightarrow 9/2_1^+$ transition in ^{25}Mg nucleus obtained with the Sk42 potential and USDA Hamiltonian using OXBASH code. Experimental data from [85].

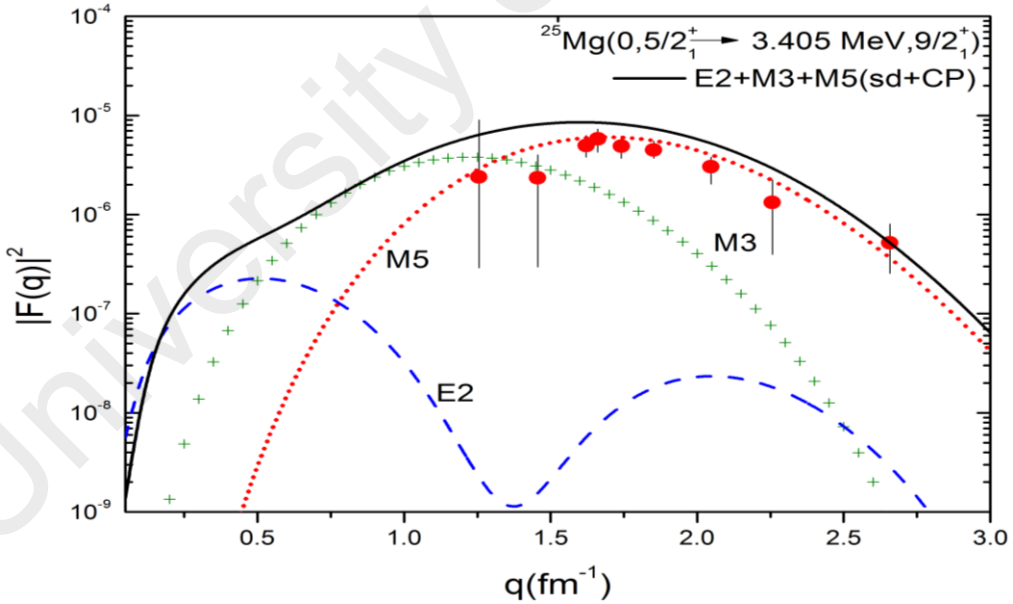

Figure 5.12: Transverse E2, M3, E4, and M5 electron scattering form factors for the $5/2_1^+ \rightarrow 9/2_1^+$ transition in ^{25}Mg nucleus calculated with core-polarization effects on the sd-shell-model wave function using CPM3Y code. Experimental data from [85].

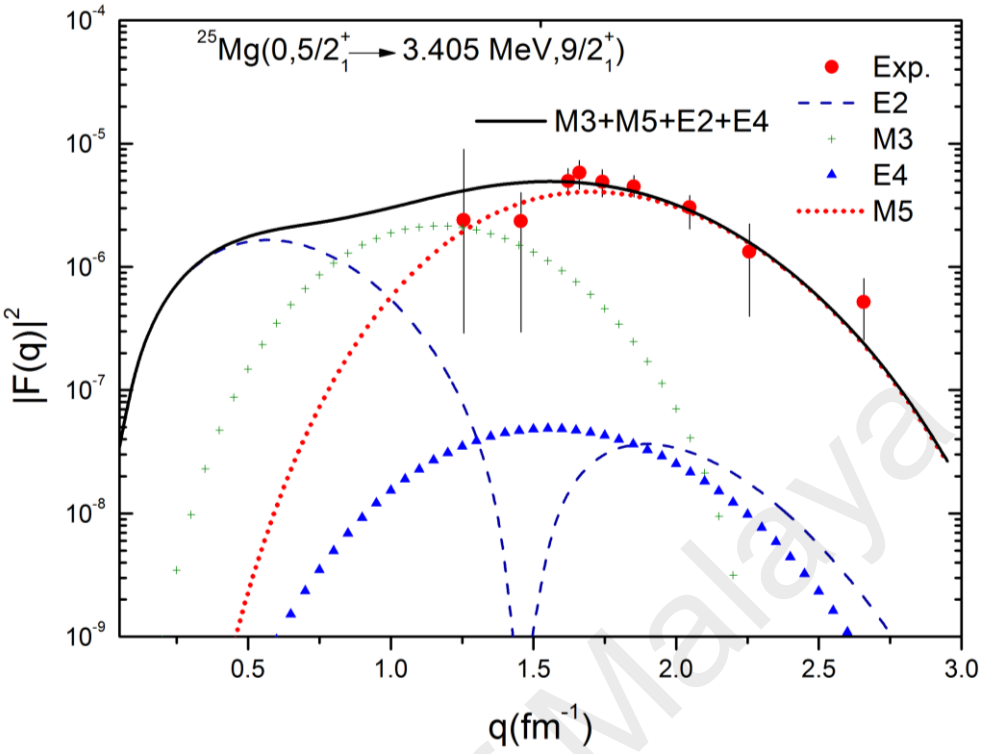

Figure 5.13: Transverse E2, M3, E4, and M5 electron scattering form factors for the $5/2_1^+ \rightarrow 9/2_1^+$ transition in ^{25}Mg nucleus obtained with the Sk42 potential, USDA Hamiltonian using OXBASH code and free-nucleon g factors with $g_s(n) = -5.5$ in the M5 calculation. Experimental data from [85].

CHAPTER 6

CONCLUSIONS AND FUTURE WORK

6.1 Introduction

In this thesis, comparison is made between theory and recent experiment of corresponding levels in odd-magnesium isotopes with neutron numbers between 9 and 17 based on energies, reduced electromagnetic transition strengths, multipole mixing ratios, and electron scattering form factors. The results obtained by employing the new sd-shell interactions USDA (universal sd-shell interaction A). Analyses of the theoretical results and experimental data have given a clear indication about the efficiency of the USDA Hamiltonian in the calculation of the nuclear structure of these isotopes. The USDA Hamiltonian efficiency has been investigated through the correspondence of its eigenvalues to the states energy and eigenvectors corresponding to the transition strengths and electron scattering form factors. In this chapter we will present our conclusions in two sections; the first is for the isotopes states energy and the second for the reduced electromagnetic transitions and electron scattering form factors. In the third section, we will present our suggestions for future work.

6.2 Isotopes States Energies

The energy states adopted in this research are of all available experimental data with non-negative parity. The study included excitation energies up to 10 MeV for most

isotopes. The results of our calculations have verify some states found experimentally and suggested some new ones in the isotope spectra where USDA shows good accuracy. The first state suggested in this work is J= $9/2_1^+$ at energy less than 3.643 MeV in the ^{21}Mg spectrum which is not observed experimentally. This suggestion is based on the reasonable agreement found between the observed states and the theoretical results obtained from USDA effective interactions in the first and second sequences for the ^{21}Mg spectrum. The USDA calculations of the energy levels show good agreement with the new experimental data in the first three sequences for all J values considered for the ^{23}Mg nucleus. According to the new experimental data and the theoretical calculations, a new rearrangement has been proposed for the states with J = $3/2^+$ and $5/2^+$. Our results show the need to experimentally investigate the J = $3/2^+$ states in ^{23}Mg spectrum.

The USDA calculations have confirmed the existence of the J = $13/2^+$ state in the second and third sequences as well as the J = $11/2^+$ and J = $7/2^+$ states in the third sequence in the ^{25}Mg spectrum where the existence of these states has previously been uncertain. The confirmation is based on the agreement between the theoretical and experimentally observed states for all three sequences. Other states have been confirmed according to the USDA calculation for sequences higher than three. The theoretical investigation using multipole mixing ratio calculations have confirmed many energy states in ^{25}Mg. Some successful confirmations have been obtained for some individual states by identifying the equivalent theoretical state and for the grouped energy level states. The good agreement between the theoretical and experimental states in the ^{27}Mg spectrum suggests a value for J = $13/2^+$ in the first sequence as well as values for the J = $11/2^+$ and $13/2^+$ states in the second sequence. All states that have been confirmed and suggested in this work are listed in Table 6.1. A poor agreement is found in the comparison between the experimental data

and theoretical results for the ^{29}Mg spectrum. This disagreement is due to the collapse of the ordinary filling of the single-particle levels in this nucleus when neutrons occupying the *pf* shell before the lower *sd* shell is fully closed and that is what makes USDA inadequate for these calculations. In general, the USDA shows an acceptable accuracy for the excited energy states especially if it compared to the realistic Hamiltonians, for example SDBA [104].

Table 6.1: Confirmed and suggested states for odd- Mg in this work

Isotope	J^+	***n***	$E(MeV)_{Theo.}$	$E(MeV)_{Exp.}$	***Status***
^{21}Mg	3/2	1	1.849	1.651	*confirmed*
	9/2	1	1.730	-	*suggested*
	9/2	2	3.439	3.643	*suggested*
	1/2	2	4.259	4.010	*confirmed*
^{23}Mg	1/2	2	4.555	4.353	*confirmed*
	7/2	3	5.363	5.689	*confirmed*
	3/2	3	6.044	-	*suggested*
	1/2	3	6.317	-	*suggested*
	9/2	3	6.198	6.238	*confirmed*
	7/2	4	6.575	6.512	*confirmed*
	15/2	1	8.929	8.943	*confirmed*
	19/2	1	14.623	14.560	*confirmed*
^{25}Mg	7/2	3	4.965	5.012	*confirmed*
	11/2	3	6.067	6.040	*confirmed*
	13/2	2	7.440	7.551	*confirmed*
	13/2	3	8.059	8.011	*confirmed*
	9/2	8	8.099	8.011	*confirmed**
	7/2	11	8.136	8.119	*confirmed**
	9/2	9	8.482	8.267	*confirmed**
	11/2	6	8.500	8.532	*confirmed**
	7/2	12	8.661	8.532	*confirmed**
	15/2	1	9.491	10.653	*confirmed*
^{27}Mg	7/2	1	3.030	3.109	*confirmed*
	7/2	2	3.487	3.427	*confirmed*
	9/2	1	4.019	3.884	*confirmed*
	9/2	2	4.310	4.398	*confirmed*
	7/2	3	4.733	4.776	*confirmed*
	9/2	3	5.239	-	*suggested*
	11/2	1	6.185	-	*suggested*
	11/2	2	6.823	-	*suggested*
	13/2	1	7.330	-	*suggested*
	13/2	2	7.819	-	*suggested*

* Confirmation based on multipole mixing ratio; see Chapter four for more details.

6.3 Electromagnetic Transition and Electron Scattering Form Factors

We now briefly summarize the main conclusions that may be reported from the calculation of the electromagnetic transition and electron scattering form factors in this work. One of the main advantages of these calculations is the dependence of the electromagnetic transition and the electron scattering form factors on the eigenvalues and eigenvectors of USDA Hamiltonian. Therefore, these calculations represent a comprehensive measure of the Hamiltonian efficiency established by the OBTD values.

For B(E2) and B(M1) values, the USDA approaches the available experimental data for ^{25}Mg and ^{23}Mg, while the USDA accuracy decreases with ^{27}Mg results. The Skyrme interaction (SK42) [98] is found to be the best than the other potential available in the OXBASH code to obtain better agreement between the experimental and theoretical results of the two form factors considered in this work. For ^{25}Mg nucleus, the results of the longitudinal form factors C2 and C4 are reproduced well data for low momentum transfer q < 1.2 fm^{-1} according to the available experimental data. Our calculations have shown a clear significance of the C4 transition especially for the region q > 1.2 fm^{-1}. The longitudinal form factor results show a reasonable accuracy of USDA in the cases of excitation to the first sequence states of the ^{25}Mg nucleus and this accuracy varies in the second sequence according to the energy of the excited state in inverse proportion.

The OBTDs obtained from USDA are appropriate to calculate the transverse form factors using OXBASH and CPM3Y codes. This is due to the good agreement with the available experimental data for the excitation to the J=$7/2_1^+$ state in ^{25}Mg nucleus. The theoretical results are in discrepancy with the experiment data for the transverse form

factors observed in the transition to the J=$9/2_1^+$ state. The interesting point in the calculations of the mixed multipolarities transverse form factors in the above cases is the sensitivity of M5 to the experimental data.

We found that the effective charges and effective g factors are necessary to describe the core-polarization effects in the OXBASH code calculations. The new effective charge (e_p = 1.36 and e_n = 0.45) and g factors ; g_s *(p)* = 5.0, g_s *(n)* = -3.5, g_l *(p)* = 1.175, and g_l *(n)* = -0.106 [95] are appropriate to show results close to the experimental values for the M1, E2 and M3 transitions. On the other hand, the effective charge e_p = 1.5 and e_n = 0. 5 are the appropriate values that can be used with E4, and the free-nucleon g factors with M5. We have found in this work that g_s*(n)* = -5.5 is the appropriate coefficient to estimate the M5 transverse form factors from the experimental data for the transition to the J=$9/2_1^+$ state .

6.4 Future Work

It is suggested to work on the following topics:

1- Extending the employing of the USDA Hamiltonian to calculate the nuclear structure of even magnesium isotopes and neighboring nuclei due to the success of the USDA in the description this the region. The theoretical values will be useful to fill the void in the knowledge of the nuclear structure of these isotopes.

2- Using the USDA values in large model space in order to minimize the core-polarization effects for down extension (*p*- shell) and contain the effects of islands of inversion in the upper extension (*fp*- shell).

3- The good description of USDA for odd magnesium isotopes structure urges us to use the USDA for calculating other nuclear characteristics in these isotopes for example, Gamow- Teller strengths and spectroscopic factors.

4- The importance of the the various constants of the one-body operator (effective charge and g factors) in the nuclear structure calculations and the possibility of changing these values according to the recent research making the development of a mathematical formula to find these values an urgent need.

LIST OF PUBLICATIONS

1. Khalid S. Jassim, Anwer A. Al-Sammarraie, Fadhil I. Sharrad, and Hasan Abu Kassim (2014), in *Elastic and inelastic electron-nucleus scattering form factors of some light nuclei:(*^{23}*Na,* ^{25}*Mg,* ^{27}*Al, and* ^{41}*Ca)*, Physical Review C, Vol. 89, pp. 014304.

2. Anwer A. Al-Sammarraie, Fadhil I. Sharrad, A. A. Aziz, Norhasliza Yusof, and Hasan Abu Kassim (2014), in *Application of USDA and SDBA Hamiltonians in calculating the excited states of odd-A magnesium isotopes*, The European Physical Journal Plus, Vol. 129, pp. 125.

APPENDIX A

The Empirical Effective Interaction Fitting Method

The starting point for the fitting method is rewrite equation (1.12) as [7, 15]:

$$H = \sum_{i=1}^{p} x_i O_i \qquad (A.1)$$

where x_i represent the single-particle energies or two-body matrix elements, O_i stand for the operators n_a and scalar two-body density, respectively. The Hamiltonian has eigenvectors ϕ_k and eigenvalues λ_k and we can express in terms of linear combination of the Hamiltonian $\vec{x}$:

$$\lambda_k = \langle \phi_k | H | \phi_k \rangle = \sum_{i=1}^{p} x_i \langle \phi_k | O_i | \phi_k \rangle = \sum_{i=1}^{p} x_i \beta_i^k \qquad (A.2)$$

The eigenvalues λ_k standard deviation can be found from:

$$\chi^2 = \sum_{k=1}^{N} \left(\frac{E_{exp}^k - \lambda_k}{\sigma_{exp}^k} \right)^2 \qquad (A.3)$$

where E_{exp}^k are the experimental energies and σ_{exp}^k are the associated errors. The minimization condition for this quantity with respect to x_i is:

$$\frac{\partial \chi^2}{\partial x_j} = \sum_{k=1}^{N} 2 \frac{\left(E_{exp}^k - \lambda_k\right)}{\left(\sigma_{exp}^k\right)^2} \frac{\partial}{\partial x_i} \left(-\sum_{i=1}^{p} x_i \beta_i^k\right) = 0 \quad . \tag{A.4}$$

By assuming that the β_i^k dependent on x_i is weak, this leads to $\frac{\partial \beta_i^k}{\partial x_i} = 0$ [16] and it produces to:

$$\frac{\partial}{\partial x_j} \left(-\sum_{i=1}^{p} x_i \beta_i^k\right) = \beta_j^k \tag{A.5}$$

where *j=1, 2, 3,..., p*. We will get the following *p* linear equations:

$$\sum_{k=1}^{N} \left(E_{exp}^k - \sum_{i=1}^{p} x_i \beta_i^k \right) \frac{\beta_j^k}{\left(\sigma_{exp}^k\right)^2} = e_j - \sum_{i=1}^{p} \gamma_{ij} x_i = 0 \quad . \tag{A.6}$$

The last term can be written in a $p \times p$ matrix:

$$G = \left(\gamma_{ij}\right) = \sum_{k=1}^{N} \frac{\beta_i^k \beta_j^k}{\left(\sigma_{exp}^k\right)^2} \tag{A.7}$$

and we have a *p*- dimensional vector

$$\vec{e} = (e_i) = \sum_{k=1}^{N} \frac{E_{exp}^k \beta_i^k}{\left(\sigma_{exp}^k\right)^2} \tag{A.8}$$

where we can write the final form of Equation (A.8) in terms of *i* [7, 15] or keeping it in terms of *j* [27]. This can be expressed through:

$$G\vec{x} = \overrightarrow{e} \quad . \tag{A.9}$$

G is a real symmetric matrix ($\beta_i^k \equiv \beta_j^k$) and we can obtain any new interaction $\vec{x}$ by:

$$\vec{x} = G^{-1}\vec{e} \, . \tag{A.10}$$

In Equation (A.10), G^{-1} is referred to the error matrix. In this fitting procedure not all matrix elements are well determined because of their dependence on available experimental data. To solve this problem, the Linear Combination (LC) method is used which we can separate the well determined from the poorly determined parameters. From Equation (A.10) if *G* is real symmetric matrix, it can be diagonalized and the least-squares fit can then be reformulated in terms of uncorrelated linear combinations of the TBME or in the other words they are orthogonal parameters:

$$D = AG^{-1}A^{T} . \qquad (A.11)$$

D is a *p-dimensional* diagonal matrix with positive elements D_i. From Equation (A.9) we can find: $D\vec{y} = \vec{c}$ for $\vec{y} = A\vec{x}$, where $\vec{y}$ is a linear combination of Hamiltonian x_i and $\vec{c} = A\vec{e}$. This leads to:

$$y_i = c_i d_i. \qquad (A.12)$$

It is clear from Equation (A.12), the c_i (variation of data) has a significant effect when d_i (x_i associated errors) has a large value or in the other words nearly identical results are obtained from largely different Hamiltonians. This linear combination is poorly determined. To separate the poorly determined from the well determined parameters we can use a certain criterion δ on the magnitude of the corresponding eigenvalues d_i. To apply the certain criterion δ method we need two linear combinations, the first one we find from Equation (A.12) and the second from a reasonable Hamiltonian such as G-matrix interaction which is used as starting Hamiltonian. Through the adoption of G-matrix values as $\vec{x}^{s}$, the second linear combination is from $\vec{y}^{s} = A\vec{x}^{s}$. The new linear combinations $\vec{y}'$ are obtained from using the results of Equation (A.12) only for well determined parameters

and using starting Hamiltonian values for the rest of the parameters by applying the equation:

$$\vec{y}' = y_i(d_i \leq \delta) + y_i^s(d_i > \delta)\,. \qquad (A.13)$$

A new Hamiltonian is obtained from $\vec{x}' = A^{-1}\vec{y}'$ and it will be used in the next iteration, where the fitted interaction is held to the starting interaction except for the part that is well determined by the data set. The process is repeated until the differences between the $(n+1)^{th}$ set and n^{th} set of the matrix elements are negligibly small.

REFERENCES

[1] M.a.J. Mayer, and J. Hans,(1955), "Elementary Theory of Nuclear Shell Structure", John Wiley and Sons , New York, pp. 1-15.

[2] W.E. Meyerhof,(1967), "Elements Of Nuclear Physics", McGRAW-Hill Book Company,, pp.3-8.

[3] S.S.M. WONG,(2004), "Introductory Nuclear Physics", Wiley-VCH Verlag GmbH & Co. KGaA, Weinheim, pp.1.

[4] R.F. Casten,(1990), "Nuclear Structure From a Simple Perspective",Oxford University Press, New York, pp.3.

[5] Ben R. Mottelson and Aage Bohr,(1998), " Nuclear Structure", World Scientific Publishing, Singapore,, Vol. 1, pp.587.

[6] B.A. Brown, and B.H. Wildenthal, *Annu. Rev. Nucl. Part. Sci.* **38**, 29 (1988).

[7] B. A. Brown, and W. A. Richter, *Phys. Rev. C* **74**, 034315 (2006).

[8] S. B. Patel,(1991), "Nuclear physics an introduction", New Age International Publishers, pp. 236-274.

[9] K. S.Krane,(1987), "Introductory Nuclear Physics", John Wiley and Sons , New York, pp.44-134.

[10] B.A. Brown,(2011), "Lecture Notes in Nuclear Structure Physics", National Superconducting Cyclotron Laboratory and Department of Physics and Astronomy Michigan State University, E. Lansing, MI 48824.

[11] A. Bürger,(2007), PhD Thesis,Rheinischen Friedrich-Wilhelms-Universität Bonn,.

[12] B.A. Brown, *Prog.Part.Nucl.Phys.* **47**, 517 (2001).

[13] J B McGrory, and B H Wildenthal, , *Annu. Rev. Nucl. Part. Sci.* **30**, 383 (1980).

[14] G.F. Bertsch, and C.W. Johnson, *Phys. Rev. C* **80**, 027302 (2009).

[15] M. Honma, B.A. Brown,T. Mizusaki, and T. Otsuka, *Nucl. Phys. **A*** **704**, 134 (2002).

[16] B.A. Brown, W.A. Richter, R.E. Julies, and B.H. Wildenthal, *Ann. Phys.* **182**, 191 (1988).

[17] M. Hjorth-Jensen, T.T.S. Kuo, and E. Osnes, *Phys. Rep.* **261**, 125 (1995).

[18] B.R. Barrett, and M.W. Kirson, *Nucl. Phys. **A*** **148**, 145 (1970).

[19] S.C. Pieper, V.R. Pandharipande, R.B. Wiringa, and J. Carlson, *Phys. Rev. C* **64**, 014001 (2001).

[20] E.K. Warburton, and B.A. Brown, *Phys. Rev. C* **46**, 923 (1992).

[21] T. Suzuki, R. Fujimoto, and T. Otsuka, *Phys. Rev. C* **67**, 044302 (2003).

[22] C. Yuan, T. Suzuki, T. Otsuka, F. Xu, and N. Tsunoda, *Phys. Rev. C* **85**, 064324 (2012).

[23] B.H. Wildenthal, *Prog.Part.Nucl.Phys.* **11**, 5 (1984).

[24] E.K. Warburton, J.A. Becker, and B.A. Brown, *Phys. Rev. C* **41**, 1147 (1990).

[25] Y. Utsuno, T. Otsuka, T. Mizusaki, and M. Honma, *Phys. Rev. C* **60**, 054315 (1999).

[26] S. Nummela *et al.*, *Phys. Rev. C* **63**, 044316 (2001).

[27] W. Chung, Ph.D. thesis, Michigan State University, 1976.

[28] A.H. J Fiase, J M Irvine and F Yazici, *J. Phys. **G**: Nucl. Part. Phys.* **14**, 9 (1988).

[29] F. Nowacki, and A. Poves, *Phys. Rev. C* **79**, 014310 (2009).

[30] Y. Utsuno *et al.* , *Phys. Rev. C* **86**, 051301 (2012).

[31] M. Honma, T. Otsuka, B.A. Brown, and T. Mizusaki, *Phys. Rev. C* **69**, 034335 (2004).

[32] M. Honma *et al.* , *J. Phys.: Conf. Ser.* **20**, 7 (2005).

[33] A. Poves, J. Sánchez-Solano, E. Caurier, and F. Nowacki, *Nucl. Phys.* ***A*** **694**, 157 (2001).

[34] T. Shizuma *et al.*, *Phys. Rev. C* **87**, 024301 (2013).

[35] B.A. Brown *et al.*, (2004),The Oxford-Buenos-Aires-MSU Shell-Model Code, MSUCL Report Number 1289.

[36] J. Krämer *et al.*, *Phys. Lett.* ***B*** **678**, 465 (2009).

[37] J.M. Yao *et al.*, *Phys. Rev. C* **83**, 014308 (2011).

[38] C.A. Diget *et al.*, *Phys. Rev. C* **77**, 064309 (2008).

[39] D.W. Visser *et al.*, *Phys. Rev. C* **78** 028802 (2008).

[40] L. Erikson *et al.*, *Phys. Rev. C* **81**, 045808 (2010).

[41] H. Comisel, C. Hategan, G. Graw, and H.H. Wolter, *Phys. Rev. C* **75**, 045807 (2007).

[42] A.L. Sallaska *et al.* , *Phys. Rev. Let.t* **105**, 152501 (2010).

[43] A.L. Sallaska *et al.*, *Phys. Rev. C* **83**, 034611 (2011).

[44] L. Collaboration *et al.*, *Phys. Rev. C* **82**, 015801 (2010).

[45] R. Longland *et al.*, *Phys. Rev. C* **80**, 055803 (2009).

[46] C. Massimi *et al.*, *Phys. Rev. C* **85**, 044615 (2012).

[47] R. Longland, C. Iliadis, and A.I. Karakas, *Phys. Rev. C* **85**, 065809 (2012).

[48] A.S.J. Murphy *et al.*, *Phys. Rev. C* **73**, 034320 (2006).

[49] W. Benenson, E. Kashy, and I.D. Proctor, *Phys. Rev. C* **8**, 210 (1973).

[50] R. C. P a r d o, Proc. Intern . Conf . Atomic Masses and Fundamental Constants, 6th, Plenum Press, New York, 1980, pp.25

[51] S. Kubono *et al.*, *Nucl. Phys.* ***A*** **537**, 153 (1992).

[52] R.B. Firestone, *Nucl. Data Sheets* **103**, 269 (2004).

[53] R.B. Firestone, *Nucl. Data Sheets* **108**, 1 (2007).

[54] O.S. Kirsebom *et al.*, Eur. Phys. J. **A 47**, 1 (2011).

[55] A. Saastamoinen *et al.*, *Phys. Rev. C* **83**, 045808 (2011).

[56] A. Gade *et al.*, *Phys. Rev. C* **83**, 054324 (2011).

[57] D.G. Jenkins *et al.*, *Phys. Rev. C* **87**, 064301 (2013).

[58] M. Bouhelal *et al.*, *Nucl. Phys.* ***A*** **864**, 113 (2011).

[59] R.K. Sheline, and R.A. Harlan, *Nucl. Phys.* **29**, 177 (1962).

[60] R.B. Firestone, *Nucl. Data Sheets* **110**, 1691 (2009).

[61] M. Shamsuzzoha Basunia, *Nucl. Data Sheets* **112**, 1875 (2011).

[62] H. Weigmann, R.L. Macklin, and J.A. Harvey, *Phys. Rev. C* **14**, 1328 (1976).

[63] P.M. Endt, *Nucl. Phys.* ***A*** **521**, 1 (1990).

[64] M. Shamsuzzoha Basunia, *Nucl. Data Sheets* **113**, 909 (2012).

[65] M. Kowalska *et al.*, *Phys. Rev. C* **77**, 034307 (2008).

[66] P. Baumann *et al.*, *Phys. Rev. C* **39**, 626 (1989).

[67] A. Johnston, and T.E. Drake, *J. Phys. A: Math. Nucl. Gen.* **7**,898 (1974).

[68] H. ÜBerall, and P. Uginčius, *Phys. Rev.* **178**, 1565 (1969).

[69] J.D. Walecka, *Nucl. Phys.* ***A*** **574**, 271 (1994).

[70] B.A. Brown, R. Radhi, and B.H. Wildenthal, *Phys. Rep.* **101**, 313 (1983).

[71] N.F. Mott, *Proc. R. Soc. Lond.* **A124**, 425 (1929).

[72] E.M. Lyman, A.O. Hanson, and M.B. Scott, *Phys. Rev.* **84**, 626 (1951).

[73] T.W. Donnelly, and I. Sick, *Rev. Mod. Phys.* **56**, 461 (1984).

[74] T. de Forest, and J.D. Walecka, *Adv. in Phys.* ***15****, 1 (1966).*

[75] H. Euteneuer *et al.*, *Phys. Rev. C* **16**, 1703 (1977).

[76] R.C. York, and G.A. Peterson, *Phys. Rev. C* **19**, 574 (1979).

[77] E.W. Lees *et al.*, *J. Phys.* ***G****: Nucl. Part. Phys.* **2**,105 (1976).

[78] E.M. de Guerra, and A.E.L. Dieperink, *Phys. Rev. C* **18**, 1596 (1978).

[79] R.A. Radhi, N.T. Khalaf, and A.A. Najim, *Nucl. Phys.* ***A*** **724**, 333 (2003).

[80] L.W. Fagg *et al.*, *Phys. Rev.* **187**, 1384 (1969).

[81] Y. Okazaki *et al.*, *Phys. Lett.* ***B*** **55**, 373 (1975).

[82] A. Nakada, Torizuka, and Yoshiharu, *J. Phys. Soc. Jpn.* **32**, 1 (1972).

[83] E.W. Lees *et al.*, *J. Phys.* ***G****: Nucl. Part. Phys.* **1**, L13 (1975).

[84] E.W. Lees *et al.*, *J. Phys.* ***G****: Nucl. Part. Phys.* **2**, 341 (1976).

[85] J.R. Marinelli, and J.R. Moreira, *Phys. Rev. C* **45**, 1556 (1992).

[86] P. J. Brussaard, and P. W. M. Glaudemans,(1977), "Shell-model Application in Nuclear Spectroscopy", North-Holland Publishing Company, Amsterdam, pp.34- 64

[87] P. Ring, and P. Schuck,(1980), "The Nuclear Many-Body Problem", Verlag Berlin Heidelberg, pp. 1-86.

[88] E. Caurier *et al.*, *Rev. Mod. Phys.* **77**, 427 (2005).

[89] V. Zelevinsky, B.A. Brown, N. Frazier, and M. Horoi, *Phys. Rep.* **276**, 85 (1996).

[90] P.-O. LÖWdin, *Rev. Mod. Phys.* **36**, 966 (1964).

[91] B.A. Brown *et al.* , *Phys. Rev. C* **32**, 1127 (1985).

[92] B. Alex Brown, *Phys. Rev. C* **58**, 220 (1998).

[93] H. Chandra, and G. Sauer, *Phys. Rev. C* **13**, 245 (1976).

[94] B.A. Brown, and W. Chung, B.H. Wildenthal, *Phys. Rev. C* **22**, 774 (1980).

[95] W.A. Richter, S. Mkhize, and B.A. Brown, *Phys. Rev. C* **78**, 064302 (2008).

[96] E.S. Paul *et al.*, *J. Phys.* ***G****: Nucl. Part. Phys.***17**, 605 (1991).

[97] http://www.nndc.bnl.gov/.

[98] B.A. Brown *et al.*, *Phys. Rev. C* **76**, 034305 (2007).

[99] M. Haaranen, M. Horoi, and J. Suhonen, *Phys. Rev. C* **89**, 034315 (2014).

[100] S. Krewald, A. Djaloeis, and S. Gopal, *Phys. Rev. C* **24**, 966 (1981).

[101] G. Bertsch, J. Borysowicz, H. McManus, and W.G. Love, *Nucl. Phys.* ***A*** **284**, 399 (1977).

[102] K.S. Jassim, Anwer A. Al-Sammarraie, F.I. Sharrad, and H. Abu Kassim, , *Phys. Rev. C* **89**, 014304 (2014).

[103] W.A. Richter, and B.A. Brown, *Phys. Rev. C* **80**, 034301 (2009).

[104] Anwer A. Al-Sammarraie, Fadhil I. Sharrad, A. A. Aziz, Norhasliza Yusof, and Hasan Abu Kassim (2014), Eur. Phys. J. Plus **129**, 125 (2014).